Russian Original Vol. 48, No. 5, May, 1980

November, 1980

SATEAZ 48(5) 281-352 (1980)

SOVIET ATOMIC ENERGY

АТОМНАЯ ЭНЕРГИЯ
(ATOMNAYA ÉNERGIYA)

TRANSLATED FROM RUSSIAN

CONSULTANTS BUREAU, NEW YORK

SOVIET ATOMIC ENERGY

Soviet Atomic Energy is a translation of *Atomnaya Énergiya*, a publication of the Academy of Sciences of the USSR.

An agreement with the Copyright Agency of the USSR (VAAP) makes available both advance copies of the Russian journal and original glossy photographs and artwork. This serves to decrease the necessary time lag between publication of the original and publication of the translation and helps to improve the quality of the latter. The translation began with the first issue of the Russian journal.

Consultants Bureau journals appear about six months after the publication of the original Russian issue. For bibliographic accuracy, the English issue published by Consultants Bureau carries the same number and date as the original Russian from which it was translated. For example, a Russian issue published in December will appear in a Consultants Bureau English translation about the following June, but the translation issue will carry the December date. When ordering any volume or particular issue of a Consultants Bureau journal, please specify the date and, where applicable, the volume and issue numbers of the original Russian. The material you will receive will be a translation of that Russian volume or issue.

Subscription (2 volumes per year)

Vols. 46 & 47: $147.50 per volume (6 Issues)
Vols. 48 & 49: $167.50 per volume (6 Issues)

Single Issue: $50
Single Article: $7.50

Prices somewhat higher outside the United States.

Soviet Atomic Energy is abstracted or indexed in *Chemical Abstracts, Chemical Titles, Pollution Abstracts, Science Research Abstracts, Parts A and B, Safety Science Abstracts Journal, Current Contents, Energy Research Abstracts,* and *Engineering Index.*

CONSULTANTS BUREAU, NEW YORK AND LONDON

c/b
227 West 17th Street
New York, New York 10011

Published monthly. Second-class postage paid at Jamaica, New York 11431.

SOVIET ATOMIC ENERGY

A translation of *Atomnaya Énergiya*

November, 1980

Volume 48, Number 5 May, 1980

CONTENTS

CONTENTS

(continued)

The Russian press date (podpisano k pechati) of this issue was 4/24/1980. Publication therefore did not occur prior to this date, but must be assumed to have taken place reasonably soon thereafter.

THE LITHIUM ZONE IN THE BLANKET OF A FUSION REACTOR

V. G. Vasil'ev, Z. V. Ershova, and E. V. Dmitrievskaya

UDC 621.039.6:621.039.573

A controlled deuterium–tritium thermonuclear reaction in a fusion reactor involves producing tritium in the reactor itself, which is then used to supply the plasma. It has been suggested that tritium can be produced by using either metallic lithium or various lithium compounds in the reactor blanket. Schemes were first proposed [1, 2] for the blanket zone in pure reactors, where the fusion neutrons are absorbed in the breeding zone of the blanket, which contains lithium materials in the molten or solid states [3-5]. In the first case, the lithium material is used also as the heat carrier. In the second case, the heat carrier is some other working body, e.g., helium. Therefore, the lithium zone in a pure reactor acts as a tritium accumulator and is a source of thermal energy. Table 1 gives the lithium materials that have been suggested for the breeding zone. A fusion reactor differs from a fission one in that the heat-transport loop is involved in the production and isolation of the tritium required for fusion. The performance of a pure reactor is examined in terms of three parameters: improvement in the efficiency of the reactor (station) as a whole, attainment of the maximum tritium breeding factor, and optimization of the working conditions in the first wall.

High efficiency involves raising the heat-carrier temperature, and this complicates various aspects related to the accumulation of tritium. Elevated temperatures increase the diffusion and dissolution of tritium in the material. Also, there are serious problems of corrosion failure in constructional materials in contact with molten lithium or salts.

The tritium breeding factor may be increased by incorporating elements into the lithium or the constructional material that undergo (n, 2n) and (n, 3n) reactions: beryllium, molybdenum, tungsten, etc.

The following major problems arise in the lithium breeding zone for a pure reactor:

1) choice of the lithium isotope composition (natural or enriched in ^{6}Li) and determination of the required macroscopic cross section;

2) provision of high temperature in the coolant, which is required for high efficiency in the station;

3) radiation safety problems arising from leakage of tritium from the loops by diffusion;

4) the interaction of the molten coolant with the constructional materials and the choice of the most stable ones for long-term operation;

5) choice of a lithium material for the blanket zone resistant to radiation damage and also thermally stable; and

6) determination of the economic features of various schemes for the accumulation and extraction of tritium.

Hybrid reactors have also been proposed, in which the blanket contains fissile material, such as depleted or natural uranium [22, 23]. This can raise the energy yield to 100 MeV per fusion neutron, which gives a substantial advantage over a pure reactor. A hybrid reactor not only produces electrical energy but also produces plutonium, while still producing tritium for the plasma. The advantages of a hybrid reactor are accompanied by some obvious disadvantages, such as increase in the radiation hazard and the need to process fissile materials.

The lithium zone is designed to breed tritium in the blanket, and the optimum dimensions and composition of the latter are determined by neutron-physics calculations. Figure 1 shows a scheme for a blanket with uranium and lithium zones [24, 25].

Translated from Atomnaya Énergiya, Vol. 48, No. 5, pp. 283-287, May, 1980. Original article submitted January 30, 1978; revision submitted March 20, 1979.

0038-531X/80/4805-0281$07.50

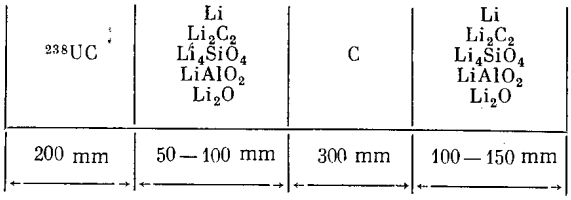

Fig. 1. Forms of blanket with various materials.

TABLE 1. Lithium Zones in Fusion Systems and Reactors

Fusion system or reactor	Lithium zone	Function	Coolant temperature, °C		Temp. of lithium material, °C	Ref.
			inlet	outlet		
T-20 blanket module	Liquid lithium	Coolant and tritium production	300/480	470/550		[6, 7]
UWMAK I			283	483		[8]
UWMAK III			630	980		[9]
			260	550		[10]
Blanket module for the LINUS fusion reactor	50% Pb—Li; 44% Pb and 6% Cd	Tritium production			~ 450°	[11]
T-20 blanket module	Molten 50% LiF—50% BeF_2	Coolant and tritium production	500	650	up to 700	[6]
Blanket for tokamak hybrid reactor	Molten 47,5% LiF—52% BeF_2, balance PuF_3 or UF_4	Tritium production, coolant helium			up to 700	[12—13]
Symbiotic system of fusion-fission reactors	Molten LiF—BeF_2	Coolant and tritium production			up to 700	[14—15]
T-20 blanket module	Solid inorganic lithium compound	Tritium production, coolant helium	300	570	up to 700	[6]
UWMAK II	$LiAlO_2$	" "	450	650	up to 900	[16]
GTRT	Solid inorganic lithium compound	» »				[17]
JAERI-M7300	Li_2O	» »	300	500	up to 600	[18—19]
Doublet DPR blanket module	Li_7Pb_2 or Li_4SiO_4	» »	275	585	up to 700	[20]
Mirror blanket module	$Li_2Be_2O_3$ + Be	Tritium production, coolant helium with lithium			⩽ 950	[21]

The lithium zone in a hybrid reactor operates under a variety of functionally conflicting conditions [17]. Most of the energy is produced in the uranium zone in a hybrid reactor, while the heat produced in the lithium zone is not more than 5-6% of the total produced in the blanket, so the lithium zone is mainly a tritium generator, where the tritium accumulates for subsequent extraction and return to the plasma.

The dimensions of the lithium zone have not been finally established; they may vary during calculation and development, but they should lie in the range 50-150 mm. Figure 1 indicates that the lithium zone consists of two sections, the first of which lies beyond the uranium zone, while the second has the lowest thermal and neutron loadings. It is found [23-26] that the ratio of the tritium formation rates in these sections is 5 : 1.

On existing proposals, a fusion reactor is designed for long-term operation (not less than 20 years), but the provision of long-term thermal stability and radiation resistance has not been finally resolved for the constructional materials in the various zones of the blanket and in the lithium material itself.

In all models, the lithium breeding involves fairly prompt extraction of the tritium and return to the reactor, which should be self-sufficient in tritium. Economy requires that the cost of the tritium stock should be minimized during the startup period. For a reactor with a thermal power of about 7 GW, the daily consumption of tritium in the plasma would be about 100 g, and the same amount of tritium must be produced in the lithium zone. The problem is to reduce the hold-up of tritium in the blanket, i.e., to begin the extraction of tritium at very low concentrations. This not only reduces the demand for tritium in the start-up period but also provides the maximum radiation safety for this element, since continuous extraction of tritium at low concentrations will keep the total amount in the blanket reasonably small (not more than 1 kg).

Experimental data are available on the isolation of tritium from irradiated inorganic compounds such as lithium fluoride, sulfate, carbonate, oxide, aluminate, chromate, and nitrate when the levels of tritium are less than 10^{-4} mass %; heat treatment under vacuum can extract 90-99% of the tritium in the range 500-800°C [21,

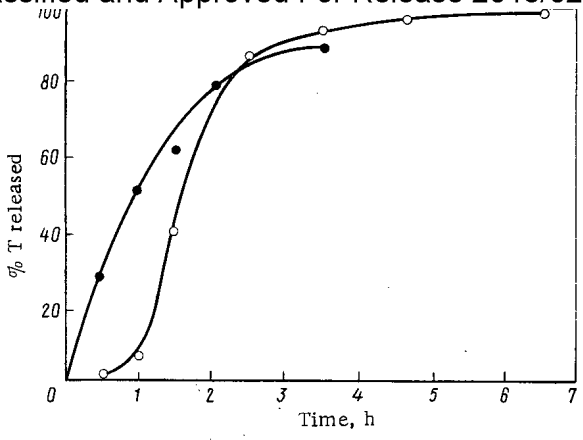

Fig. 2

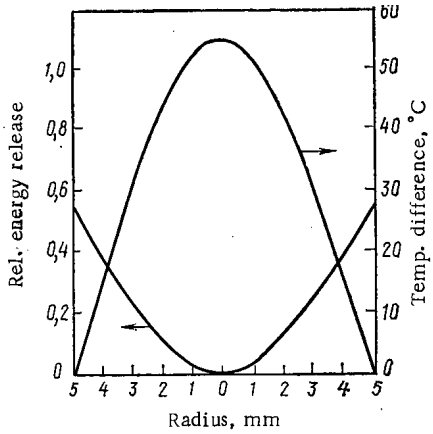

Fig. 3

Fig. 2. Release of tritium from irradiated lithium sulfate for an initial tritium concentration of $1 \cdot 10^8$ Bq/g at 15-550°C (○) and $1 \cdot 10^7$ Bq/g at 550°C (●).

Fig. 3. Energy production and temperature difference in a sphere of diameter 10 mm with $\lambda = 1$ W/m·°C, $q = 8$ W/cm^3.

27, 28]. Figure 2 shows the extraction of tritium from irradiated lithium sulfate during heat treatment under vacuum. Preliminary estimates indicate that the tritium diffusion coefficient is 10^{-10} cm^2/sec at 550°C.

At present one envisages the following modes of operation for the lithium zone in a hybrid reactor, which provide for fairly independent production of the temperatures needed for the accumulation and extraction of tritium (Table 2).

1. Low-temperature (100-200°C) irradiation of the lithium material for instance in the form of spheres with hard coating or in some other form. In that case, the lithium material may be cooled to the required temperature for example with helium. Figure 3 shows the energy production and the temperature difference over the radius of the sphere for a thermal output of 8 W/cm^3 on the assumption that the thermal conductivity of the lithium material is $\lambda \approx 1$ W/m·°C ($\lambda \approx 1.7$ W/m·°C for lithium aluminate and oxide) at room temperature [16, 18]. A gap of 0.5 mm between the shell and the contents of the sphere may result in an additional temperature difference of about 200°C if the gap is filled with argon or about 20°C if the gap is filled with helium. This provides for minimal loss of tritium from the breeding zone during irradiation and minimum contamination of the helium coolant with tritium.

2. Operation of the lithium zone with helium as coolant at about 500°C; in that case the tritium is released from the lithium material by diffusion and is continuously carried out of the zone by the helium. This requires continuous treatment of the helium to extract the tritium. The operation of the lithium components may be complicated by the fact that the helium formed in ^{6}LI (n, α) T cannot be extracted from the lithium component without breaking the sealing in the sheath. The accumulation of helium within the lithium components causes a gradual increase in pressure, and within a year of operation the helium in a sphere of diameter 10 mm with a free volume of 0.05 cm^3 will give rise to a pressure of $9.8 \cdot 10^6$ Pa. In addition to the gas released from the lithium elements, one has to consider the temperature at the wall of the lithium zone. A preliminary calculation on the leakage of tritium through the hot outer wall of this zone shows that this can be minimized. Then the main difficulties in the isolation of tritium from the helium, where the partial pressure of tritium is to be kept not more than 13.3 Pa, are transferred to the processing section. The tritium can be extracted from the zone continuously or periodically, as in the production of tritium by continuous irradiation in fission reactors [29-31].

The energy production in the parts of the lithium zone of about $3 \cdot 10$ W/m^3 is distributed as 5 : 1 between them [26]. Figure 4 shows the expected distribution of the temperatures in zone I for two-sided cooling and for zone II with one-sided cooling. However, it is clear that one can produce conditions required for tritium extraction throughout the lithium zone. Compounds of lithium such as the aluminate, silicate, and oxide having $\lambda \approx 1$-2 W/m·°C can result in temperature differences of several hundred degrees in the first 5-10 mm of the layer. The lithium material in the central part of the zone will be at the melting point.

Table 2 gives characteristics for the lithium zone in a hybrid reactor; further research is required on the operation of the lithium zone, particularly the complications arising in continuous isolation of the tritium.

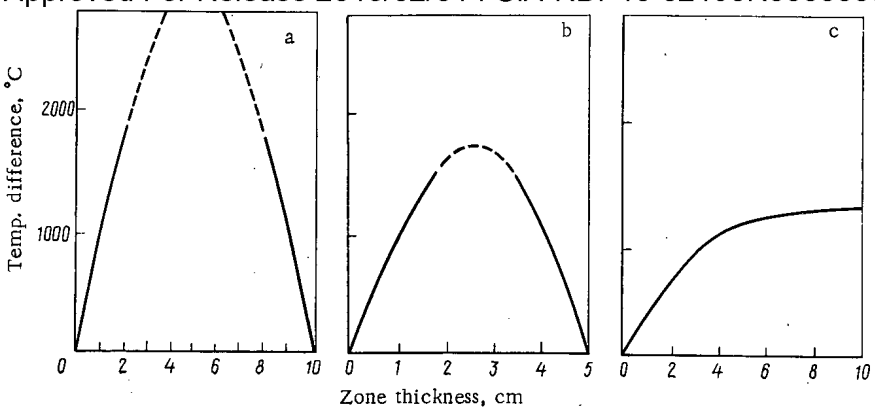

Fig. 4. Distribution of temperature differences in lithium material in the zones of a blanket for $\lambda = 1$ W/m·°C and $q = 3 \cdot 10^6$ W/m^3; t_m $LiAlO_2$ = 1600°C, t_m Li_4SiO_4 = 1250°C: a) zone I, thickness 10 cm; b) zone I, thickness 5 cm; c) zone II, thickness 10 cm.

TABLE 2. Characteristics of the Lithium Zone in a Hybrid Reactor

Features	Lithium zone cooled to 200°C by helium (wall temp. 200°C, spherical elements)	Lithium zone cooled to 600°C by helium (wall temp. 500-600°C, spherical elements)	Lithium zone at a high temp., wall temp. 200°C, temp. of lithium material between 600°C and the melting point
Advantages	Safe operational zone with minimum trition loss from elements	Continuous isolation of tritium with a minimum level in the blanket	Continuous isolation of tritium with a minimum level in the blanket
	Scope for rapid change of elements under emergency situations	Prolonged operation of elements without replacement	Elimination of radiation damage by melting of the tritium material in the zone
	Tritium extraction outside the reactor	Scope for rapid change of elements under emergency situations	Production of tritium in concentrated form
Disadvantages	Tritium hold-up in reactor	Maintenance of a small temperature difference between the spherical elements for tritium isolation	Severe working conditions in the lithium zone with pressure differences
	Periodic or continuous displacement of elements for trition extraction	Considerable dilution of the tritium with helium	Change in the composition of the lithium material by mass transport
	Increased consumption of initial material and formation of radioactive wastes	Contamination of the coolant and need to cool the walls to reduce diffusion leakage	

A hybrid reactor allows one to control the temperature of the lithium zone and to isolate the tritium under safe conditions of operation. Here it is necessary to consider the construction of the lithium components for the blanket in order to provide reliable operation in the lithium zone. This requires lithium material of high thermal stability and good radiation resistance on exposure to integral fluxes of 10^{21}-10^{22} neutrons/cm^2, as well as constructional materials for the sheaths compatible with the lithium materials, and improved design of the blanket as a whole and of the lithium zone in particular.

LITERATURE CITED

1. D. J. Rose and M. Clark jun., Plasmas and Controlled Fusion [Russian translation], Gosatomizdat, Moscow (1963).
2. W. Homeyer, "Thermal and chemical aspects of the thermonuclear blanket problem," MIT TR-435 (1965).

3. G. Kulcinski and R. Conn, in: Fusion Reactor Design Problems, Proceedings of an IAEA Workshop Held at Culham, UK, Jan. 29 to Feb. 15, 1975, p. 51; F. Tenney, ibid., p. 17; K. Sako et al., ibid, p. 27.
4. J. Darvas, in: Proceedings of the International Conference, Gatlinburg, 1-3 Oct. 1975. Conf. 750985, v. III.
5. Z. V. Ershova et al., in: Proceedings of the All-Union Conference on Engineering Problems of Controlled Fusion [in Russian], Vol. IV, NIIEFA, Leningrad (1975), p. 14.
6. V. A. Glukhikh, N. A. Monoszon, and G. F. Churakov, ibid., Vol. 1 (1977), p. 42.
7. G. N. Zhemchuzhnikov, A. M. Benevolenskii, and A. N. Topil'skii, in: Proceedings of the Second Soviet–American Seminar [in Russian], Atomizdat, Moscow (1978), p. 164.
8. B. Badger et al., "UWMAK I, A Wisconsin toroidal fusion reactor-design," Nucl. Eng. Dept. Report UWFDM-68, University of Wisconsin at Madison (1974), Vol. 1 (1975), Vol. 2.
9. B. Badger et al., "UWMAK III, A conceptual noncircular tokamak power reactor design," Nucl. Eng. Dept. Report UWFDM-150, University of Wisconsin at Madison (1976).
10. S. Majumbar and B. Misra, Trans. Am. Nucl. Soc., 27, 73 (1977).
11. A. Robson, ibid, p. 45.
12. W. Price et al., "The Princeton beam-driven tokamak fusion–fission hybrid study," PPPL-TM-299. Feb. (1977).
13. F. Tennly, in: Proceedings of the US–USSR Symposium on Fusion–Fission Reactors. Conf. 760733. Livermore, 13-16 July (1976), p. 71.
14. V. L. Blinkin and V. M. Novikov, IAE Preprint 28-19, Moscow (1977). Proceedings of the Second Soviet–American Fusion–Fission Seminar [in Russian], Atomizdat, Moscow (1978).
15. V. Blinkin and V. Novikov, Nucl. Fusion, 18, 893 (1978).
16. B. Badger et al., "UWMAK III, A conceptual noncircular tokamak power reactor design," Nucl. Eng. Dept. Report UWFDM-112, University of Wisconsin at Madison (1975).
17. E. P. Velikhov et al., [6], Vol. 1, p. 5.
18. K. Sako et al., First Preliminary Design of an Experimental Fusion Reactor, JAERI-M 7300 (1977).
19. H. Kubo, K. Tanaka, and H. Amano, J. Inorg. Nucl. Chem., 40, 363 (1978).
20. D. Kearney et al., Mechanical and Thermal Design of a Gas-Cooled Fusion Blanket Module GA-A14671, September (1977).
21. T. Galloway, in: Proceedings of the Conference of the Second Topical Meeting on the Technology of Controlled Nuclear Fusion, Richmond, 21-23 Sept. (1976). 760935. v. III, p. 1351.
22. I. N. Golovin, At. Energ., 39, No. 6, 379 (1975).
23. G. E. Shatalov, Izv. Akad. Nauk SSSR, Ser. Energ. Transport, No. 6, 85 (1975).
24. S. V. Marin et al., "Some parameters of the blanket around a fission reactor containing fissile material," Paper at the USSR–USA Joint Seminar, Leningrad, December 9 (1974).
25. V. Kotov and G. Shatalov, [13], p. 129.
26. V. Gur'ev et al., [13], p. 119.
27. I. Owen, [4], p. 433.
28. Z. V. Ershova and V. G. Vasil'ev, in: Proceedings of the All-Union Conference on Engineering Problems of Controlled Fusion [in Russian], Vol. IV, NIIEFA, Leningrad (1975), p. 3.
29. Czechoslovak Patent No. 103871, cl. 12.01. Publ. 13.06.1962.
30. U.S.A. Patent No. 3079317, cl. 204.154.2. Publ. 26.02.63.
31. V. G. Vasil'ev, Z. V. Ershova, and E. V. Dmitrievskaya, At. Energ., 44, No. 5, 440 (1978).

TEMPERATURES IN THE GRAPHITE STACKS IN THE REACTORS AT THE BILIBINSK NUCLEAR POWER STATION

O. V. Komissarov, N. I. Logosha,
M. E. Minashin, G. E. Soldatov,
N. V. Filippova, and V. N. Sharapov

UDC 621.039.516.5

The reactions at the Bilibinsk combined heat and power station each have a pile of graphite blocks, in which there are vertical technological channels TC and control and protection channels CPC [1]. The pile is contained in a sealed volume filled with nitrogen to prevent rapid burnup of the graphite at high temperatures. The heat deposited in the graphite by neutron moderation and γ-ray absorption is output in the main to the TC and CPC, although some part passes through the reflectors to the foundations and to the biological shielding tank filled with water.

The thermal power of each of the four reactors in the station is 62 MW, of which 12 MW is utilized in electrical form and 29 MW represents the heat load. Figure 1 shows a cross section of one-quarter of a reactor. Five three-zone thermocouples are installed at various distances from the center of the core to monitor the temperature of the graphite. Each measures the temperature at three points along the height of the graphite stack. Temperature measurements are also made on the metal jacket surrounding the graphite and on the foundations and upper cover of the reactor.

Temperature Distribution in a Technological-Channel Cell. Figure 2a shows the cross section of a cell in a technological channel; the channel consists of six tubular fuel rods within the core, which are enclosed in graphite sleeves around the central tube. The outside diameter of the fuel rods is 20 mm, while the central tube in the channel is of diameter 25 mm, and the graphite sleeves have diameters of 88 mm. There is the gas gap δ_1 between the central tube and graphite sleeve, while between a fuel rod and a sleeve there is the gap δ_2, together with the gap δ_3 between the channel sleeve and the graphite blocks in the stack. The coolant moves in the channel by natural circulation.

The heat released in the graphite in a TC cell in the main is transmitted to the fuel rods, whose surface temperature is about 310°C. The maximum temperature in the graphite is dependent on the channel power. Figure 3 shows an example of the calculated temperature distribution along the radius for a cell of output 250 kW. The calculations were performed by simulation with conducting paper. This method has been described [2] in application to temperature distribution determination for reactor cells. Figure 3 shows that the temperature of the graphite is determined mainly by the thermal resistance of the gas gaps.

These gaps should provide ready extraction of the channels from the reactor and free movement of the fuel rods in the graphite sleeves. They must be chosen in accordance with the thermal and radiation-induced changes in the sizes of the graphite and in the fuel rods throughout the time spent by the latter in the reactor, but on the other hand they should be small enough to prevent an unacceptable temperature rise in the graphite.

In a reactor with natural circulation, the distribution of the heat flux from the graphite to the fuel rods and to the central tube is dependent on the relation between δ_1 and δ_2. To prevent the natural circulation from being interrupted when the emergency protection gear operates, when the heat flux from the graphite becomes comparable with the residual heat production in the uranium, it is necessary to minimize the amount of heat transmitted to the central tube [3]. Figure 4 shows the proportion of heat transmitted from the graphite to the central tube as a function of δ_1 for various gaps between the fuel rods and the graphite sleeves.

Most of the heat from the graphite must pass to the fuel rods, so the gap between these and the graphite sleeves should not be large. When the fuel rods are a close fit to the graphite sleeves, the part of the fuel-rod surface facing the central tube is screened and plays little part in removing heat from the graphite, which causes the temperature to rise. In the TC at this station, the minimum size of the graphite wall between fuel rods is about 8 mm. Then the heat flux from the graphite via the surfaces facing the central tube is half that through the surface facing the graphite block.

Translated from Atomnaya Énergiya, Vol. 48, No. 5, pp. 287-291, May, 1980. Original article submitted February 5, 1979; revision submitted July 16, 1979.

0038-531X/80/4805-0286$07.50

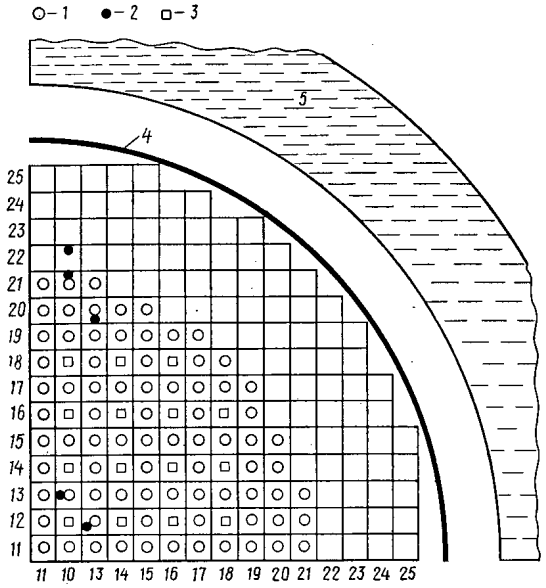

Fig. 1. Cross section of a reactor: 1) TC; 2) CPC; 3) thermocouples for measuring graphite temperature; 4) reactor jacket; 5) biological shield.

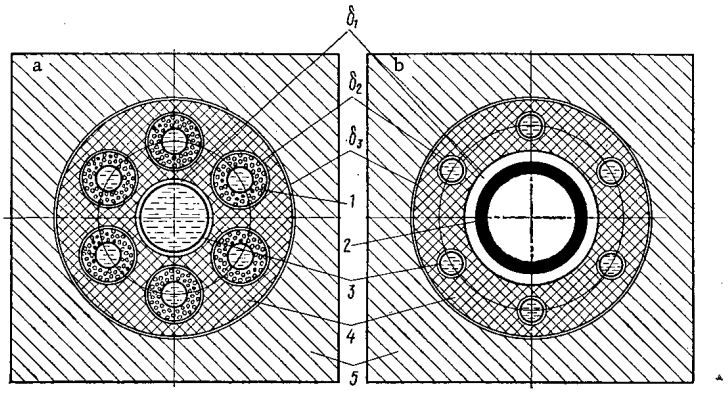

Fig. 2

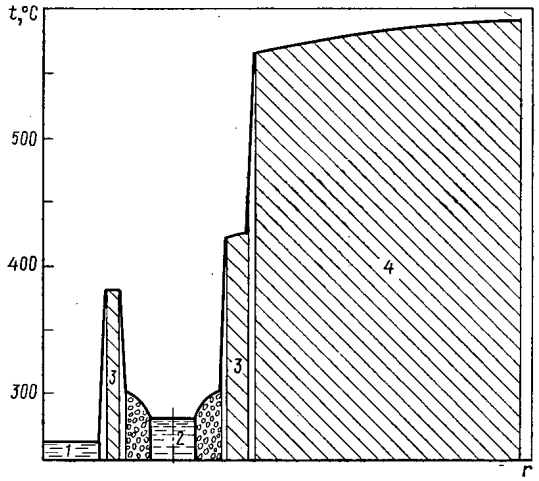

Fig. 3

Fig. 2. Cross sections of a TC cell (a) and a CPC cell (b): 1) fuel rod; 2) absorbing rod; 3) channel tube; 4) graphite sleeves; 5) graphite block.

Fig. 3. Temperature distribution over the radius of a TC cell: 1) channel tube; 2) fuel rod; 3) graphite sleeve; 4) graphite block.

Figure 5 shows the theoretical relationship between the maximum temperature of the graphite block and δ_2 derived on the basis of the uneven distribution of the heat flux at the outer surface of the fuel rods. This relationship has been used on the basis of possible rod swelling during operation to choose δ_2 in the cold state.

If we choose for the cold state $\delta_2 = 0.25$ mm, $\delta_3 = 0.35$ mm, while the heat production in the graphite in a cell is 8.7% of the power and the coefficient representing the nonuniformity over the height of the reactor is 1.35, we get the maximum graphite temperature in relation to TC power as shown by curve 1 of Fig. 6. This relationship was derived for fuel rods coaxially placed in the holes in the graphite sleeves and the same for the sleeves in the holes in the graphite blocks. Under real conditions, these elements are always in contact. Calculations by electrical simulation show that the maximum temperature of the pile may be reduced by considerably more than 10° on account of the contact. There is a temperature reduction of about 10°C on account of heat leakage over the height of the graphite stack.

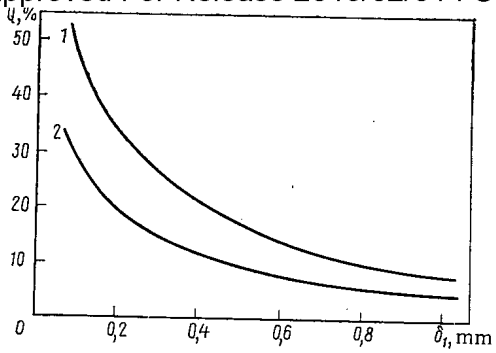

Fig. 4

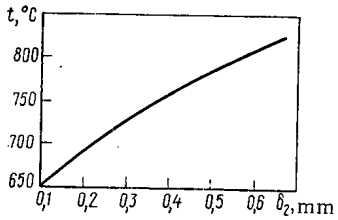

Fig. 5

Fig. 4. Proportion of heat transferred from graphite to central TC tube, power 340 kW, δ_2 = 0.7 mm (1) and 0.2 mm (2).

Fig. 5. Theoretical dependence of maximum graphite temperature on δ_2 (TC power 340 kW; δ_1 = 1 mm; δ_3 = 0.35 mm).

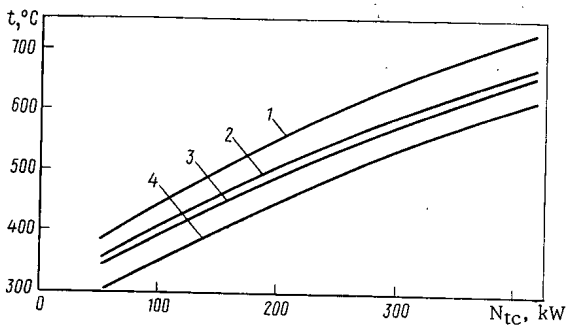

Fig. 6

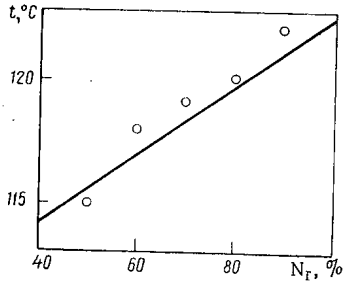

Fig. 7

Fig. 6. Theoretical dependence of maximum graphite temperature on TC power (dimensions in TC cell: δ_1 = 1 mm, δ_2 = 0.25 mm, δ_3 = 0.35 mm, in CPC cell: δ_1 = 3 mm, δ_2 = 0.20 mm, δ_3 = 0.35 mm): 1) homogeneous TC lattice; 2) TC cell with angular disposition relative to CPC cell; 3) TC cell adjacent to CPC cell; 4) CPC cell.

Fig. 7. Water temperature at the exit from a CPC channel in relation to reactor power for t_{in} = 104°C: solid line from calculation with allowance for contact between fuel rod and CPC channel tubes; points from experiment.

Effects of CPC on Graphite Temperature. In a homogeneous TC lattice, the heat production in the graphite constitutes 8.7% of the channel power, but in the presence of CPC the graphite in the latter produces 5.0% of the heat, while the graphite in the TC cells in line with the CPC cells and at angles to them will produce, respectively, 7 and 8.4%. The CPC cells in the pile reduce the maximum graphite temperature by about 70°C (Fig. 6).

Figure 7 shows theoretical and experimental data on water heating in the CPC in relation to reactor power. The temperature rise is almost independent of whether the absorbing rods have been withdrawn from the core or not, and about 70% is due to heat produced in the CPC cells (including heat from the absorbing rods), while about 30% is accounted for by heat coming from adjacent TC cells. The set of CPC extracts about 2% of the thermal power of the reactor into the deaerator.

Graphite Temperature in the Core. The graphite temperature was measured at three points along the height of the pile: at the center of the core and at the interfaces with the upper and lower reflectors, where the temperature does not greatly exceed the fuel-rod temperature and is about 350°C for the top and bottom at the nominal reactor power.

The graphite temperature is maximal at the center of the core; the value increases with the reactor power and does not exceed 510°C at the nominal power. The temperature variations in the graphite over the radius of the core are not more than 20°C although the TC power at the center is 1.5 times that at the periphery. This is because the CPC channels lie predominantly at the center of the core, and calculations (Fig. 6)

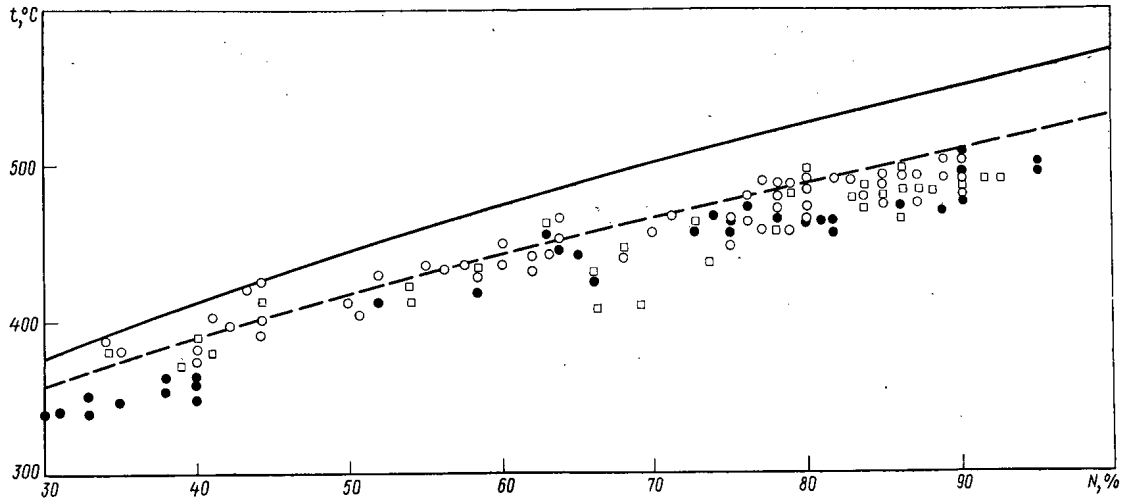

Fig. 8. Maximum graphite temperature in relation to reactor power: ○, □, ●) from experiment (first, second, and third reactors); solid line) calculation without allowance for contact between fuel rods and channel tubes in CPC; broken line) calculation on the basis of contact, by use of reduced concentric gaps (δ_2 = 0.12 mm in TC, δ_2 = 0.1 mm in CPC).

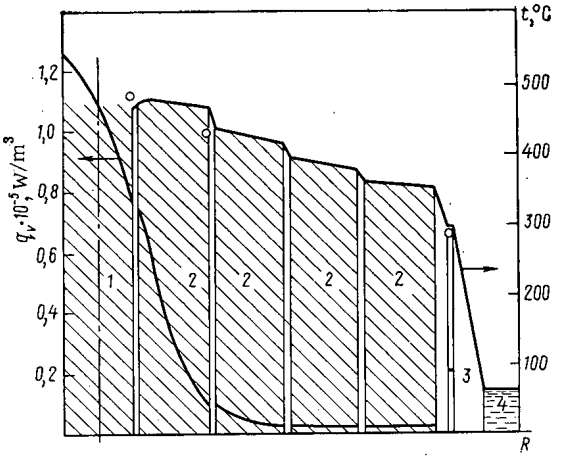

Fig. 9. Calculated distributions of heat production and temperature over the radius of the lateral reflector at the minimal power: 1) TC cell; 2) reflector layers; 3) reactor jacket; 4) biological shield; ⊙ temperature measurements at 93% of the nominal power.

show that this tends to equalize the graphite temperatures in the central and peripheral TC cells. Figure 8 shows how the temperature of the graphite in the center of the core varies with the reactor power.

Graphite Temperature in the Lateral Reflector. Calculation indicates that the total heat production in the laterial reflector is about 400 kW; measurements of the water flow rate and temperature rise for the foundations and biological shield indicate heat removal of about 500 kW, i.e., 100 kW more. The difference is due to the additional influx of heat from the lower end reflector and the core. Figure 9* shows the distribution of the heat production and the temperature pattern in the lateral reflector. The temperature distribution has been derived on the basis of the axial heat leak.

Conclusions. The graphite stack temperature in the Bilibinsk reactors is maximum in the core and is measured as 510°C at the nominal power. The calculated temperature for average gas gaps is about 50°C

*The heat production in the peripheral layers of the reflector and in the reactor jacket was calculated by L. B. Kuznetsova and A. P. Suvorov.

higher. The measured temperatures of the graphite at the center and edge of the core are virtually identical, in spite of differences in the TC power. This occurs because the central thermocouples lie near the CPC cells, whose channels are cooled by water at only about 120°C. When the graphite pile temperature is calculated, it is necessary to correct for the reduction in thermal resistance of the gas gaps arising from contact between the components of the pile.

LITERATURE CITED

1. A. A. Vaimugin et al., At. Energ., 39, No. 1, 3 (1975).
2. O. V. Komissarov et al., in: Calculation of Physical Fields by Simulation Methods [in Russian], Mashinostroenie, Moscow (1968), p. 200.
3. V. M. Abramov et al., in: Proc. IAEA Symposium on Small and Medium Power Reactors, 1970. IAEA, Vienna (1971), p. 363 (IAEA/SM-140/16).

SAFETY IN SERVICING OPERATIONS AT THE BOR-60 NUCLEAR POWER STATION

V. D. Kizin, V. I. Polyakov,
Yu. V. Chechetkin, and L. M. Levin

UDC 621.039.58:621.039.526.004.6

The high levels of radioactivity and chemical activity in the sodium coolant in a fast reactor often lead to pessimistic evaluation of the radiation environment in a nuclear power station during servicing operations. Complicated multitone shielded equipments have been built for removal systems, along with complicated decontamination systems, and means of cleaning the gas in the first loop. Some experience has been accumulated with servicing operations on working fast reactors, particularly the BOR-60, especially for equipment in contact with the coolant and contaminated by fission products and corrosion deposits.

Servicing the First Loop. During the planned prophylactic servicing on the BOR-60, various operations were performed on modifying and replacing the transducers for the monitoring and measuring instruments, and checks were made on the states of certain parts of the hot zones, which were serviced, and further checks were made on the cabling systems, the fire alarms, the transducers in the monitoring systems, etc., with replacement of various items subject to wear (pumps, valve gear, nonreturn valves), etc.

The units in the first and second loops (heat exchangers, pumps, and valve gear) were designed in such a way that parts showing wear could be replaced without entering the first-loop space or cutting the main pipelines. In each case the equipment consisted of a body welded to the pipelines and a removable part containing the components and items needing servicing.

The most complicated servicing operation is to extract the removable parts of the heat exchangers and pumps, which is followed by transport and decontamination. When these removable parts are being demounted, there may be high-intensity radiation fields at the working site, and the films of coolant on the surfaces may ignite, with the production of large amounts of oxide within the loop, which hinders installation of the removable parts after servicing. Further, such operations often give rise to aerosols, which may enter the working location.

The following servicing operations involving the removal and replacement of parts from the first loop were performed during the working cycle of the BOR-60:

1) removal of filters installed in the bodies of the valve gear during the start-up period, with replacement by standard removable parts of this gear;

2) replacement of removable parts of the nonreturn valves;

3) replacement of parts in slides after prolonged operation;

Translated from Atomnaya Énergiya, Vol. 48, No. 5, pp. 291-294, May, 1980. Original article submitted April 23, 1979.

 0038-531X/80/4805-0290$07.50

TABLE 1. Staff Irradiation in Servicing Operations on the BOR-60

Operation	Dose rate μR/sec	Total dose, ber
Operations in the heat-exchanger sections of the first loop, including examination and modification (checks on smoke detectors, examination of thermocouples, replacement of electric lamps, replacement of vibrational transducers, etc.)	200-300	0.04-0.1
Servicing in the heat-exchange sections for the first loop (connection of electrical flowmeters, replacement of electrical heaters on parts of pipelines, servicing of thermal insulation, servicing of base of oxide trap, etc.)	200-300	0.5-3.0
Replacement of removable parts (pump level gauge, pump, etc.)	200-1000	0.2-0.7
Reloading of fuel-rod and experimental assemblies	1-25	1-3

4) removal and replacement of pump components; and

5) replacement of reloading tubes and experimental devices in the core.

No major servicing and replacement operations were performed in the heat-exchanger segments of the first loop, and only one small leak of sodium (about 1-2 kg) was detected as coming from a butt weld under the thermal insulation. The removable parts of the equipment were extracted in a working hood (without biological shielding) flushed by argon, either with a low level for the sodium (without drainage of the bodies) or with the coolant completely removed from the loop. When the removable part of the pump was being extracted, argon was injected into the body, while nitrogen was injected under the working hood. The use of a sealed hood made of a plastic film facilitated the transport and other operations during the reloading, and this also prevented the ignition of the sodium and formation of oxides in the body, as well as the production of aerosols in the working site.

Radiation Environment during Servicing. The BOR-60 has now operated about seven years with the coolant contaminated by fission products. The number of fuel pins with ruptured sheaths is 0.1-1% of the load. The level of radioactivity in the gas phase in the reactor with this number of defective pins is governed by ^{133}Xe and has risen to 1200 Ci.* However, the gas system is sealed, so this level of radioactivity has not resulted in any difficulties. The gas release from the reactor to the environment is governed by ^{41}Ar (in the shield cooling) and is not more than 25 Ci/day. The protective gas was purified on activated charcoal before the reactor was opened for reloading.

The fission-product activity in the sodium at certain periods has greatly exceeded the radioactivity arising from the main long-lived activation isotopes ^{22}Na (0.7 mCi/kg) and ^{110m}Ag (0.2 mCi/kg). This has resulted in increased radiation fields outside the heat exchangers in the first loop, which have risen to 300-500 μR/sec. Up to 8% contribution to the dose rate comes from the γ rays of ^{137}Cs and ^{134}Cs, and the specific activity of ^{137}Cs has varied from 2 to 20 mCi/kg at different times.

See [1] for the isotope compositions of the surface contaminants on various parts of the loop and more detailed information on the radioactivity in the coolant. The $^{140}Ba-^{140}La$ and ^{95}Nb activities, which govern the contamination of the surfaces in the loop, are dependent on the run time since the defects were formed in the fuel-pin sheaths in the core; at certain times, the γ rays from these nuclides contributed up to 65% of the dose rate from the pipelines. Drainage of the coolant from the loop then did not reduce the dose rate in the heat-exchanger sections below 100-150 μR/sec. The activity due to ^{60}Co and ^{54}Mn, which are nuclides of corrosion origin, increased on the surfaces during the years of operation of the reactor, but they never contributed more than 10% of the dose rate from the pipelines.

*1 Ci = $3.700 \cdot 10^{10}$ Bq; 1R = $2.58 \cdot 10^{-4}$ Cu/kg; 1 ber = 0.01 J/kg.

When the nuclear power station is operated normally, there is no leak of radioactive gases and aerosols into the working locations, nor are there any sources of surface contamination of the equipment and buildings. Some such contamination occurred during reactor reloading, particularly during removal of the loading tube and effector mechanism for the CPC, which involved modification and servicing of the loading machine. The contamination levels of the surfaces were not more than the equivalent of 4000 β particles per minute per cm^2, which were due to ^{95}Nb, ^{137}Cs, and ^{141}Ce. When equipment was removed from the reactor into the central bay, there were brief episodes of radioactive aerosols, whose concentrations were not more than $1 \cdot 10^{-10}$ Ci/liter (mainly ^{137}Cs).

A coefficient was formulated to characterize the escape of radionuclides from the contaminated surfaces into the atmosphere as aerosols (the ratio of the activity in the air to that at the surface) by reference to measurements, which gave $3 \cdot 10^{-2}$ m^{-1} for ^{137}Cs and ^{134}Cs or $(1-5) \cdot 10^{-4}$ m^{-1} for ^{141}Ce, ^{95}Nb, ^{60}Co, and ^{54}Mn; the high cesium activity in the coolant and the high volatility of the element make it obligatory to use respirators in servicing operations. The surface contamination in the central bay was purely local in character and was readily flushed away.

Personal Exposure during Servicing. We examined the exposure records arising from planned prophylactic servicing after prolonged operation with fill pins that had begun to leak; we found that examination and minor servicing of monitoring and measuring equipments in parts of the first loop involved certain does levels to a comparatively large number of staff (Table 1).

During operations in the heat-exchanger sections for the first loop, the γ-ray doses to the hands were 30-40% higher than those to the body as a whole; the exposure due to β rays was not more than 3% of the total dose. The mean radiation dose per person was 0.3-0.5 ber per year. Not more than 2-3% of the staff received doses of 1.5-5 ber.

We now consider the radiation environment and staff irradiation during one of the major servicing operations, namely replacement of the replacable parts of pumps in the first loop, which are extracted by a special technique using an isolating cover without biological shielding. The cover was supplied with nitrogen to prevent combustion of the sodium on the pump surfaces.

The exposure dose rate from γ rays from the extracted part was 200-300 μR/sec at a distance of 3-5 m. The radioactive aerosol concentration in the building at that time was not more than 10^{-13} Ci/liter. The total working time from start of lifting for the removable part to immersion in the decontamination tank was about 1 h. The total dose to the staff concerned with preparatory operations and removing the part of the pump was 0.7 ber. The use of an isolating plastic-film cover in place of a special shielded container enabled us to remove the part of the pump rapidly and did not lead to contamination of the building or any considerable staff irradiation. The removable part of the pump was placed in a decontamination tank. The exposure dose rate from the pump after removing the remaining sodium and decontamination was reduced to 0.4-5 μR/sec.

Estimates show that replacement of the cables, valve gear, electrical heaters, etc. in the heat-exchanger segments give rise to a collective staff dose of 100-500 ber at the level of contamination of the coolant and surfaces corresponding to prolonged operation with pins with leaking sheaths. Consequently, such operations must be performed after drainage or purification of the coolant, and sometimes after the loop has been decontaminated.

Consequences of Sodium Ignition during Servicing. The radioactivity of aerosols during reloading and servicing operations seldom exceeded $1 \cdot 10^{-11}$ Ci/liter, which represents no hazard if individual protection is used. However, there may be unacceptable effects from the chemical action of sodium oxide on the skin and eye. Also, sodium oxide rapidly becomes caustic soda and sodium carbonate in contact with air, and these materials can corrode construction materials. The most hazardous consequences arise from combustion of the residual film of sodium on the surfaces of removable parts during extraction when there are coolant leaks. The resultant dense clouds of sodium oxide greatly reduce visibility and may hinder the escape of staff from the hazard zone. A concentration of 50 mg/m^3 of sodium combustion products can be tolerated by the respiratory system for only 2.5 min. A rise in concentration from 50 to 100 mg/m^3 irritates the eyes and lungs and interferes with vision.

When the removable part of the pump was being extracted from the BOR-60 with an isolating hood, there was some combustion of the sodium film on account of lack of match between the nitrogen supply to the hood and the lifting of the component. However, the smoke lasted only a short time and the sodium aerosol concentration in the working site was low (the radioactivity of the aerosol was about 10^{-13} Ci/liter, while the sodium concentration was below 1 mg/m^3).

TABLE 2. Nuclide Concentrations in the Air of the Central Bay on Burning of Sodium Film on the Surfaces of Intermediate Heat Exchanger

Nuclide	Activity on surfaces, Ci	Activity in air, Ci	Conc., Ci/m³		
			$t=0$ min*	$t=15$ min	$t=60$ min
^{22}Na	$3\cdot10^{-2}$	$4{,}5\cdot10^{-3}$	$1{,}7\cdot10^{-7}$	$5{,}3\cdot10^{-8}$	$6\cdot10^{-9}$
^{110m}Ag	$1{,}2\cdot10^{-3}$	$1{,}8\cdot10^{-4}$	$7\cdot10^{-8}$	$2{,}2\cdot10^{-9}$	$3\cdot10^{-10}$
^{137}Cs	1,1	0,66	$2{,}5\cdot10^{-5}$	$7{,}8\cdot10^{-6}$	$9\cdot10^{-7}$
^{134}Cs	0,1	$6\cdot10^{-2}$	$2{,}3\cdot10^{-6}$	$7{,}1\cdot10^{-7}$	$8\cdot10^{-8}$

*t is the time after burning.

As a limiting case one can consider the combustion of the residual sodium film on the very extensive surface of the heat exchanger. We assumed that the surfaces of the removable parts bore a sodium film about 0.2 mm thick. This corresponds to about 50 kg of sodium for the BOR-60 heat exchanger. We do not propose to consider all the possible emergencies and envisage the case where the inert-gas supply to the isolating cover is interrupted for some reason. The sodium film on the surfaces of the heat exchanger burns up very rapidly (in about 18 sec). The maximum sodium concentration in the air may rise to 290 mg/m³. Calculations were performed on the sodium aerosol concentration and the radioactivity due to the main nuclides in the air of the central bay of the BOR-60 for this situation on the assumption of instantaneous mixing with the ventilation disconnected, using the maximum observed values for the nuclide activities in the coolant (Table 2). The coefficients representing transition of the nuclides into the aerosol in the combustion of sodium were taken from [2]. The nuclide activities and the sodium concentration in the air of the central bay would greatly exceed the permissible values. It would be impossible to enter this space, and the building would have to be evacuated temporarily. If the ventilation was not working, about 80% of the combustion products would settle on the floor, 18% on the walls, and 2% on the ceiling. All the surfaces would be contaminated and require decontamination.

Experience with the BOR-60 thus indicates the following positive factors occurring in sodium-cooled systems:

1) retention of a large proportion of the radionuclides escaping from the fuel pins;

2) low activity in nuclides of corrosion origin in the coolant and in deposits;

3) reliable operation of the main units and equipments;

4) prolonged perfect sealing in the first loop at high sodium temperatures;

5) the possibility of cutting pipelines containing frozen sodium;

6) low surface contamination of buildings and low aerosol activities; and

7) low radioactive gas releases from the nuclear power station, with consequently no effect on environmental radioactivity.

However, there still are some problems to be envisaged in the design and operation of sodium-cooled reactors, which arise mainly during servicing operations:

1) the high level of radioactivity in the coolant on prolonged operation with leaking fuel rods, which requires efficient means of purifying the coolant;

2) ignition of the residual sodium film on the surfaces of removable units at elevated temperatures, where protective hoods with inert atmospheres must be used;

3) production of oxides in the loop on opening, which tend to be deposited at the points of installation of removable parts. It is necessary to maintain an inert atmosphere at such a point throughout servicing;

4) the possibility of sodium leakage, which requires reliable systems for detecting and suppressing combustion in buildings containing the loops; and

5) the possibility that aerosols containing sodium combustion products will enter the buildings if the sodium burns. It is then necessary to protect the organs of respiration and the eyes from chemical effects of the sodium.

LITERATURE CITED

1. V. D. Kizin et al., At. Energ., 44, No. 6, 492 (1978).
2. Yu. V. Chechetkin, I. G. Kobzar', and G. I. Poznyak, At. Energ., 35, No. 6, 401 (1973).

SEMIEMPIRICAL METHOD OF CALCULATING ISOTOPIC COMPOSITION OF URANIUM AND PLUTONIUM IN IRRADIATED FUEL FROM A WATER-COOLED – WATER-MODERATED REACTOR

B. A. Bibichev, A. V. Lovtsyus, V. P. Maiorov, M. A. Razuraeva, A. V. Stepanov, and P. I. Fedotov

UDC 621.039.524.4

The method of fission-product γ spectrometry is widely used to measure the burnup of power-reactor fuel. However, such measurements do not contain direct information on the concentration of heavy nuclides in the fuel. Broader prospects for the method of fission-product γ spectrometry may be secured by combining γ-spectrometric measurements with theoretical calculations [1].

The concentration of fission products in irradiated fuel depends on the initial isotopic composition of the fuel, on the conditions of irradiation (the duration of each irradiation cycle and the mean relative thermal power of the given fuel element in each irradiation cycle), and also on the neutron-flux parameters and their variation in the course of irradiation of the given fuel element. This allows the neutron-flux parameters in the course of fuel irradiation to be determined and the concentration of heavy nuclides to be calculated from the known initial fuel composition and the measured concentration of certain fission products, for known irradiation conditions.

The change in isotopic composition of the fuel in the course of irradiation is described by the following system of equations

$$dN_i(t)/dt = \Phi_{th}\hat{\sigma}^c_{i-1}N_{i-1}(t) - (\Phi_{th}\hat{\sigma}^a_i + \lambda_i)N_i(t); \quad (1)$$

$$dN_j(t)/dt = \Phi_{th}\sum_i Y_{ji}\hat{\sigma}^f_i N_i(t) + \Phi_{th}\hat{\sigma}^c_{j-1}N_{j-1}(t) - (\Phi_{th}\hat{\sigma}^a_j + \lambda_j)N_j(t), \quad (2)$$

where $N_i(t)$ is the concentration of the i-th heavy nuclide; $N_j(t)$, concentration of the j-th fission product; Φ_{th}, thermal-neutron flux density; $\hat{\sigma}^f_i$, effective cross section of the i-th nuclide; Y_{ji}, yield of the j-th fission product in the fission of the i-th heavy nuclide; $\hat{\sigma}^c_{i-1}$, effective cross section of the (n, γ) reaction at the (i – 1)-th nuclide; $\hat{\sigma}^a_i$, effective absorption cross section for the i-th nuclide; λ_i, decay constants of the i-th nuclide.

In solving Eqs. (1) and (2), the neutron spectrum is divided into two groups: thermal and superthermal. In addition, in calculating the contribution of ^{238}U to the formation of fission products, the fission neutron spectrum is also considered. The effective cross section for all nuclides except ^{238}U is determined from the formula

$$\hat{\sigma} = \sigma_{th} + \alpha I, \quad (3)$$

where σ_{th} is the thermal cross section; I, resonance integral; α, hardness of the neutron spectrum.

For ^{238}U, the product $\sigma^f_{238U} \cdot r$ is taken as $\hat{\sigma}^f_{238U}$, where σ^f_{238U} is the ^{238}U fission cross section averaged over the fission neutron spectrum; r is the ratio of the fission-neutron flux density to Φ_{th}. In the calculations, use is made of the dependence of the variation of Φ_{th} and α on the concentration of fissile nuclides from [2]. On passing from the n-th irradiation cycle, with relative thermal power R_n, to the (n+1)-th cycle, Φ_{th} is multiplied by R_{n+1}/R_n.

There are three free parameters in Eqs. (1) and (2): $\Phi_{th}(0)$ and $\alpha(0)$, which are the values of Φ_{th} and α at the beginning of irradiation, and also r. In [1] it was noted that r has a weak influence on the fission-product concentration, and therefore in the present calculations the value of r is taken from theoretical calculations for a water-cooled–water-moderated reactor [3]. Having measured concentrations of ^{137}Cs and ^{134}Cs, a

Translated from Atomnaya Énergiya, Vol. 48, No. 5, pp. 294-297, May, 1980. Original article submitted October 30, 1978; revision submitted October 14, 1979.

0038-531X/80/4805-0294$07.50

TABLE 1. Uranium-Isotope Concentrations in Fuel-Element Samples, 10^{18} atom/g U

Sample No.	Fuel-element No.	Position over fuel-element height, mm	Calculated burnup, kg/ton U	^{235}U		^{236}U	
				expt.	calc.	expt.	calc.
1	98	125	6,2	58,5	60,1 (+2,7) *	2,87	3,09 (+7,7)
2	76	2125	10,7	49,1	49,9 (+1,6)	5,02	4,86 (—3,2)
3	4	375	12,8	44,9	45,3 (+0,9)	5,30	5,59 (+5,5)
4	4	1125	14,6	41,6	41,8 (+0,5)	5,89	6,14 (+4,2)
5	107	50	15,0	40,0	41,0 (+2,5)	6,22	6,25 (+0,5)
6	87	375	28,5	20,8	21,3 (+2,4)	9,38	9,04 (—3,6)
7	76	375	28,9	21,1	21,4 (+1,4)	9,29	9,04 (—2,7)
8	68	1625	33,7	15,8	16,0 (+1,3)	9,65	9,58 (—0,7)

*The figure in brackets is the discrepancy between the calculated and experimental results, %.

specified irradiation program, and the initial isotopic concentration of the fuel, the values $\Phi_{th}(0)$ and $\alpha(0)$ are found by fitting the calculated values N_{137} and N_{134} $(N_{137})^2$ to measured values. The values of N_{137} and $N_{134}/(N_{137})^2$ may expediently be used for finding the parameters $\Phi_{th}(0)$ and $\alpha(0)$, since each value strongly depends on only one of the parameters: N_{137} on $\Phi_{th}(0)$ and $N_{134}/(N_{137})^2$ on $\alpha(0)$. For example, for a fuel burnup of around 20 kg/ton on U

$$\frac{\delta \ln N_{137}}{\delta \ln \Phi_{th}(0)} = 1.0; \quad \frac{\delta \ln N_{137}}{\delta \ln \alpha(0)} = 0.18;$$

$$\frac{\delta \ln [N_{134}/(N_{137})^2]}{\delta \ln \Phi_{th}(0)} = 0.05; \quad \frac{\delta \ln [N_{134}/(N_{137})^2]}{\delta \ln \alpha(0)} = 0.60.$$

Numerical integration is used to solve Eqs. (1) and (2), with an irradiation time step of 1 day. The values of $\Phi_{th}(0)$ and $\alpha(0)$ are found by the gradient method. The following nuclides are included in the system of equations: ^{235}U, ^{236}U, ^{238}U, ^{239}Pu, ^{240}Pu, ^{241}Pu, ^{242}Pu, ^{137}Cs, ^{133}Cs, ^{134}Cs, ^{144}Ce, ^{106}Ru. Note that the accuracy obtained in calculating the burnup and isotopic composition of the fuel within the framework of the given method depends significantly on the choice of nuclear data: σ_{th}, I, and Y. In the present calculations, values of σ_{th} and I for heavy nuclides calculated using the ROR program [3] are taken as the basis. However, these values change as burnup proceeds, and so averaged values of σ_{th} and I for burnup from 0 to 35 kg/ton on U are used. The value of Y is taken from [4].

The error in calculating the concentration of uranium and plutonium isotopes was verified experimentally on fuel-element samples by destructive methods. To this end, eight samples were cut from fuel elements of two cassettes of the VVÉR-365 reactor, with an initial ^{235}U enrichment of 3% and with various irradiation histories. Samples 1-4 were cut from DR-3 No. 80 cassette, with a mean burnup of 12.7 kg/ton on U, and the remainder from cassette RP-3 No. 223 with a mean burnup of 30.2 kg/ton on U. The numbers of the fuel elements and the positions over the height of the fuel element at which the samples were cut are shown in Table 1 (the total fuel-element height is 2500 mm). The samples were dissolved, and the concentrations of ^{137}Cs and ^{134}Cs and also the concentrations of uranium and plutonium isotopes were measured in aliquots of the solutions. The ^{137}Cs and ^{134}Cs solutions were measured by a γ-spectrometric method. The uranium concentration was determined by potentiometric titration using the Davis and Gray method, and the plutonium concentration by the method of isotopic dilution with α-spectrometric termination and using ^{238}Pu as isotopic label. The isotopic composition of uranium and plutonium was determined using a mass-spectrometric method (Tables 1 and 2). The error in measuring the ^{137}Cs and ^{134}Cs concentrations in the samples was, on average, 1.5%; for ^{235}U, 0.8%; for ^{236}U, 1.3%; for ^{239}Pu, 0.8%; for ^{240}Pu, 1.2%; for ^{241}Pu, 1.5%; and for ^{242}Pu, 1.8%.

Note that the measured concentrations of uranium and plutonium isotopes in sample 8 were used in correcting σ_{th}^f and σ_{th}^c for ^{235}U and ^{239}Pu; I^c for ^{240}Pu and ^{133}Cs; and also for correcting r. The values of these quantities were chosen in accordance with the condition of best agreement between the calculated and experimental values for sample 8. For the remaining samples these quantities were chosen in the same way as for sample 8. The important point in the correction of σ_{th} and I is the choice of I_{f33}^c, since the rather stronger resonances of the reactions (n, γ) on ^{133}Cs and ^{238}U partially overlap, which leads to I_{133}^c blocking. Table 3 shows the values of σ_{th} and I for uranium, plutonium, and cesium nuclides used in the calculations.

The greatest discrepancies between the calculated and measured concentrations for ^{235}U and ^{236}U (see Table 1) are 2.7% and 7.7%, respectively. The difference in calculated and measured concentrations for plutonium isotopes is larger (see Table 2) than for uranium isotopes. The greatest discrepancy for ^{239}Pu, observed in end samples, may be explained in that the thermal-power distribution over the irradiation period may differ

TABLE 2. Plutonium-Isotope Concentrations in Samples

Sample No.	^{239}Pu, 10^{18} atom/g U		^{240}Pu, 10^{18} atom/g U		^{241}Pu, 10^{17} atom/g U		^{242}Pu, 10^{16} atom/g U		Pu, 10^{18} atom/g U	
	expt.	calc.	expt.	calc.	expt.	calc.	expt.	calc.	expt.	calc.
1	6,76	7,28 (+7,7) *	0,75	0,73 (—2,7)	2,08	1,25 (—40)	1,16	0,60 (—48)	7,73	8,14 (+5,3)
2	10,3	10,4 (+1,0)	1,76	1,72 (—2,3)	7,53	4,83 (—36)	6,94	4,29 (—38)	12,9	12,6 (—2,3)
3	10,8	11,0 (+1,9)	2,20	2,20 (0)	9,98	7,00 (—30)	12,2	7,77 (—36)	14,1	14,0 (—0,7)
4	11,3	11,2 (—0,9)	2,54	2,59 (+2,0)	11,9	8,85 (—26)	17,4	11,6 (—33)	15,2	14,8 (—2,6)
5	9,26	10,9 (+18)	2,27	2,65 (+17)	8,74	8,74 (0)	14,1	12,1 (—14)	12,5	14,5 (+16)
6	13,1	13,4 (+2,3)	5,02	5,19 (+3,4)	27,6	29,0 (+5,1)	96,2	94,0 (—2,3)	21,8	22,4 (+2,8)
8	13,1	13,2 (+0,8)	5,64	5,77 (+2,3)	31,8	34,7 (+9,1)	140	146 (—4,3)	23,3	23,9 (+2,6)

*The figure in brackets is the discrepancy between the calculated and experimental results, %.

TABLE 3. Thermal Cross Sections and Effective Resonance Integrals Used in Calculations

Nuclide	σ^f_{th}	I^f	σ^c_{th}	I^c	Nuclide	σ^f_{th}	I^f	σ^c_{th}	I^c
^{235}U	307	292	58,0	119	^{241}Pu	744	459	267	331
^{236}U	—	—	3,73	350	^{242}Pu	—	—	9,91	1210
^{238}U	0,349	0,349	1,45	23,5	^{133}Cs	—	—	16,6	300
^{239}Pu	672	286	374	180	^{134}Cs	—	—	80,2	—
^{240}Pu	—	—	173	3400	^{137}Cs	—	—	0,063	—

for end and central sections of the fuel element. In addition, I^c_{238} may also differ somewhat for end and central sections of the fuel element. The considerable discrepancy between the calculated and experimental data for the ^{241}Pu and ^{242}Pu concentrations in samples with small fuel burnup is related to the strong dependence of I^c_{240} on the fuel burnup. Since the value of I^c_{240} was chosen for sample 8 with large fuel burnup, it is not optimal for samples with small burnup.

To estimate the contribution of the error in measuring N_{137} and N_{134} to the total error in determining the concentrations of uranium and plutonium isotopes, the change in isotopic composition of uranium and plutonium in samples 4 and 8 when N_{137} and N_{134} change by 1.5% was calculated. The change in the concentrations of uranium and plutonium isotopes in sample 4 was as follows: ^{235}U by 1.1%; ^{236}U by 1.0%; ^{239}Pu by 1.2%; ^{240}Pu by 2%; ^{241}Pu by 0.003%; ^{242}Pu by 2.4%. In sample 8, the corresponding figures were as follows: ^{235}U by 4.3%; ^{236}U by 0.7%; ^{239}Pu by 3.5%; ^{240}Pu by 1.5%; ^{241}Pu by 1.7%; and ^{242}Pu by 2.5%. It is evident from Tables 1 and 2 that, except for the ^{235}U concentration, the discrepancy between the calculated and measured concentrations of uranium and plutonium isotopes in all the samples, taken as an average over the sample, considerably exceeds the error due to N_{137} and N_{134}.

Note, in conclusion, that experimental and calculated data for a considerably larger number of samples are necessary for reliable estimation of the error of the method. In addition, it is also necessary to verify the correction of the most important effective cross sections used in the calculations over the whole set of experimental data on the isotopic composition of the fuel in the fuel-element samples. After correcting the effective cross sections, the method may be used for nondestructive measurements of the content of uranium and plutonium isotopes in the fuel elements and cassettes of water-cooled – water-moderated reactors. The ^{137}Cs and ^{134}Cs concentrations in intact fuel elements and cassettes may be measured γ-spectrometrically.

LITERATURE CITED

1. O. Eder and M. Lammer, in: Proceedings of IAEA Symposium on Nuclear Data in Science and Technology, Vol. 1, Vienna (1974), p. 233.
2. T. S. Zaritskaya, A. K. Kruglov, and A. P. Rudik, At. Energ., 41, No. 5, 321 (1976).
3. V. D. Sidorenko and E. D. Belyaeva, Preprint IAÉ-1171 (1966).
4. M. Meek and B. Rider, Compilation of Fission Product Yields, Vallecitos Nuclear Center, NEDO-12154-1 (1974).

EFFECTS OF TRANSDUCER LOCATION ON THE AZIMUTHAL AND RADIAL STABILIZATION IN A REACTOR

B. Z. Torlin

UDC 621.039.56

A form factor μ analogous to the Randall form factor [1] has been introduced for a reactor with N fast-acting astatic regulators* [2, 3] as an eigenvalue for the system

$$\begin{cases} \Delta\varphi + B_0^2\varphi + \Phi_0 \sum_{j=1}^{N} F_j s_j + \mu\varphi = 0; & \text{(1a)} \\ \int_V K_j \varphi \, dV = 0, \quad j = 1, 2, \ldots, N, & \text{(1b)} \end{cases}$$

where B_0 and Φ_0 are the unperturbed material parameter and the neutron-flux distribution, while F_j describes the spatial localization of the reactivity s_j introduced by control rod j and K_j is the weighting function in the formation of the transducer signals for control of this rod. The spatial stability of a reactor for slow processes is the greater the higher the minimum value μ_{min} [1-6]. Various control systems influence μ_{min}, and a study has been made [3] of the effects of various arrangements of the transducers and control rods for a height problem. The same method has been applied [7] to the effects of a central automatic regulator on the spatial stability for the cylindrical case. Such a regulator cannot correct the azimuthal distortion in the neutron distribution, and this requires eccentrically placed control rods. The BASIRA program has been used with a BÉSM-6 in detailed analysis of the stability of such a system with a complicated distribution of the parameters; however, the situation can be analyzed qualitatively without resort to a computer. We consider a homogeneous cylindrical reactor of unit radius with zero boundary conditions ($B_0 = 2.405$).

If the thin control rods are placed at points with coordinates (R_j, ϑ_j), j = 1, 2, ..., N, then the solution to (1a) will [8] be the sum

$$\varphi(r, \theta) = \sum_{j=1}^{N} a_j f_j(r, \theta), \qquad (2)$$

where

$$f_j(r, \theta) = N_0(Br_j) - \sum_{n=-\infty}^{\infty} J_n(BR_j) J_n(Br) \frac{N_n(B)}{J_n(B)} \cos n(\theta - \vartheta_j). \qquad (2a)$$

Here J_n and N_n are Bessel and Neumann functions, respectively, of order n, $B^2 = B_0^2 + \mu$, and r_j is the distance from control rod j to the point with coordinates (r, θ).

The relation between the a_j and the eigenvalues B can be derived from (1b); it has been shown [2, 3] that conditions (1b) become $\varphi(r_j, \theta_j) = 0$; j = 1, 2, ..., N ($r_j$ and θ_j are the polar coordinates of transducer j) if each regulator is designed to maintain a given neutron flux at the position of its transducer.

We consider six control rods symmetrically disposed in azimuth at a radius ρ and six transducers at radius r_g on the same radii as the control rods. We put $f_1 = f_1(r_g, 0)$, $f_2 = f_1(r_g, \pi/3)$, $f_3 = f_1(r_g, 2\pi/3)$, and $f_4 = f_1(r_g, \pi)$, and instead of (1b) we have $\hat{A}\mathbf{a} = 0$, where $\mathbf{a}$ is a vector with components a_j and matrix $\hat{A}$ takes the form

*It is assumed that the regulators have fast-process stability.

Translated from Atomnaya Énergiya, Vol. 48, No. 5, pp. 297-300, May, 1980. Original article submitted July 2, 1979.

0038-531X/80/4805-0297$07.50

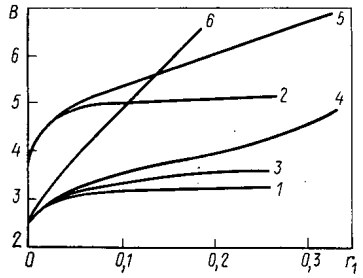

Fig. 1. B as a function of the distance between control rod and transducer for the first roots of: 1) (3a); 2) (3b); 3) (5); 4) (6a); 5) (6b); 6) (7).

$$\hat{A}=\begin{Vmatrix} b_1 & b_2 & b_3 & b_4 & b_3 & b_2 \\ b_2 & b_1 & b_2 & b_3 & b_4 & b_3 \\ b_3 & b_2 & b_1 & b_2 & b_3 & b_4 \\ b_4 & b_3 & b_2 & b_1 & b_2 & b_3 \\ b_3 & b_4 & b_3 & b_2 & b_1 & b_2 \\ b_2 & b_3 & b_4 & b_3 & b_2 & b_1 \end{Vmatrix},$$

where $b_l = f_l$.

Matrix $\hat{A}$ belongs to the circulant class [9]. We use a property of such matrices to convert it to diagonal form and get the following four transcendental equations for B:

$$\begin{aligned} &b_1 + 2(b_2 + b_3) + b_4 = 0; \\ &b_1 + b_2 - b_3 - b_4 = 0; \\ &b_1 - b_2 - b_3 + b_4 = 0; \\ &b_1 - 2(b_2 - b_3) - b_4 = 0. \end{aligned} \tag{3}$$

We substitute the corresponding expressions for the b_l and get after elementary steps

$$N_0(Br_1) + 2N_0(Br_2) + 2N_0(Br_3) + N_0(Br_4) - 6\sum_{n=-\infty}^{\infty} U_{|6n|} = 0; \tag{3a}$$

$$N_0(Br_1) + N_0(Br_2) - N_0(Br_3) - N_0(Br_4) - 6\sum_{n=-\infty}^{\infty} U_{|1+6n|} = 0; \tag{3b}$$

$$N_0(Br_1) - N_0(Br_2) - N_0(Br_3) + N_0(Br_4) - 6\sum_{n=-\infty}^{\infty} U_{|2+6n|} = 0; \tag{3c}$$

$$N_0(Br_1) - 2N_0(Br_2) + 2N_0(Br_3) - N_0(Br_4) - 6\sum_{n=-\infty}^{\infty} U_{|3+6n|} = 0, \tag{3d}$$

where $U_k = J_k(B\rho)\, J_k(Br_g)\, \frac{N_k(B)}{J_k(B)}$, r_1 is the distance from the first control rod to transducer i, and $r_1 = |r_g - \rho|$.

Apart from the sum of (2), the solution to (1) for this example is provided by functions of the form $J_{3n}(Br) \sin 3n\theta$ for those values of B for which

$$J_{3n}(B) = 0, \quad n = 1, 2, \ldots \tag{3e}$$

Therefore, the minimum eigenvalue $B^2_{min} = B^2_0 + \mu_{min}$ should be selected from the complete set of roots of these equations.

The simplest of the equations is (3e). The least of the set of values defined by this is B = 6.380. This is not dependent on ρ or on r_g, so such a system in principle cannot provide stability in the reactor if the latter is unstable on more than two azimuthal modes in the absence of the regulators. Although the other equations are complicated in form, they can be analyzed quite simply, and the least roots can be estimated even without a computer. Equation (3a) is related to the scope for radial stabilization (including the fundamental), while (3b), (3c), and (3d) are related mainly to the scope for eliminating dipole, quadrupole, and higher-order azimuthal perturbations in the neutron distribution. These considerations alone indicate that one should seek the minimum eigenvalue primarily alongst the roots of (3a). The same conclusion is reached by considering the

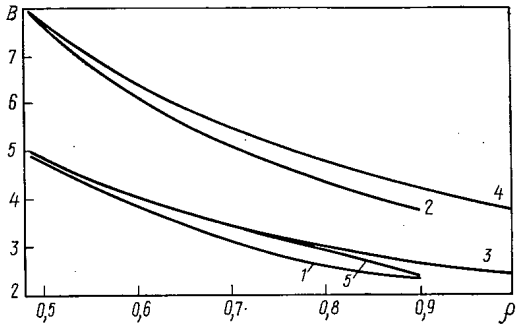

Fig. 2. Dependence of B on control rod placing: 1 and 2) first roots of (3a) and (3b) respectively; 3 and 4) first root of (4) for $l = 0$ and $l = 1$; 5) first root of (5).

limiting case $r_1 \to 0$. Then $N_0(Br_1) \to -\infty$. The structure of the expressions for U_k shows that the roots of all equations are then zeros of Bessel functions. Therefore, the minimum roots of (3a)-(3d) will be correspondingly 2.405, 3.832, 5.136, and 6.380. The same technique can be applied to the performance of eccentrically disposed control rods [8] for r_1 small to demonstrate readily that these values of B increase with r_1. It is difficult to demonstrate analytically that there is monotone growth of these throughout the entire range in r_1, but this is confirmed by numerical calculations, and it is demonstrated also below analytically for large r_1. Therefore, one should not seek the B_{min} among the roots of (3d), and this equation can be eliminated from the subsequent analysis. If only the first azimuthal mode is unstable, we can also eliminate (3c) from consideration. Very often, the minimum eigenvalue is found from the equation related to radial stabilization, i.e., (3a) in this example.

An important feature of the sums appearing in (3) is the rapid convergence; as a rule, it is sufficient to take the term in the sum with the least subscript in order to determine the least of the roots. These are correspondingly U_0, U_1, and U_2 for (3a), (3b), and (3c). Figure 1 shows the r_1 dependence of the least roots of (3a) and (3b) for $\rho = 2/3$. The solution was obtained graphically. Incorporation of the second term in the sum results in a correction to the root not exceeding 3%. Figure 1 shows that the stability of the system is limited by the least root of (3a), i.e., the fundamental mode is actually stable. Further, the stability is increased within rather narrow limits as the transducer recedes from the control rod to the edge of the core. However, such displacement of the transducer has a much greater effect on the azimuthal stability (curve 2). Figure 2 shows the effects of control-rod position on the least roots of (3a) and (3b) for $r_g = 0.9$. It is clear that the stability can be varied widely via the separation between the control rod and the transducer. Stability on the fundamental is the limiting factor throughout the range.

Curves 3 and 4 of Fig. 2 are described by $B = 2.405/\rho$ and $B = 3.832/\rho$; Fig. 2 shows that the divergence between curves 1 and 3 decreases as the distance between the transducer and the control rod is increased, and the same applies to curve 2 and 4. This is explained as follows. The addition theorem [10] for Neumann functions enables us to transform (3) into

$$\sum_{n=-\infty}^{\infty} V_{|l+6n|} = 0, \qquad l = 0, 1, 2, 3, \tag{4}$$

where

$$V_k = \begin{cases} J_k(B\rho)\left[N_k(Br_g) - J_k(Br_g)\dfrac{N_k(B)}{J_k(B)}\right] \\ \qquad\qquad \text{for} \quad \rho < r_g; \\ J_k(Br_g)\left[N_k(B\rho) - J_k(B\rho)\dfrac{N_k(B)}{J_k(B)}\right] \\ \qquad\qquad \text{for} \quad \rho > r_g. \end{cases}$$

If the terms of (4) are arranged in order of increasing subscript, then the sums will converge the more rapidly the greater the difference between ρ and r_g. If this difference is sufficiently large, we can restrict ourselves to the following equations in estimating the least roots:

$$V_l \approx 0, \quad l = 0, 1, 2. \tag{4a}$$

These equations have previously been published [7], where it was pointed out that the ρ dependence of the least

[illegible] with dashed line for it shown in Fig. 2 (curves 3 and 4) for $l = 0$ and $l = 1$ for r_g sufficiently large. Figure 2 shows that curves 1 and 3 almost coincide for $r_g = 0.9$ and $\rho \lesssim 0.5$, and the same applies to curves 2 and 4, i.e., the terms other than the one with the least subscript in (4) are unimportant.

In this example, the number of transducers was equal to the number of control rods; if there are more transducers than control rods, one has redundant information, which can be utilized in the best fashion. For example, one can specify minimality in the square of the deviations $\sum_{i=1}^{M} \varphi_i^2$ of the neutron distribution from the steady-state distribution, which means that (1b) becomes

$$\sum_{i=1}^{M} \varphi_i \psi_{ij} = 0, \quad j = 1, 2, \ldots, N,$$

where M is the number of transducers and φ_i and ψ_{ij} are, respectively, the deviation of the neutron distribution from the stationary value and the influence function of control rod j at sensor i.

If the system of the previous example is supplemented with six sensors symmetrically distributed in azimuthal angle ϑ at radius r_g, then (1b) will still take the form $\tilde{A}a = 0$. On the other hand, the matrix elements will now have a more complicated dependence via f_l and the influence functions of the rods:

$$b_1 = f_1\psi_1 + 2f_2\psi_2 + 2f_3\psi_3 + 2f_4\psi_4 + 2f_5\psi_5 + 2f_6\psi_6 + f_7\psi_7;$$

$$b_2 = f_3\psi_1 + (f_2+f_4)\,\psi_2 + (f_1+f_5)\,\psi_3 + (f_2+f_6)\,\psi_4 + (f_3+f_7)\,\psi_5 + (f_4+f_6)\,\psi_6 + f_5\psi_7;$$

$$b_3 = f_5\psi_1 + (f_4+f_6)\,\psi_2 + (f_3+f_7)\,\psi_3 + (f_2+f_6)\,\psi_4 + (f_1+f_5)\,\psi_5 + (f_2+f_4)\,\psi_6 + f_3\psi_7;$$

$$b_4 = f_7\psi_1 + 2f_6\psi_2 + 2f_5\psi_3 + 2f_4\psi_4 + 2f_3\psi_5 + 2f_2\psi_6 + f_1\psi_7,$$

where

$$f_l = f_1(r_g, \vartheta_l); \quad \vartheta_l = \pi/6\,(l-1); \quad \psi_l = \psi_{l,1}.$$

However, diagonalization of $\hat{A}$ results in the same four equations of (3). Substitution of the appropriate expressions in place of b_l causes only the first to differ from (3a). The other equations are the same as (3b)-(3d). Therefore, the azimuthal stability of a system with twelve sensors is the same as that of one with six. Instead of (3a) we get

$$N_0(Br_1) + 2\sum_{l=2}^{6} N_0(Br_l) + N_0(Br_7) - 12\sum_{n=-\infty}^{\infty} U_{|12n|} = 0. \tag{5}$$

Figures 1 and 2 show the r_1 dependence of the least root of this equation; the reactor stability is still limited by the behavior of the fundamental, and the stability for a system with twelve sensors is shown by curve 3 of Fig. 1 and curve 5 of Fig. 2 to be only slightly higher than that for a system with six transducers.

The situation is substantially altered if a sensor at the center of the active zone supplements the six or twelve sensors uniformly disposed at radius r_g. In that case the least root for the fundamental is even higher than 6.38. The reactor stability is governed by the least root of (3b), since the central sensor does not affect the form of (3b)-(3d). Therefore, the central sensor greatly increases the stability.

In conclusion we consider the situation characteristic of a reactor controlled by local automatic regulators. We first consider six control rods placed as in the previous examples, namely uniformly in angle ϑ at radius ρ. The control sensors are placed around each control rod at distances r_1. The minimum eigenvalues for such a system are to be found in the roots of the equations

$$N_0(Br_1) + J_0(Br_1)\,[2N_0(B\rho_2) + 2N_0(B\rho_3) + N_0(B\rho_4) - 6\sum_{n=-\infty}^{\infty} v_{|6n|}] = 0; \tag{6a}$$

$$N_0(Br_1) + J_0(Br_1)\,[N_0(B\rho_2) - N_0(B\rho_3) - N_0(B\rho_4) - 6\sum_{n=-\infty}^{\infty} v_{|1+6n|}] = 0, \tag{6b}$$

which are related primarily to the fundamental and dipole modes respectively. Here ρ_i is the distance between the first control rod and control rod i, while $v_l = J_l^2(B\rho)\,\frac{N_l(B)}{J_l(B)}$. Figure 1 shows the r_1 dependence of the least root of (6a) and (6b) for $\rho = 2/3$ (curves 4 and 5, respectively).

In the case of these local automatic regulators, the dependence of B on the distance between the sensors and the control rods is more pronounced than that in all previous examples. One can provide stability of the reactor within wider limits by increasing the distance between the sensor and the control rod. However, six control rods do not allow us to raise B_{min} above 4.8 (here $r_1 = 1/3$). The limiting mode is again the fundamental one. The stability can be improved substantially if a further control rod surrounded by sensors at radius r_0 is placed at the center of the reactor. Clearly, this local control does not influence the azimuthal stability, and (6b) remains unchanged. The equation (6a) is replaced by a more complicated one:

$$\left\{N_0(Br_1)+J_0(Br_1)\left[2N_0(B\rho_2)+2N_0(B\rho_3)+N_0(B\rho_4)-6\sum_{n=-\infty}^{\infty}U_{|6n|}\right]\right\}\left[N_0(Br_0)-\right. \tag{7}$$

$$\left.-J_0(Br_0)\frac{N_0(B)}{J_0(B)}\right]=6J_0(Br_0)J_0(Br_1)\left[N_0(B\rho)-J_0(B\rho)\frac{N_0(B)}{J_0(B)}\right]^2.$$

Curve 6 of Fig. 1 shows the r_1 dependence of the least root of this equation for $r_0 = r_1$ and $\rho = 2/3$.

The stability is determined by the root of (7), i.e., by the fundamental, when the sensors for the local automatic controls are arranged around the control rods at distances of less than 0.14 of the radius of the reactor. If the sensors are further from the control rods, the dipole mode becomes the limiting one (curve 5). Then $B_{min} = 6.38$ when the sensors are at a distance of 0.26 of the radius of the reactor from the control rods, and any further increase in the distance does not improve the stability. In the case of the RBMK-1000 reactor, this corresponds to about six steps in the lattice. A system of seven local automatic controls with this disposition of the transducers provides stability in a reactor that on Randall's criterion would be unstable on two azimuthal modes and one radial one. The sensors arranged around the control rods at distances of not less than three steps in the lattice can provide stability in a reactor that would be unstable on the first azimuthal harmonic without the local automatic controls.

All these effects of the transducer disposition on the stability have been confirmed by calculations via the BASIRA program. More details of this will be given in a forthcoming paper.

I am indebted to A. D. Galanin, Ya. V. Shevelev, A. M. Afanas'ev, I. B. Basina, B. B. Bergel'son, and others for interest in this work and discussion of the results, and to E. F. Sabaev and I. S. Postnikov for directing attention to the properties of circulant matrices.

LITERATURE CITED

1. D. Randall and D. John, Nucleonics, 16, 82 (1958).
2. A. Hitchcock, Nuclear Reactor Stability [Russian translation], Gosatomizdat, Moscow (1963).
3. A. M. Afanas'ev and B. Z. Torlin, At. Energ., 43, No. 4, 243 (1977).
4. I. Ya. Emel'yanov, P. A. Gavrilov, and B. N. Seliverstov, Control and Safety in Nuclear Power Reactors [in Russian], Atomizdat, Moscow (1975).
5. A. M. Afanas'ev and B. Z. Torlin, in: Nuclear Science and Technology, Dynamics of Nuclear Control Systems [in Russian], Issue 2(6), Izd. TsNIIatominform, Moscow (1974), p. 91.
6. I. S. Postnikov, ibid., Issue 1, 5 (1971).
7. B. Z. Torlin, At. Energ., 54, No. 6, 457 (1978).
8. A. D. Galanin, Theory of Thermal-Neutron Nuclear Reactors [in Russian], Atomizdat, Moscow (1959).
9. O. S. Sobolev, One-Loop Coupled Control Systems [in Russian], Énergiya, Moscow (1973).
10. I. S. Gradshtein and I. M. Ryzhik, Tables of Integrals, Series, and Products, Academic Press (1966).

EFFECTS OF NEUTRON-DISTRIBUTION PATTERN ON THE STABILITY OF A POWER REACTOR

I. Ya. Emel'yanov, L. N. Podlazov, A. N. Aleksakov, and V. M. Panin

UDC 621.039.512

The energy-production pattern alters during the operation of a power reactor because of change in the isotope composition of the fuel and because of displacements of the control rods, and this may have a marked effect on the stability.

It is important to establish how changes in the configuration reduce the stability, and if possible to avoid the development of such changes. It has been shown [1] that there is a loss of stability in a cylindrical reactor with a plateau in the center if the size of the latter increases. The real changes do not amount only to change in the size of the plateau, so the stability analysis must be performed for more complex configurations.

Here we present a method of calculating the stability in the energy production pattern for any stationary neutron-flux distribution $\Phi_0(r)$ together with tables of parameter values that can be used to determine the instability development period.

Formulation. A one-group equation in the diffusion approximation is used in a cylindrical coordinate system to describe the neutron balance. Relatively slow processes are envisaged, where one can neglect the delayed neutrons, and where the neutron multiplication factor is a function of the reactor power and the moderator temperature, with due allowance for the instantaneous power feedback due to the fuel temperature and steam content. We assume also that there is hydraulic profiling of the coolant flow in the core. A first-order differential equation for the moderator reactivity is employed. We then assume that the variables can be separated and average all changes in the parameters with respect to the square of the neutron flux to get the equations for the reactor dynamics in terms of deviations as

$$\begin{cases} M^2\left[\frac{1}{R}\frac{\partial}{\partial R}\left(R\frac{\partial\varphi}{\partial R}\right)+\frac{1}{R^2}\frac{\partial^2\varphi}{\partial\theta^2}\right]+ \\ \quad+(k_0-1)\varphi+(a_\Phi\varphi+a_m t_m)\Phi_0=0; \end{cases} \tag{1}$$

$$\varphi|_{R=R_0}=0; \tag{2}$$

$$C_m\frac{\partial t_m}{\partial\tau}=\alpha\varphi-t_m, \tag{3}$$

where M^2 is the neutron migration area; Φ_0 and k_0, energy distribution and neutron multiplication coefficient under steady-state conditions; a_Φ and a_m, power and moderator-temperature reactivity coefficients, respectively; R_0, extrapolated core radius; and C_m, moderator time constant.

We introduce the dimensionless quantities $r = R/R_0$; $\varkappa_0 = R_0^2(k_0-1)/M^2$; $\gamma_\Phi = R_0^2 a_\Phi \max\Phi_0/M^2$; $\gamma_m = R_0^2 a_m \alpha \max\Phi_0/M^2$; $\varphi' = \varphi/\max\Phi_0$; $f_0 = \Phi_0/\max\Phi_0$ and use a Laplace transform to get from (1)-(3) that

$$\begin{cases} \frac{1}{r}\frac{\partial}{\partial r}\left(r\frac{\partial\bar{\varphi}}{\partial r}\right)+\frac{1}{r^2}\frac{\partial^2\bar{\varphi}}{\partial\theta^2}+\varkappa_0\bar{\varphi}+ \\ +\left(\gamma_\Phi+\frac{\gamma_m}{C_m s+1}\right)\bar{\varphi}f_0=0; \end{cases} \tag{4}$$

$$\bar{\varphi}|_{r=1}=0, \tag{5}$$

where $\bar{\varphi}(s, r, \theta) = \mathbf{L}[\varphi'(t, r, \theta)]$.

We assume that the steady-state neutron distribution is dependent only on the radius, and then the expression for $\varkappa_0$ can be put as

$$\varkappa_0=-\frac{1}{f_0}\frac{1}{r}\frac{\partial}{\partial r}\left(r\frac{\partial f_0}{\partial r}\right).$$

The latter equation enables us to put (4) as

Translated from Atomnaya Énergiya, Vol. 48, No. 5, pp. 301-303, May, 1980. Original article submitted July 23, 1979.

 0038-531X/80/4805-0302$07.50

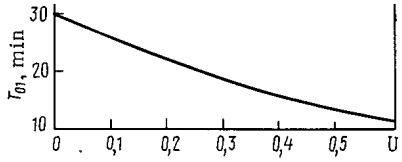

Fig. 1. Instability buildup period for the first azimuthal harmonic in relation to the dip in the neutron flux at the center of the core for $r_1 = 0.7$, $C_m = 40$ min, $R_0^2/M^2 = 792$; $a_m = 3.9 \cdot 10^{-5}$ 1/°C; $a_\varphi = 0$, and a mean moderator temperature of 300°C.

TABLE 1. Eigenvalues ν_{01} Corresponding to the First Azimuthal Harmonic

U	r_1						
	0,1	0,2	0,3	0,4	0,5	0,6	0,7
0	13,63	11,76	9,85	8,29	7,02	5,80	5,01
0,05	13,57	11,65	9,68	8,10	6,89	5,69	4,89
0,1	13,51	11,54	9,51	7,91	6,75	5,58	4,77
0,15	13,45	11,43	9,34	7,71	6,61	5,46	4,64
0,2	13,39	11,32	9,17	7,52	6,47	5,34	4,50
0,25	13,32	11,21	9,00	7,32	6,33	5,22	4,36
0,3	13,25	11,09	8,83	7,12	6,18	5,10	4,21
0,35	13,18	10,97	8,66	6,92	6,03	4,98	4,05
0,4	13,11	10,85	8,49	6,72	5,88	4,86	3,89
0,45	13,04	10,72	8,32	6,51	5,73	4,73	3,75
0,5	12,96	10,59	8,16	6,31	5,58	4,61	3,56
0,55	12,88	10,46	7,99	6,11	5,43	4,49	3,39
0,6	12,80	10,33	7,83	5,92	5,27	4,37	3,22

$$f_0\left[\frac{1}{r}\frac{\partial}{\partial r}\left(r\frac{\partial\bar{\varphi}}{\partial r}\right)+\frac{1}{r^2}\frac{\partial^2\bar{\varphi}}{\partial\theta^2}\right]+\left[\nu f_0^2-\frac{1}{r}\frac{\partial}{\partial r}\left(r\frac{\partial f_0}{\partial r}\right)\right]\bar{\varphi}=0, \tag{6}$$

where

$$\nu=\gamma_\Phi+\frac{\gamma_m}{C_m s+1}, \tag{7}$$

i.e., the stability problem for an arbitrary $\Phi_0(r)$ amounts to finding the eigenvalues for the boundary-value problem of (5) and (6).

We solve the problem of (5) and (6) approximately by representing the desired eigenfunction $\bar{\varphi}_i$ as

$$\bar{\varphi}_i=W_i(r)(a_i\cos i\theta+b_i\sin i\theta). \tag{8}$$

We substitute (8) into (6), multiply the resulting equation by $\cos i\theta$ ($\sin i\theta$) for $i=0, 1, 2, \ldots$, and integrate with respect to θ from zero to 2π to get

$$f_0\left[\frac{1}{r}\frac{\partial}{\partial r}\left(r\frac{\partial W_i}{\partial r}\right)-\frac{i^2}{r^2}W_i\right]+\left[\nu_i f_0^2-\frac{1}{r}\frac{\partial}{\partial r}\left(r\frac{\partial f_0}{\partial r}\right)\right]W_i=0 \tag{9}$$

The functions $R_i(r)$ can be represented approximately as a sum:

$$W_i(r)=\sum_{j=1}^{n}\alpha_{ij}\psi_{ij}(r), \tag{10}$$

where ψ_{ij}, $j = 1, 2, \ldots$ is a system of linearly independent coordinate functions with the corresponding boundary conditions.

We substitute (10) into (9), multiply by ψ_{ij}, and integrate with respect to r to get a linear homogeneous algebraic system of equations for the coefficients α_{ij}, $j = 1, 2, \ldots n$:

$$\sum_{j=1}^{n}A_{kj}^{i}\alpha_{ij}=0, \quad k=1, 2, \ldots, n,$$

where

$$A_{kj}^{i}=\int_0^1\left\{\psi_{ij}\frac{\partial}{\partial r}\left(r\frac{\partial\psi_{ik}}{\partial r}\right)-\frac{i^2}{r}\psi_{ij}\psi_{ik}+\nu_i\psi_{ij}\psi_{ik}rf_0-\frac{\partial}{\partial r}\left(r\frac{\partial(\psi_{ij}\psi_{ik})}{\partial r}\right)\right\}f_0\,dr.$$

TABLE 2. Values of $\bar{f}_0(0, r_1)$

r_1	$\bar{f}_0$
0	0,216
0,1	0,228
0,2	0,249
0,3	0,275
0,4	0,303
0,5	0,332
0,6	0,364
0,7	0,396

TABLE 3. Calculated Values of $(\lambda_{01} R_0)^2$ as a Function of R_1/R_0 and U

U	R_1/R_0						
	0,1	0,2	0,3	0,4	0,5	0,6	0,7
0	8,70	8,17	7,42	6,69	5,98	5,16	4,63
0,05	8,67	8,11	7,30	6,52	5,84	5,02	4,47
0,1	8,64	8,05	7,18	6,35	5,69	4,88	4,30
0,15	8,61	7,98	7,05	6,18	5,54	4,74	4,14
0,2	8,57	7,92	6,93	6,01	5,40	4,60	3,97
0,25	8,54	7,85	6,80	5,83	5,25	4,46	3,81
0,3	8,50	7,79	6,67	5,66	5,11	4,33	3,64
0,35	8,47	7,72	6,55	5,49	4,96	4,19	3,47
0,4	8,43	7,64	6,42	5,32	4,82	4,06	3,31
0,45	8,39	7,57	6,30	5,15	4,68	3,94	3,14
0,5	8,35	7,49	6,18	4,99	4,54	3,81	2,97
0,55	8,31	7,42	6,06	4,82	4,40	3,69	2,81
0,6	8,26	7,34	5,95	4,66	4,26	3,58	2,65

We equate the determinant of this system to zero to get an approximate equation for the eigenvalues ν_i (i = 0, 1, 2, ...):

$$|A_{kj}^i| = 0. \tag{11}$$

Stability on the First Azimuthal Harmonic. If the radial and azimuthal energy distributions are unstable on several harmonics, then the most unstable is the first azimuthal harmonic (the fundamental is usually stabilized by the automatic power regulator), and therefore from the practical viewpoint the period of instability buildup will be characterized by the period corresponding to that harmonic. From (7), the expression for this period can be put as

$$T_{01} = C_m \Big/ \Big(\frac{\gamma_m}{\nu_{01} - \gamma_\Phi} - 1 \Big). \tag{12}$$

At the present time, T_{01} is one of the most important dynamic characteristics of a power reactor of large physical dimensions.

To determine eigenvalue ν_{01} we can take the coordinate functions in the form $\psi_{1i} = r^i (1-r)$, i = 1, 2, ..., n; numerical analysis shows that one obtains an acceptable accuracy for ν_{01} if the first eight terms in the expansion of (10) are taken. There may be a dip in the neutron pattern in the center of a cylindrical reactor on account of burnup and displacement of the control rods. To estimate the effects of this on the stability we take the depth of the dip at the center of a core $U = 1 - 1/f_0(r)|_{r=0}$ as the adjustable parameter,

$$f_0(r) = \begin{cases} U(r^2/r_1^2 - 1) + 1 & \text{for } r < r_1; \\ A[J_0(\mu_0 r) Y_0(\mu_0) - Y_0(\mu_0 r) J_0(\mu_0)] & \\ \qquad \text{for } r_1 \leqslant r \leqslant 1; & \end{cases}$$

$r_1 = R_1/R_0$ is the relative radius of the region with the dip in the neutron flux, and μ_0^2 is the material parameter for the case corresponding to a plateau in the energy distribution with plateau radius r_1.

Table 1 gives numerical results for ν_{01} as a function of r_1 and U, which shows that the stability deteriorates appreciably as the dip in the center increases. Extrapolation to $r_1 = 0$ along all lines in Table 1 gives $\nu_{01} = 15.38$ with an error of up to 1%. Figure 1 shows how the instability buildup period varies for a constant total reactor power. The period of the first azimuthal harmonic decreases monotonically as U increases.

The calculations may be performed for a constant reactor power to relate the value to max Φ_0 : max $\Phi_0 = \Phi_0/2\bar{f}_0$, where

$$\overline{\Phi}_0 = \int_0^{2\pi} \int_0^{R_0} \Phi_0 R\, dR\, d\theta / (\pi R_0^2);$$

$$\bar{f}_0 = \int_0^1 f_0 r\, dr.$$

The value of $\bar{f}_0$ is dependent on U and r_1. The U dependence may be put as

$$\bar{f}_0(U, r_1) = \bar{f}_0(0, r_1) - r_1^2 U/4.$$

Table 2 gives numerical values of $\bar{f}_0$ (0, r_1).

Table 1 can also be used to estimate one of the reactivity coefficients. For example, the energy distribution $\Phi_0(r)$ may be derived from detectors within the core [2] and all the parameters of the system may have been determined by experiment, including T_{01} [3], apart from a_m, in which case (12) can be used with Table 1 to derive γ_m and then a_m. The method can then be used to identify the system parameters.

A method has been given [1] for calculating the stability of a reactor with an equalized neutron flux. In order to use the results of [1] it is necessary to determine the eigenvalues for the boundary-value problem

$$\begin{cases} \Delta\varphi + (\varkappa_0 + \lambda^2)\varphi = 0; \\ \varphi|_{R=R_0} = 0. \end{cases}$$

It is of interest to compare the eigenvalues calculated as above for U = 0 with $(\lambda_{01}R_0)^2$ of [1]; Table 3 shows that the difference does not exceed 2%, which is quite acceptable for practical calculations.

Conclusions. A method has been developed for calculating the stability of a power reactor with any stationary power distribution $\Phi_0(r)$; tables have been formulated for the values of the parameters that can be used to determine the instability buildup period for the radial and azimuthal power distribution. A dip in the steady-state neutron distribution at the center of the core has an appreciable effect on the instability buildup period, e.g., a 30% dip at the center of the core reduces the period by about a factor 1.5. This method can be used with the method of measuring the instability period of [3] in identifying the individual dynamic parameters of a power reactor.

LITERATURE CITED

1. A. Hitchcock, Nuclear Reactor Stability [Russian translation], Gosatomizdat, Moscow (1963).
2. M. Levin and D. Diamond, At. Tekh. Rubezhom, No. 5, 10 (1973).
3. A. N. Aleksakov et al., At. Energ., 46, No. 4, 227 (1979).

THERMOHYDRAULIC CALCULATION OF MULTIROD HEAT-LIBERATING PILES COOLED BY SINGLE-PHASE HEAT CARRIER

G. S. Mingaleeva and Yu. V. Mironov

UDC 621.039.5:536.27

The possibility of increasing the power and reliability of rod heat-liberating piles (HLP) in gas-cooled fast reactors is determined primarily by the maximum fuel temperature at the center of the fuel element and its shell and the maximum temperature difference over the fuel-element perimeter. In studying these parameters, it is necessary to take account of bias of the heat liberation in the cassette cross section, the influence of the unheated shell, and other factors producing nonuniform gas heating in the different parts of the channel cross section; this is done by means of numerical methods in which the channel cross section is arbitrarily divided into elementary cells. For each cell, mass, momentum, and energy balance equations are written, taking into account the interaction of the heat-carrier fluxes in the elementary channels. On this basis, both within and outside the Soviet Union, computer programs for the calculation have been developed [1-3]. A considerable proportion of these are oriented toward the analysis of the evaporating channels of boiling reactors, the HLP of which contain a relatively small number of fuel elements. The development of special algorithms which are very rapid and economical in the use of computer memory is necessary for the calculation of the characteristic gas-cooled-reactor piles with a large number of fuel elements.

In the present work, the PUCHOK-BM (high-power) program intended for thermohydraulic calculations of multirod HLP cooled by a single-phase heat carrier is described. This program has the following features:

for a system of interrelated channels, it solves the steady problem with initial conditions at the channel inlet;

it allows the three-dimensional temperature distribution of the heat carrier in the pile and at the fuel-element surface to be obtained (without taking into account the leakage of heat over the perimeter in fuel elements) for an arbitrary energy-distribution curve in the fuel elements over the pile height and cross section;

it takes three mechanisms of transverse flow mixing into account: convective redistribution of the flows due to equalization of the longitudinal pressure gradients; turbulent energy and momentum diffusion through the cell boundaries; and local transverse currents due to distance pieces obstructing the flow;

the system of differential mass, momentum, and energy balance equations is integrated by the Euler method with automatic choice of step, depending on the given error;

The program is written in Fortran, taking the requirements of the BÉSM-6 computer's translator into account.

Suppose that the active channel cross section is divided into N cells. The cross section of the k-th cell will be denoted by F_k, and the perimeters of the fuel elements and shells appearing in this cell by Π_k^j, where j is the numbering of the walls in the cell. A flow of flow rate m_k and heat content i_k passes through the cell. The frictional stress at the j-th surface is denoted by τ_k^j and the heat flux by q_k^j. Let the k-th cell be adjoining some n-th cell. The length of the boundary between these cells is Π_{kn}, and the mass transfer per unit height of the pile from the n-th cell to the k-th is W_{kn} ($W_{kn} = -W_{nk}$).

The turbulent frictional stress and heat flux at the boundary between two cells will be denoted by τ_{kn} and q_{kn}. Then the mass, momentum, and energy balance equations for the k-th cell may be written

Translated from Atomnaya Énergiya, Vol. 48, No. 5, pp. 303-308, May, 1980. Original article submitted June 26, 1979.

0038-531X/80/4805-0306$07.50

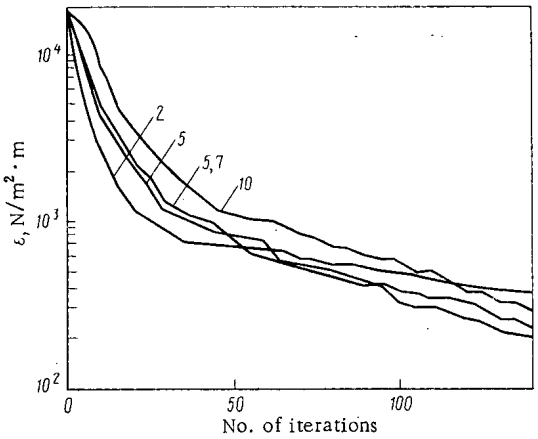

Fig. 1. Dependence of maximum imbalance of pressure gradients in cells on the number of iterations for different values of k (given on the curves).

$$\frac{dm_k}{dz} = \sum_n W_{kn};$$

$$\frac{1}{F_k}\frac{d}{dz}\left(\frac{m_k^2}{\rho_k}\right) + F_k\frac{dp_k}{dz} = \sum_n W_{kn}u_{kn}^* + \sum_n \tau_{kn}\Pi_{kn} - \sum_j \tau_k^j\Pi_k^j; \quad (1)$$

$$\frac{d}{dz}\left[m_k\left(i_k + \frac{m_k^2}{2\rho_k^2F_k^2}\right)\right] = \sum_n W_{kn}i_{kn}^* + \sum_n q_{kn}\Pi_{kn} + \sum_j q_k^j\Pi_k^j,$$

where z is the longitudinal coordinate along the channel axis; ρ_k and p_k, gas density and pressure in the k-th cell; u_{kn}^* and i_{kn}^*, longitudinal momentum and energy of the transverse current W_{kn}, equal to the momentum and energy of the flow in the donor cell.

To close the system in Eq. (1), additional relations are required for determining the currents between cells. Remaining within the framework of hydraulic assumptions, the following relation may be used to determine W_{kn}

$$p_n - p_k = \zeta_{kn}\frac{W_{kn}|W_{kn}|}{2\bar{\rho}_{kn}\Pi_{kn}^2}, \quad (2)$$

where ζ_{kn} is the drag coefficient of the transverse current between the k-th and n-th cells; $\bar{\rho}_{kn}$ is the mean gas density in the considered cells.

In some programs, a complete form of the momentum balance in the transverse direction is used, including the convective terms. However, it was shown in [4, 5] that the difference between these approaches only becomes pronounced in channels with strong perturbation of the flow, for example, in the vicinity of a compression of part of the channel cross section. On the other hand, a more complete form also requires more empirical parameters, the values of which have been inadequately investigated as yet.

Thus, Eqs. (1) and (2) form a system of ordinary differential equations of order 3N in the unknowns p_k, m_k, and i_k. To integrate this system, 3N initial conditions must be specified – the values of the unknowns at the channel inlet: when z = 0

$$p_k = p_0, \quad m_k = m_{0k}, \quad i_k = i_0. \quad (3)$$

However, direct numerical integration of the equations obtained leads to rapidly appearing instability. For example, if there is a random increase in pressure in one of the cells of the system which is in mechanical equilibrium, this will lead to a discharge into a neighboring cell according to Eq. (2), and the gas velocity in the considered cell will decrease. Then the retardation of the flux and the decrease in hydraulic losses, in turn, lead to further rise in pressure in the cell. The opposing factors (turbulent momentum transfer and heating of the gas) are unable to balance this process.

In the present work, stabilization of the system is achieved by introducing an approximate equalization of the pressure in the cells by an iterational method, with subsequent averaging of the pressure over the channel cross section. In Eq. (1), the pressure gradients in the cell may be written in the form

$$dp_k/dz = B_k + \sum_n \delta_{kn}W_{kn}, \quad (4)$$

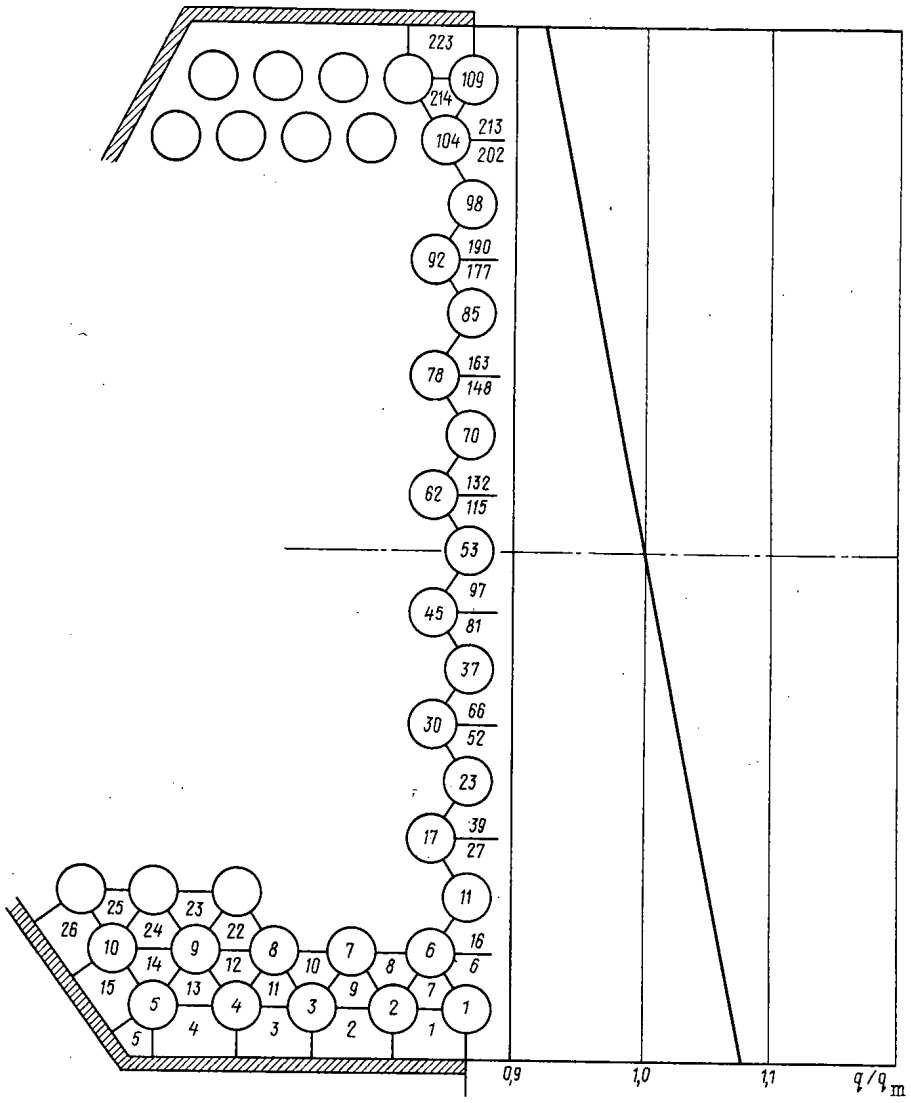

Fig. 2. Numbering of cells and fuel elements for 217-rod HLP and energy distribution over channel cross section.

where B_k combines terms independent of W_{kn}, and the factor δ_{kn} includes the parameters of the transverse flow u^*_{kn} and i^*_{kn}, i.e., depends only on the direction of these currents.

Thus, suppose that at the i-th iteration the maximum difference in gradients is observed between cells numbered r and s. The pressure gradients existing at this iteration are then used in Eq. (2) to calculate the vector W^*_{kn} characterizing the direction of the change in the set of values W^i_{kn}. Then the new currents for the (i+1)-th iteration are found from the formula

$$W^{i+1}_{kn} = W^i_{kn} + \alpha W^*_{kn}, \tag{5}$$

where α is an as-yet unknown number.

The difference in gradients between cells r and s at the (i+1)-th iteration may be written, in the first approximation, in the form

$$\varepsilon^{i+1}_{rs} \approx \varepsilon^i_{rs} + \alpha \left(\sum_n \delta^i_{rn} W^*_{rn} - \sum_n \delta^i_{sn} W^*_{sn} \right). \tag{6}$$

Requiring ε^{i+1}_{rs} to vanish in Eq. (6), an expression for α is obtained

$$\alpha = - \frac{\varepsilon^i_{rs}}{\sum_n \delta^i_{rn} W^*_{rn} - \sum_n \delta^i_{sn} W^*_{sn}}. \tag{7}$$

Using Eq. (5), the following approximation is obtained. The process ends after reducing the imbalance ε_{rs} to the specified level. In the PUCHOK-BM program, provision is also made for exit from the iteration

after a specified number of iterations or the reduction of the corrections to the currents to a specified value. Calculations have shown that it is expedient to substitute into Eq. (5) not the parameter α determined from Eq. (7) but $\alpha' = \alpha/k$, where k is a parameter whose optimal value is determined, on the basis of specific calculations, from the criterion of maximum rate of convergence of the iterative process.

The behavior of the maximum imbalance of the pressure gradients in the cells in the iterative process as a function of the parameter k is shown in Fig. 1. Calculations were carried out for a pile of 271 rods cooled by helium at a pressure of 160 bar, with uniform spacing of the fuel elements in a triangular grid with spacing $s/d = 1.32$. At the beginning of the iteration, zero currents were specified. An acceptable reduction in the pressure-gradient imbalances to 250-500 $N/m^2 \cdot m$ is observed with $k = 5.7$ after 80-130 iterations. Note that, if in the subsequent calculations of the coefficients in Eq. (1) the currents obtained in the previous calculations are used as the initial approximation for the iterative process, the number of iterations required is reduced to 12-18. Experience of calculations shows that k depends only weakly on the parameters of the flow conditions, and is mainly determined by the number and geometry of the cells. Usually k = 2-6. If the value of k optimal for the given pile is used, the machine time required may be reduced by an order of magnitude. For the given form of cassette, the time required for the calculation (with $k = 5.7$) is 8-12 min per 1 m length (depending on the specified level of error). In this case, the above equalization of pressure gradients resulted in a pressure difference in the cells after one integration step, equal to ~ 0.01-0.05 m, that was within the limits of 10-20 N/m^2. This allows the pressures in the cells to be regarded as practically equal.

The terms characterizing the turbulent momentum and energy transfer in Eq. (1) are expressed in terms of the velocity difference or heat-content difference in the considered cells

$$\tau_{kn} = W'_{kn}(u_n - u_k);$$
$$q_{kn} = W'_{kn}(i_n - i_k), \qquad (8)$$

where W'_{kn} is the turbulent-diffusion intensity at the cell boundary. In recent years, there have been numerous investigations of the dependences for turbulent mixing between cells of beams, many of them having been considered in the review [1]. In the PUCHOK-BM program, provision is made for the use of different relations for the calculation of W'_{kn}, so that the investigator may choose the one which he judges to be best.

Local resistance in the channel with the rod bundles (distance pieces and annular grids) may have a pronounced influence on the flow distribution over the channel cross section. The mass, momentum, and energy balance equations for the grid are written in integral form, without any terms taking the turbulent interaction of elementary channels into account. The friction distributed over the length is then replaced by local losses expressed in terms of the local drag coefficients of the grid in the cells. In the absence of more accurate information, these coefficients may be calculated taking into account the decrease in cross section of the elementary channel on the basis of data for the grid as a whole.

The PUCHOK-BM program was used for a thermophysical analysis of the HLP of a gas-cooled fast reactor, considering 217 rod fuel elements arranged in a triangular lattice with relative step s/d equal to 1.32, and relative distance to the wall ($2s_{cm}/d$) equal to 1.33. The numbering scheme adopted for the rods and elementary cells is shown in Fig. 2, together with curves of the energy distribution in the cassette cross section. The cassette is cooled by helium with an initial pressure of 160 bar.

In the calculations, the equation of state of an ideal gas and the temperature dependence of the viscosity and heat conduction of helium were used. The diffusional mass flux in Eq. (8) was determined from the data of [6]. The heat-transfer coefficients were calculated from the averaged presser dependence [7]. In calculating the hydraulic drag of the cell, a special form factor was introduced, taking into account the difference in characteristics from a circular tube. For the central cells this factor is calculated from the data of [8], while for the peripheral cells the theoretical results of [9] are used, taking into account the influence of the nonisothermal flow conditions by means of a temperature factor in accordance with [10].

The temperature distribution of the gas and the fuel-element surface is shown in Fig. 3 for cells arranged along the pile symmetry axis. At the channel exit the gas temperature in cells 1 and 223 differs by 97°C. The maximum surface temperature of the fuel elements is observed at $z/L = 0.625$, i.e., the value is somewhat shifted downstream with respect to the center of the active region and the maximum of the energy-liberation curve, varying in almost cosinusoidal fashion in the central region of the zone (where $0.25 \leq z/L \leq 1.75$). However, more unfavorable effects were observed for the corner fuel elements. Calculations show a considerable rise in gas temperature in corner cell 5. This is due to the decrease in mass velocity of the gas in the corner cell, since its hydraulic diameter in much less than that of the central "triangular" cells. Decrease in mass velocity in cell 5 leads to an increase in surface temperature of the corner fuel element, the

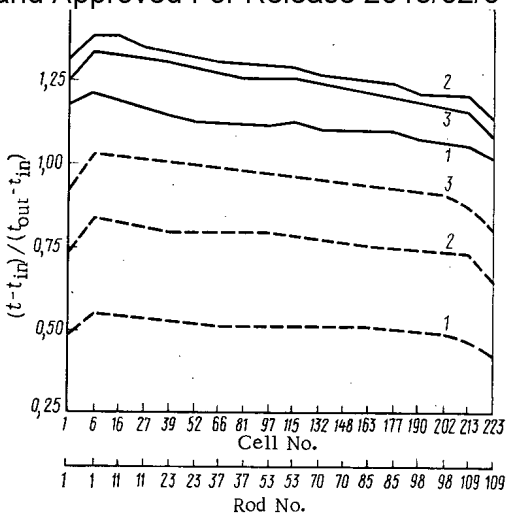

Fig. 3

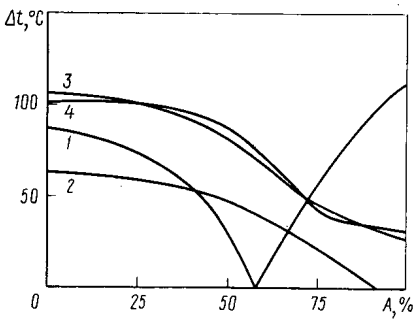

Fig. 4

Fig. 3. Temperature distribution of gas (dashed curves) and fuel-element surface (continuous curves) along the symmetry line of a 217-rod gas-cooled pile with z/L = 0.5 (1), 0.625 (2), and 0.75 (3).

Fig. 4. Maximum temperature drop over the perimeter for corner fuel elements of a 217-rod gas-cooled pile as a function of the energy liberation (A, %) in fuel element 5 with z/L = 0.625; curves 1-4 are for fuel elements 5, 9, 4, and 10, respectively.

extent of which increases with increase in gas temperature in the corner cell, since the heat-transfer coefficient is proportional to Reynolds number to the power 0.8. At the same time, the calculations show a considerable temperature drop over the perimeter of the corner fuel element, reaching 90°C at z/L = 0.625. Therefore, further efforts were directed toward the discovery of constructional means of smoothing the observed corner effects. The simplest method, involving decrease in the degree of enrichment of the fuel in the corner rod, does not lead to significant improvement in the situation. In Fig. 4, the change in maximum temperature drop over the perimeter of the group of fuel elements is shown as a function of the energy liberation in fuel element 5. With decrease in enrichment in the corner rod, the heat flow into the adjacent cells 4 and 15 is reduced, as a result of which the temperature drops at rods 4 and 10, which appear in these cells, are increased. Consequently, equalization of the temperature requires, on the one hand, a certain decrease in the fuel enrichment in the corner fuel element, to decrease the gas heating in the corner cell and, on the other, some kind of "squeezing" of cells 4 and 15, to raise the gas temperature in them. This may be achieved by changing the fuel enrichment in the corner fuel element in combination with change in its diameter or with the fitting of a displacer in cells 4 and 15. The results of calculations for an alternative version in which cells 4 and 15 are fitted with cylindrical displacers, reducing the active cross section of these cells by 16% and reducing the energy liberation in fuel element 5 to 65% of the nominal value, shows that this approach has possibilities. In this case the maximum temperature drop over the perimeter of the corner fuel elements is no more than 32°C.

Thus, the above method and the PUCHOK-BM program allow the problem of thermohydraulic optimization of gas-cooled-cassette construction to be considered in the first approximation. The program will be useful in generalizing experimental data and more accurate modeling, on this basis, of cassette behavior under different conditions.

LITERATURE CITED

1. J. Weisman and R. Bowring, Nucl. Sci. Eng., 57, 255 (1975).
2. V. I. Abramov et al., in: TF-4 Seminar on the Investigation of Critical Heat Fluxes in Rod Bundles in Steady and Nonsteady Heat-Transfer Conditions [in Russian], Izd. SÉV, Moscow (1974), p. 201.
3. Yu. V. Mironov and S. V. Shpanskii, At. Energ., 39, No. 6, 403 (1975).
4. J. Weisman, Nucl. Eng. Design, 52, No. 1, 67 (1979).
5. A. Tapucu, Nucl. Eng. Design, 52, No. 1, 69 (1979).
6. D. Rowe, Trans. Am. Nucl. Soc., 12, No. 2, 805 (1969).
7. V. I. Subbotin et al., Hydrodynamics and Heat Transfer in Atomic Power Plants [in Russian], Atomizdat, Moscow (1975).

8. P. A. Ushakov, in: Liquid Metals. FÉI Proceedings [in Russian], Atomizdat, Moscow (1974), p. 263.
9. W. Eifler and R. Nijsing, Atomkernenerg., 18, No. 3, 189 (1971).
10. Yu. Vilemas et al., Heat Transfer in Gas-Cooled Circular Channels [in Russian], Moklas, Vilnius (1977).

NONSTATIONARY SLOWING DOWN OF NEUTRONS FROM A PLANE PULSED SOURCE IN A SYSTEM OF TWO MEDIA WITH A PLANE INTERFACE

Yu. A. Medvedev and E. V. Metelkin

UDC 621.039.512.4

The investigation of the nonstationary slowing down of neutrons is of great interest for the solution of certain problems of nuclear physics, reactor physics, nuclear geophysics, shielding physics, etc. [1-3]. While the problem of nonstationary slowing down of neutrons in homogeneous media can be considered adequately studied [4-8], the slowing down of neutrons in spatially inhomogeneous media has been far from completely investigated. In [9, 10] nonstationary space–energy spectra of neutrons elastically slowed down in slightly inhomogeneous media were calculated analytically. At the same time, it is necessary to investigate the directly opposite situation, which is frequently encountered in practice, when neutrons are slowed down in a system consisting of homogeneous media with different moderating properties.

In the present article we consider the case with the simplest geometry: slowing down of neutrons from a plane pulsed source in a system consisting of two different media with a plane interface. The space–energy dependence of the average slowing-down time of neutrons in each medium is calculated on the basis of the age approximation. It is assumed that neutrons slow down as a result of elastic collisions, the mean free path of neutrons in each medium is constant, and there is no absorption of neutrons. It should be noted that the steady-state problem of neutron slowing down in a system of two media with a plane interface was solved in [11-14] within the framework of the age approximation.

The Boltzmann equation describing the nonstationary elastic slowing down of neutrons in the age approximation without absorption has the form [11]

$$\frac{1}{v\xi\Sigma}\frac{\partial}{\partial t}F(u, \mathbf{r}, t)+\frac{\partial}{\partial u}F(u, \mathbf{r}, t)-\frac{\Delta F(u, \mathbf{r}, t)}{3\xi\Sigma^2(1-\mu)}=S(u, \mathbf{r}, t), \tag{1}$$

where $F = \xi v\Sigma f(u, \mathbf{r}, t)$ is the neutron slowing-down density; $f(u, \mathbf{r}, t)\,dudr$, number of neutrons in the interval $(u, u+du; \mathbf{r}, r+dr)$ at time t; $u = \ln(E^+/E)$, lethargy; E, energy of the neutrons undergoing moderation; v, their velocity; E^+, maximum energy of the neutrons emitted by the source; Σ, neutron scattering cross section; ξ, average change in lethargy as the result of a single collision; μ, average cosine of the neutron scattering angle in the laboratory coordinate system; and $S(u, \mathbf{r}, t)$, a function which characterizes the space–energy and temporal distribution of the neutron sources.

We assume that the neutrons are slowed down in a system consisting of two media separated by the plane $z = 0$, and that a plane pulsed monoenergetic neutron source lies in the plane $z = d$. In this case Eq. (1) will have the following form in the different media:

$$\tau_i e^{u/2}\frac{\partial}{\partial t}F_i(u, z, t)+\frac{\partial}{\partial u}F_i(u, z, t)-R_i^2\frac{\partial^2}{\partial z^2}F_i(u, z, t)=\delta(u)\,\delta(t)\,\delta(z-d)\,\delta_{i1}, \tag{2}$$

for $z > 0$ $i = 1$, and for $z < 0$ $i = 2$; δ_{ij} is the Kronecker symbol:

$$R_i^2=\frac{1}{3\xi_i\Sigma_i^2(1-\mu_i)};\quad \tau_i=\frac{1}{\xi_i\Sigma_i v^+}\qquad (i=1, 2). \tag{3}$$

Taking Laplace transforms with respect to time and lethargy

$$F_i(u, z, p)=\int_0^\infty dt e^{-pt}F_i(u, z, t), \tag{4}$$

Translated from Atomnaya Énergiya, Vol. 48, No. 5, pp. 308-313, May, 1980. Original article submitted April 23, 1979.

0038-531X/80/4805-0311$07.50

$$F_i(s, z, t) = \int_0^\infty du e^{-su} F_i(u, z, t) \tag{5}$$

and shifting the inhomogeneity into the boundary conditions, Eqs. (2) can be written in the form

$$sF_i(s, z, p) - R_i^2 \frac{\partial^2}{\partial z^2} F_i(s, z, p) + p\tau_i F_i\left(s - \frac{1}{2}; z, p\right) = 0. \tag{6}$$

Equation (6) must be solved for the following boundary conditions:

$$\begin{aligned} &F_1(s, p, z) \to 0 \quad \text{as} \quad z \to \infty; \\ &F_2(s, p, z) \to 0 \quad \text{as} \quad z \to -\infty; \end{aligned} \tag{7}$$

$$F_1(s, p, d) = \tilde{F}_1(s, p, d); \; R_1^2\left[\frac{\partial}{\partial z}\tilde{F}_1(s, d, p) - \frac{\partial}{\partial z}F_1(s, d, p,)\right] = 1; \tag{8}$$

$$\tau_1\tilde{F}_1(s, 0, p) = \tau_2 F_2(s, 0, p); \; R_2^2\frac{\partial}{\partial z}F_2(s, 0, p) - R_1^2\frac{\partial}{\partial z}\tilde{F}_1(s, 0, p) = 0, \tag{9}$$

where $F_1(s, z, p)$ and $\tilde{F}_1(s, z, p)$ are solutions of Eqs. (6) in the regions $z \geq d$ and $0 \leq z \leq d$, respectively.

We seek a series solution of Eqs. (6) in powers of p:

$$F_i(s, z, p) = \sum_{n=0}^\infty \frac{(-1)^n}{n!} p^n F_i^{(n)}(s, z). \tag{10}$$

After determining the functions $F_i^{(n)}(s, z)$ it is easy to find the times from the corresponding distribution functions of slowing-down neutrons, defined as

$$\langle t_i^n(z, u)\rangle = \left[\int_0^\infty dt t^n F_i(u, z, t)\right] \Big/ \left[\int_0^\infty dt F_i(z, u, t)\right]. \tag{11}$$

Actually, using (4) it is easy to see that

$$\langle t_i^n(z, u)\rangle = (-1)^n\left[\frac{\partial^n}{\partial p^n}F_i(u, z, p)|_{p=0}\right] \Big/ \left[F_i(u, z, p)|_{p=0}\right]. \tag{12}$$

Substituting (10) into (12), we obtain

$$\langle t_i^n(u, z)\rangle = F_i^{(n)}(u, z)/F_i^{(0)}(u, z). \tag{13}$$

Substituting series (10) into Eqs. (6) and equating terms with the same powers of p, we obtain a chain of equations describing the functions $F_i^{(n)}(s, z)$

$$sF_i^{(0)} - R_i^2\frac{\partial^2}{\partial z^2}F_i^{(0)}(s, z) = 0 \quad (i = 1, 2); \tag{14}$$

$$sF_i^{(n)}(s, z) - R_i^2\frac{\partial^2}{\partial z^2}F_i^{(n)}(s, z) - n\tau_i F_i^{(n-1)}\left(s - \frac{1}{2}; z\right) = 0 \; (n \geqslant 1, \; i = 1, 2). \tag{15}$$

Substituting series (10) into boundary conditions (7)-(9) and equating terms with the same powers of p, we find that the functions $F_i^{(n)}(s, z)$ for n = 0 must satisfy conditions (7)-(9), and for $n \geq 1$ conditions (7)-(9) with the only difference that the right-hand side of the second of Eqs. (8) will be zero instead of unity

Equations (14) and (15) are linear differential equations of the second order with constant coefficients which can be solved successively by using appropriate boundary conditions. For the functions $F_i^{(0)}$ and $F_i^{(1)}$ (i = 1, 2) which determine the average slowing-down time of neutrons in each medium (cf. (13)), we obtain

$$F_i^{(0)}(s, z) = \frac{(R_1\tau^2 - R_2\tau_1)}{(R_1\tau_2 + R_2\tau_1)}\frac{\exp\{-(\sqrt{s}/R_1)(z+d)\}}{2R_1\sqrt{s}} + \frac{\exp\{-(\sqrt{s}/R_1)(z-d)\}}{2R_1\sqrt{s}}; \tag{16}$$

$$\begin{aligned} F_1^{(1)}(s, z) = {} & \frac{\tau_1(R_1\tau_2 - R_2\tau_1)}{R_1(R_1\tau_2 + R_2\tau_1)}\left\{\frac{1}{\sqrt{s-0.5}}\exp\left[-\frac{\sqrt{s-0.5}}{R_1}(z+d)\right] - \frac{1}{\sqrt{s}}\exp\left[-\frac{\sqrt{s}}{R_1}(z+d)\right]\right\} + \\ & + \frac{\tau_1}{R_1}\left\{\frac{1}{\sqrt{s-0.5}}\exp\left[-\frac{\sqrt{s-0.5}}{R_1}(z-d)\right] - \frac{1}{\sqrt{s}}\exp\left[-\frac{\sqrt{s}}{R_1}(z-d)\right]\right\} - \frac{2\tau_1\tau_2 R_2(\tau_2 - \tau_1)}{(R_1\tau_2 + R_2\tau_1)^2} \times \\ & \times\left[\frac{1}{\sqrt{s}} - \frac{1}{\sqrt{s-0.5}}\right]\exp\left[-\frac{\sqrt{s}}{R_1}z - \frac{\sqrt{s-0.5}}{R_1}d\right]; \end{aligned} \tag{17}$$

$$F_2^{(0)}(s, z) = \frac{\tau_1}{R_1\tau_2 + R_2\tau_1}\frac{1}{\sqrt{s}}\exp\left\{\sqrt{s}\left(\frac{z}{R_2} - \frac{d}{R_1}\right)\right\}; \tag{18}$$

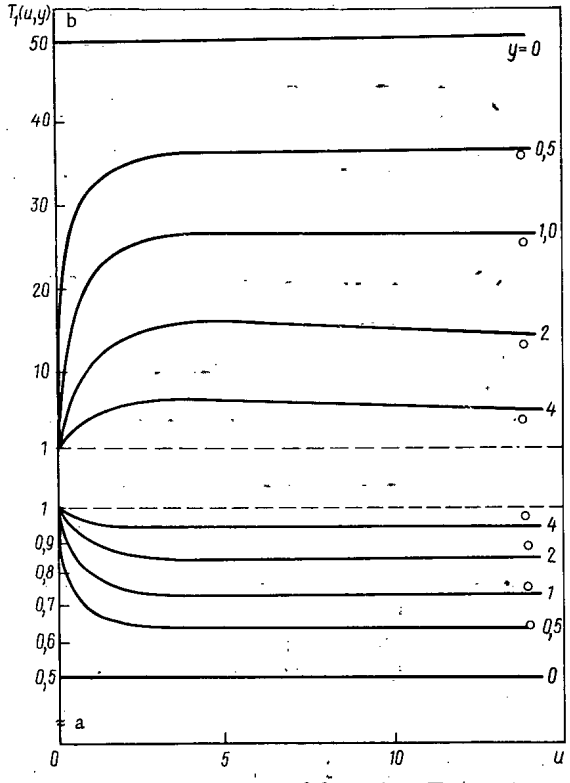

Fig. 1. Dependence of function $T_1(y, u)$ on lethargy in a system of two identical media of different densities: a) in the less dense medium for $Q = 10^4$; b) in the more dense medium for $Q = 10^{-4}$; ○) values of T_1 calculated by approximate Eq. (24).

$$F_2^{(1)}(s, z) = \frac{2\tau_1\tau_2}{R_1\tau_2 + R_2\tau_1}\left\{\frac{1}{\sqrt{s-0.5}}\exp\left[+\sqrt{s-0.5}\left(\frac{z}{R_2}-\frac{d}{R_1}\right)\right]-\frac{\tau_1}{\tau_2}\frac{1}{\sqrt{s}}\times\right.$$

$$\left.\times\exp\left[\sqrt{s}\left(\frac{z}{R_2}-\frac{d}{R_1}\right)\right]\right\}-\frac{2R_1\tau_1^2(\tau_2-\tau_1)}{(R_1\tau_2+R_2\tau_1)^2}\left[\frac{1}{\sqrt{s}}+\left(\frac{R_1\tau_2}{R_2\tau_1}\right)\frac{1}{\sqrt{s-0.5}}\right]\exp\left[\frac{\sqrt{s}}{R_2}z-\frac{\sqrt{s-0.5}}{R_1}d\right]. \quad (19)$$

The expressions for the functions $F_i^{(0,1)}$ (cf. remark following Eq. (9)) are obtained from Eqs. (16) and (17) by replacing the difference $z - d$ which appears in them by $d - z$. Hence it follows that by taking the inverse Laplace transforms with respect to s of the functions $\tilde{F}_1^{(0,1)}(u, z)$ and $F_1^{(0,1)}(u, z)$ we obtain corresponding expressions, as can easily be verified directly.

By using (16)-(19) for a homogeneous medium ($\tau_1 = \tau_2$; $R_1 = R_2$) it is easy to find from Eq. (12)

$$\langle t_i(u)\rangle_{\text{homo}} = 2\tau_i(e^{u/2}-1) = \frac{2}{\xi_i v\Sigma_i}\left(1-\frac{v}{v^+}\right). \quad (20)$$

This expression agrees with the analogous expression derived earlier in [4, 5].

Let us consider first the simplest case when the neutron source is on the interface of the two media (d = 0). Here the simplest result is obtained for the neutron slowing-down time in the plane z = 0. Taking inverse Laplace transforms of Eqs. (16) and (17) for z = d = 0 [15], and using Eq. (12), we obtain

$$T_1(u, 0) \equiv \frac{\langle t_1(u, 0)\rangle}{\langle t_1(u)\rangle_{\text{homo}}} = \frac{1+(1/\sqrt{Q})}{1+\sqrt{\delta}}, \quad (21)$$

where, as in [13]

$$Q = \frac{R_1^2}{R_2^2}\frac{\Sigma_2^2\xi_2(1-\mu_2)}{\Sigma_1^2\xi_1(1-\mu_1)}; \quad \delta = \frac{\xi_2(1-\mu_1)}{\xi_1(1-\mu_2)}.$$

It is known [13] that for an air (i = 1) – ground (i = 2) system $Q = 10^6$ and $\delta \approx 2.1$. Using these constants, we find that at the air – ground interface the neutron slowing-down time is only 0.4 times shorter than the neu-

$$T_1(u, y, D) = 1 - \frac{\sqrt{\delta}[(1/\sqrt{Q\delta})-1]}{(1+\sqrt{\delta})^2} \frac{\sqrt{u/\pi}}{e^{u/2}-1} \frac{\int_0^u \frac{du'}{[u'(u-u')]^{3/2}} [uD - u'(y+D)] \exp\left\{\frac{u'}{2} \frac{D^2}{4u'} \frac{y^2}{4(u-u')}\right\}}{\left\{\exp\left[\frac{(y-D)^2}{4u}\right] + \left(\frac{1-\sqrt{\delta}}{1+\sqrt{\delta}}\right) \exp\left[-\frac{(y+D)^2}{4u}\right]\right\}}, \quad (26)$$

where $y = z/R_1$; $D = d/R_1$ (for $y > 0$);

$$T_2(u, y, D) = \frac{(e^{u/2} - \sqrt{Q\delta})}{e^{u/2}-1} - \frac{\sqrt{\delta}(1-\sqrt{Q\delta})}{2(1+\sqrt{\delta})} \times \quad (27)$$

$$\times \frac{\sqrt{u/\pi}}{e^{u/2}-1} \exp\left[\frac{(y-D)^2}{4u}\right] \int_0^u \frac{du'}{[u'(u-u')]^{3/2}} \left[uD - u'\left(D + \frac{y}{\sqrt{\delta}}\right)\right] \exp\left\{\frac{u'}{2} - \frac{D^2}{4u'} - \frac{y^2}{4(u-u')}\right\},$$

where $y = z/R_2$; $D = d/R_1$ (for $y < 0$).

From the results of Eqs. (26) and (27) it is easy to determine that at early times ($u \to 0$) the function T_1 approaches the constant limit unity. At the same time as $u \to 0$ the function T_2 approaches a limit which depends on y and D. Its form in the two limiting cases for $y \ll D$ and $y \gg D$ is determined respectively by the expressions:

$$T_2(u, y, D) \xrightarrow[u\to 0]{} T_2(y, D, 0) \approx \sqrt{Q\delta} - \frac{1-\sqrt{Q\delta}}{1+\sqrt{\delta}}\left(\frac{y}{D}\right); \quad (28)$$

$$T_2(u, y, D) \xrightarrow[u\to 0]{} T_2(y, D, 0) \approx 1 + (1-\sqrt{Q\delta}\left(\frac{D}{y}\right). \quad (29)$$

Figures 4 and 5 show the dependence of the functions $T_1(u, y, D)$ and $T_2(u, y, D)$ on lethargy, plotted from Eqs. (26) and (27) for $|y| = 1$ and for various positions of the source in the first medium for a system consisting of two identical media ($\delta = 1$) with different densities. An analysis of these results shows that the displacement of the source into the first medium (an increase in D) decreases the effect of the second medium on the average slowing-down time of neutrons in the first medium (cf. Figs. 4a and 5b), but on the other hand increases the effect of the first medium on the average slowing-down time in the second medium (cf. Figs. 4b and 5a). This character of the dependence of T_1 and T_2 on the position of the source results from the fact that the displacement of the source into the first medium leads to an increase in the time which slowing-down neutrons spend in the first medium, and to a decrease in the time they spend in the second medium.

The authors thank N. S. Potapovaya for help in performing the numerical calculations.

LITERATURE CITED

1. Theoretical and Experimental Problems of Nonstationary Neutron Transport [in Russian], Atomizdat, Moscow (1972).
2. Slow Neutron Spectra [in Russian], Atomizdat, Moscow (1971).
3. The Biological Shield of Mobile Reactor Power Plants [in Russian], Atomizdat, Moscow (1969).
4. M. V. Kazarnovskii, in: Proc. Fiz. Inst. Akad. Nauk, 11, 176 (1959).
5. I. G. Dyad'kin and É. P. Batalina, at. Energ., 10, No. 1, 5 (1961).
6. D. A. Kozhevnikov and V. S. Khavkin, At. Energ., 27, No. 2, 142 (1969); 29, No. 5, 365 (1970); 29, No. 6, 448 (1970).
7. Yu. A. Medvedev et al., At. Energ., 38, No. 3, 156 (1975).
8. Yu. A. Medvedev and E. V. Metelkin, At. Energ., 42, No. 4, 331 (1977).
9. E. V. Metalkin and G. Ya. Trukhanov, At. Energ., 37, No. 6, 466 (1974).
10. E. V. Metelkin, At. Energ., 40, No. 1, 45 (1976).
11. R. Marshak, Rev. Mod. Phys., 19, No. 4, 185 (1947).
12. R. Bellman, R. Marshak, and M. Wing, Phil. Mag., 40, 297 (1949).
13. P. A. Yampol'skii, Neutrons of an Atomic Explosion [in Russian], Atomizdat, Moscow (1961).
14. I. A. Kozachok, V. V. Kulik, and V. I. Pirogov, At. Energ., 30, No. 6, 536 (1971).
15. H. Bateman and A. Erdelyi, Tables of Integral Transforms, McGraw-Hill, New York (1954).

RETARDATION IN MEDIUM OF VARIABLE DENSITY

A. A. Kostritsa

UDC 621.039.5

The theory of neutron transfer in varying media was considered in [1], where gas-phase reactors were the subject of discussion. In [2], the behavior of neutron gas was investigated in the case when the density ρ of the medium and the scattering path length l_S undergo significant variation in the residence time of the neutrons in the densifying medium. The variation of ρ and l_S amounts to $\sim(1+u_0/v)^3$, where u_0 is the velocity of the boundary of the medium toward its center, and v is the neutron velocity. This variation may be significant for thermal-neutron diffusion in a gaseous medium with u_0 larger than the velocity of sound (if l_S is comparable with the dimensions of the medium, and scattering is taken into account), and for retardation and diffusion of fast neutrons in the case of supercompression of the medium.

Consider the retardation of neutrons when the density of the medium changes; so as to be specific, rise in density will always be considered. The initial kinetic equation for the neutron distribution function f may be written in the form

$$\frac{\partial f}{\partial t}+v\left(\mu\frac{\partial f}{\partial r}+\frac{1-\mu^2}{r}\frac{\partial f}{\partial \mu}\right)+(\nu_s+\nu_a)f=\nu_s\int d\mathbf{v}'\,f'\int d\mathbf{u}\,\varphi(\mathbf{u})\,G(\mathbf{v}'\to\mathbf{v};\,\mathbf{u}) \tag{1}$$

$$+\frac{S(\mathbf{v})}{4\pi r^2}\,\delta(\mathbf{r})\,\delta(t-t_0),$$

where μ is the cosine of the angle between $\mathbf{v}$ and $\mathbf{r}$; $\varphi(\mathbf{u})$, distribution function of the atoms of the medium over the velocity u; the pulsed source $S(\mathbf{v})$ lies at the point $\mathbf{r}=0$ and emits neutrons isotropically in all directions; ν_S and ν_a, frequencies of scattering collisions and collisions leading to absorption, and are assumed to be independent of the neutron velocity, which implies decrease in the cross section with rise in neutron energy. The assumption that the collision frequency is independent of velocity is very sweeping, but allows the basic features of the considered phenomenon to be retained. The probability of change in velocity in scattering is determined by the function

$$G(\mathbf{v}'\to\mathbf{v};\,\mathbf{u})=\frac{(1+m)^2}{4\pi\,|\mathbf{v}'-\mathbf{u}|}\,\delta\left[\frac{|\mathbf{v}'-\mathbf{u}|^2}{2}-\frac{|\mathbf{v}-\mathbf{u}|^2}{2}-\frac{m}{2}(\mathbf{v}'-\mathbf{v})\right], \tag{2}$$

where m is the mass ratio of the neutron and the nucleus; scattering is assumed to be isotropic in the center-of-mass system.

The moments of the distribution function are now introduced; these are quantities averaged over the velocity and coordinate spaces, i.e., quantities of the form

$$\langle r^2\rangle=\frac{\int_0^\infty dr\,4\pi r^2\int d\mathbf{v}\,r^2 f}{\int_0^\infty dr\,4\pi r^2\int d\mathbf{v}\,f}. \tag{3}$$

A velocity distribution of the atoms that is isotropic over all directions is assumed, and the system of equations for the moments is written

$$\frac{d\langle r^2\rangle}{dt}=2\langle rv\mu\rangle; \tag{4}$$

$$\frac{d\langle rv\mu\rangle}{dt}+\frac{\nu_s}{1+m}\langle rv\mu\rangle=\langle v^2\rangle; \tag{5}$$

$$\frac{d\langle v^2\rangle}{dt}+\frac{2m\nu_s}{(1+m)^2}\langle v^2\rangle=\frac{2\nu_s u_T^2}{(1+m)^2}+\langle v_0^2\rangle\,\delta(t-t_0), \tag{6}$$

where u_T^2 is the mean square velocity of the atoms; $\langle v_0^2\rangle$ is the mean square velocity of neutrons emitted by the source.

Translated from Atomnaya Énergiya, Vol. 48, No. 5, pp. 313-315, May, 1980. Original article submitted June 4, 1979.

0038-531X/80/4805-0317$07.50

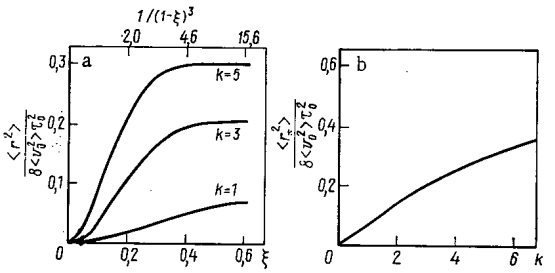

Fig. 1

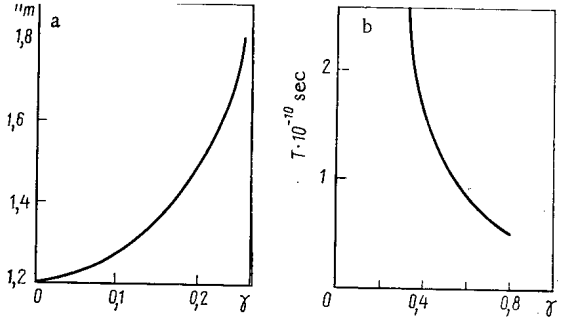

Fig. 2

Fig. 1. Mean-square distance of neutrons from source and dependence on time and degree of compression for m = 0.5 (a) and maximum value of $\langle r_*^2 \rangle$ as a function of the compression rate for m = 0.5 (b).

Fig. 2. Evolution of pulse with initial distribution of energy over the ^{238}U fission spectrum in an infinite medium: a) number of particles at the peak referred to the initial number; b) period of exponential increase in neutron pulse as a function of γ.

From Eqs. (4)-(6), it is easy to find the time dependence of the mean-square velocity of the neutron gas, $\langle v^2(t) \rangle$, and of the mean-square distance of neutrons with such a mean energy from the source, $\langle r^2(t) \rangle$. It is assumed that u_T^2 is constant, the time t is measured from t_0, and two particular cases are considered.

1. Suppose that ν_S is independent of the time. Then

$$\langle v^2(t) \rangle = \frac{u_T^2}{m} + \left(\langle v_0^2 \rangle - \frac{u_T^2}{m} \right) \exp\left[-\frac{2mt}{(1+m)\tau_1} \right], \tag{7}$$

where $\tau_1 = (1+m)\tau$; $\tau = 1/\nu_S$ is the mean time between scattering collisions and

$$\langle r^2(t) \rangle = 2\tau_1 \left\{ \frac{u_T^2}{m} \left[t - \tau_1 \xi_1 - \frac{1+m}{1-m} \tau_1 \left(\frac{1+m}{2m} \xi_2 - \xi_1 \right) \right] + \frac{1+m}{1-m} \langle v_0^2 \rangle \tau_1 \left(\frac{1+m}{2m} \xi_2 - \xi_1 \right) \right\}, \tag{8}$$

where

$$\xi_1(t) = 1 - \exp\left(-\frac{t}{\tau_1} \right);$$
$$\xi_2 = 1 - \exp\left(-\frac{2m}{1+m} \frac{t}{\tau_1} \right). \tag{9}$$

If the thermal motion of the atoms is neglected, the linear dependence of $\langle r^2 \rangle$ on t, which is characteristic of diffusion, disappears, and attention is confined to the retardation stage. If in the course of retardation the energy changes by 6-7 orders of magnitude, then $\langle r^2(t) \rangle$ stops changing somewhat earlier than the relaxation of $\langle v^2(t) \rangle$ is complete, and becomes equal to

$$\langle r^2(\infty) \rangle = \frac{(1+m)^3}{m} \tau^2 \langle v_0^2 \rangle. \tag{10}$$

At small m (medium of heavy nuclei), the migration area is larger, but its minimum value occurs at m = 0.5 and not at m = 1.

2. Suppose that ν_S increases with time according to the formula $\nu_S = \nu_{S0}/(1-\xi)^3$. If a sphere of initial radius R is compressed, and the boundary moves toward the center of the sphere at a velocity u_0, then $\xi = u_0 t/R$.

Then Eqs. (4)-(6) give

$$\langle v^2(t) \rangle = \frac{u_T^2}{m} \left\{ 1 - \exp\left[-\frac{2m}{(1+m)^2} \zeta(t) \right] \right\} + \langle v_0^2 \rangle \exp\left[-\frac{2m}{(1+m)^2} \zeta(t) \right]; \tag{11}$$

$$\langle r^2(t) \rangle = 2\frac{u_T^2}{m} \int_0^t dt' \exp\left[-\frac{\zeta(t')}{1+m} \right] \int_0^{t'} dt'' \exp\left[\frac{\zeta(t'')}{1+m} \right] + 2\left(\langle v_0^2 \rangle - \frac{u_T^2}{m} \right) \int_0^t dt' \times$$

$$\exp\left[-\frac{\zeta(t')}{1+m} \right] \int_0^{t'} dt'' \exp\left[\frac{1-m}{(1+m)^2} \zeta(t'') \right], \tag{12}$$

where

$$\zeta(t) = \int_0^t \nu_s\, dt'. \tag{13}$$

Now consider the neutron migration area under the assumption $u_T^2 = 0$, or specifically

$$\frac{\langle r^2(t)\rangle}{8\langle v_0^2\rangle \tau_0^2} = k^2 \int_0^{\xi} dz \exp\left\{-\frac{k}{1+m}\left[\frac{1}{(1-z)^2}-1\right]\right\} \int_0^{z} dy \exp\left\{\frac{1-m}{(1+m)^2}\, k\left[\frac{1}{(1-y)^2}-1\right]\right\}, \tag{14}$$

where $k = R\nu_{S0}/2u_0$; $\xi = u_0 t/R$; $\tau_0 = 1/\nu_{S0}$.

It is simple to pass from ξ to t using the relation $t/\tau_0 = 2k\xi$. The quantity k characterizes the compression rate $u_0/\langle v_0\rangle = R/2kl_{S0}$ if $l_{S0} = \langle v_0\rangle \tau_0$. Small k corresponds to rapid compression.

The dependence of $\langle r^2\rangle$ on ξ and the degree of compression is shown in Fig. 1a. As a result of the increase in density of the medium, the neutrons quickly perform the number of collisions necessary to reach a standstill in a cold medium. The limiting value $\langle r_*^2\rangle$ to which $\langle r^2(t)\rangle$ quickly tends is significantly less than $\langle r^2(\infty)\rangle$ as given by Eq. (10). When $k \sim 1$, $\langle r_*^2\rangle \leqslant l_{s0}$ and weakly depends on m. The dependence of $\langle r_*^2\rangle$ on k for m = 0.5 is shown in Fig. 1b. With increase in compression rate, the minimum of $\langle r_*^2\rangle$ (which corresponds to m = 0.5 in the absence of compression) is shifted toward smaller m.

To what degree are the results obtained here by the moment method applicable to a finite region of radius R? A rigorous condition of applicability is the requirement that neutrons on a straight path are not able, in the course of retardation, to pass beyond the limits of the region, which is equivalent to the inequality $R/l_{s0} \geqslant 2k\xi/(1-\xi)$. It is evident from Fig. 1a that when k = 5 the retardation process ends when $\xi \approx 0.35$–0.4, i.e., it is necessary that $R/l_{S0} \approx 6$. The mean-square distance of neutrons from the source amounts in this case to $\langle r_*^2\rangle \approx 0.3 \cdot 8 \times \langle v_0^2\rangle \tau_0^2 \approx 2.4\, l_{s0}^2$, but the condition $R/l_{S0} \geqslant 1.6$ would be too weak.

The above discussion, based on Eqs. (4)–(6), has a significant deficiency, in that it takes no account of the velocity of directed motion of the medium toward the center of the target. The entrainment of neutrons to the center is a complex process, since the heating of the neutron gas plays an important role, especially in a medium of heavy nuclei [2]. The heating of the neutron gas amplifies its migration. At a small target, those neutrons which undergo major collisions remain, but they accumulate energy in collisions in the centrally symmetric flow of heavy nuclei, i.e., a phenomenon inverse to diffusional cooling is observed. In [3], it was noted that when the velocity of directed nuclear motion is $\sim 5 \cdot 10^6$ m/sec, heating of the neutron gas, together with the increase in energy of the medium due to fission neutrons may compensate the neutron energy losses in inelastic collisions on ^{238}U. This conclusion may be illustrated by the results of numerical calculation for centrally symmetric uniform motion of heavy nuclei. In Fig. 2a, the number of neutrons n_m at the pulse peak (in an infinite medium of ^{238}U) is shown as a function of $\gamma = u_0/v_1$, where v_1 is the velocity of neutrons with an energy of 1 MeV. The initial number of neutrons is taken to be unity, and their initial energy is distributed over the fission spectrum. The time for the number of neutrons to rise by a factor of e is shown as a function of γ in Fig. 2b.

LITERATURE CITED

1. V. M. Novikov and S. B. Shikov, Preprint IAÉ-2340, Moscow (1973); Preprint IAÉ-2381, Moscow (1974).
2. A. A. Kostritsa, Izv. Akad. Nauk Kaz. SSR, Ser. Fiz.-Mat., No. 4, 67 (1977).
3. A. A. Kostritsa, Izv. Akad. Nauk Kaz. SSR, Ser. Fiz.-Mat., No. 2, 90 (1979).

IRRADIATION LEVELS OF PROFESSIONALLY EXPOSED GROUPS AND RADIATION-MONITORING OPTIMIZATION

V. I. Ivanov, I. P. Korenkov, and O. N. Salimov

UDC 621.039.76(063)

The extensive use of atomic energy for peaceful purposes is one of the characteristic features of the present time; techniques based on ionizing radiation not only provide technical progress but also bring an enormous economic return, which is over 250 million rubles a year in this country [1].

In earlier times, the use of ionizing radiations for peaceful purposes was the concern of a restricted number of organizations, but now it is difficult to name any sphere of the economy where radiation is not employed. In recent years alone, Soviet industry has produced over 10,000 γ-ray flaw detectors, 60,000 radioisotope instruments, and over 50 high-power γ-ray systems containing sources up to 50 Ci (1 Ci = $3.700 \cdot 10^{10}$ Bq) [2].

Radioisotopes are particularly widely used in medicine; in 1965, there were 17,500 x-ray sections in this country, which were equipped with 35,000 x-ray sets and 21,000 fluorographs, while there were over 200 departments of radiology. At the beginning of 1977, the number of x-ray sections exceeded 30,000, with over 48,000 x-ray sets, and there were more than 600 radiological departments [3].

The uses of radioisotopes in COMECON member-countries also increased considerably. For example, the use of radioisotopes in Czechoslovakia has increased by a factor 6-7 in the last 10 years, while the number of medical organizations employing radioactive preparations has increased by a factor 2.5. The annual increase in the consumption of radioactive medical preparations is 20-30% [4].

Radioisotopes are also widely used in other countries. Data from the United States Atomic Energy Commission indicate that 5000 American clinics and hospitals use radioactive substances for therapeutic and diagnostic purposes. The value of the annual output of isotopes for medical radiology is 700 million dollars [5].

Particularly promising lines of radioisotope use in medicine include afterloading methods, the use of ^{252}Cf for intracavity and intratissue therapy, and the use of short-lived isotope generators for diagnostic purposes [6-8].

Any use of ionizing radiation involves a radiation hazard, so it is particularly important to monitor irradiation levels of staff in view of the increasing scales of the use of atomic energy. Also, data from such observations are of great practical significance in evaluating the performance of protection measures and the relative hazards of various technological processes.

During the past 15 years we have used film dosimetry to determine individual radiation doses for ionizing-radiation workers in various branches of the economy. We used IFK-2, 3 M, and IFKU cassettes placed on the chest, with exposure times of 30 days. The films were calibrated of VNIIM. The usual methods were employed to process the working and monitor films.

Figure 1 shows that the irradiation levels for various professionally exposed groups range from 0.2 to 4.0 rad/yr (1 rad = 0.01 Gr). The largest doses were received by workers in medical organizations concerned with intracavity therapy, x-ray diagnosis, and radioisotope diagnosis by means of short-lived isotope generators.

An important part in routine monitoring is occupied by sample choice for the various professional groups. The mean or collective dose is used in evaluating the remote effects of irradiation:

$$\langle D \rangle = \int_0^\infty Dw(D)\,dD;$$

$$S = \int_0^\infty DN(D)\,dD,$$

Translated from Atomnaya Énergiya, Vol. 48, No. 5, pp. 315-318, May, 1980. Original article submitted July 3, 1979.

0038-531X/80/4805-0320$07.50

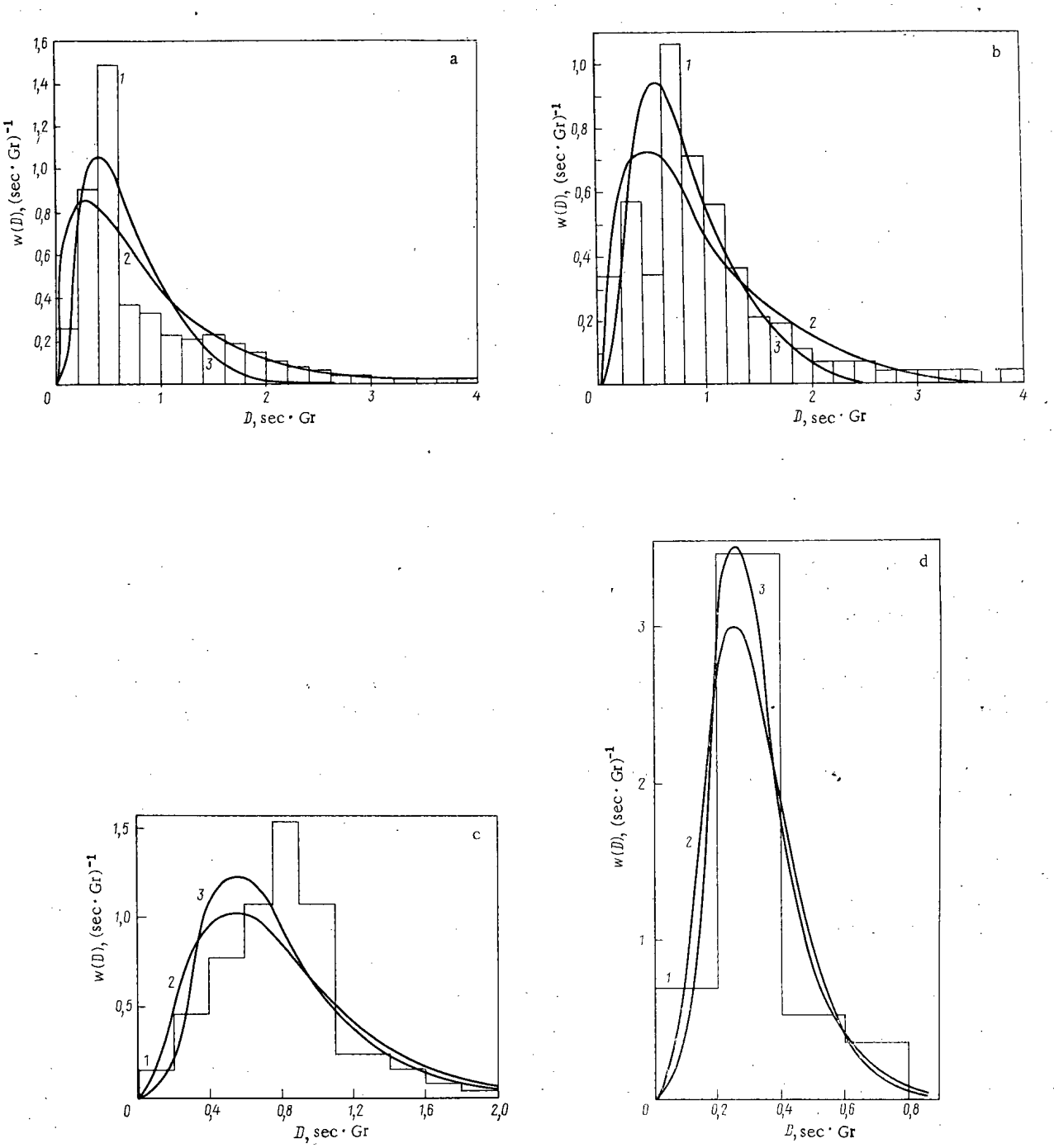

Fig. 1. Approximation of the annual dose distribution for medical staff performing: a) x-ray diagnosis; b) intracavity therapy; c) radioisotope diagnosis; d) teletherapy: 1) actual distribution; 2) γ distribution; 3) log-normal distribution; 1 centiGray (cGr) = 0.01 Gray (Gr).

where N is the total number of persons irradiated and w(D) is the dose distribution, which is related to the former by N(D) = w(D)N.

However, the mean number of remote radiobiological effects may vary with the dose distribution for identical values for the mean and for the same dose-effect response. A set of moments gives a fuller description [9] of any dose distribution:

$$m_n = \int_0^\infty D^n w(D)\, dD \quad (d = 1, 2, \ldots).$$

One can approximate the dose distribution analytically in order to standardize the data on the population dose structure. A log-normal distribution has been used [10], while the γ distribution has been employed also [11, 12]:

$$\gamma(D) = \frac{\beta^{\alpha}}{\Gamma(\alpha)} D^{\alpha-1} e^{-\beta D},$$

where α and β are parameters of the dose distribution; $\Gamma(\alpha) = \int_0^{\infty} y^{\alpha-1} e^{-y} dy$, Γ function; and y, variable of integration.

The origin moments for the dose distribution are then given by

$$m_n = \Gamma(\alpha+n)/\Gamma(\alpha)\beta^n \quad (n = 1, 2, \ldots). \tag{1}$$

The parameters α and β are found from the origin moments m_1 and m_2:

$$\beta = m_1/(m_2 - m_1^2); \quad \alpha = m_2\beta.$$

The position of the peak D_0 in the γ distribution can be determined by equating the first derivative to zero:

$$[\gamma(D)\Gamma(\alpha)]' = D^{\alpha-1} e^{-\beta D}\left(\frac{\alpha-1}{D} - \beta\right) = 0.$$

Then

$$D_0 = (\alpha-1)/\beta. \tag{2}$$

Figure 1 shows the approximation results for medical staff performing various procedures; one can select an analytical approximation and compare for example the third central moments for the actual and approximating distributions.

A knowledge of the distribution enables one to use the sample volume for routine dosimetric monitoring; it also allows one to define the optimum technique. Subject to certain assumptions one can obtain the relative error δ_1 in determining the first moment (mean dose) as expressed by the following [11]:

$$\delta_1 = \delta + b_1 N^{-1/2}, \tag{3}$$

where δ is the relative error in measuring the individual dose and

$$N = \sum_i N_i; \quad b_1 = \frac{1}{m_1} \int_0^{\infty} D \sqrt{w(D)}\, dD;$$

where N_i is the number of workers receiving doses in the range from D_i to $D_i + \Delta D_i$ (subscript i characterizes the division of the doses into intervals ΔD_i). One can calculate the necessary sample volume N subject to given errors in the mean dose and a given error in measuring the individual doses. It follows from (3) that

$$N = [b_1/(\delta_1 - \delta)]^2.$$

Numerical values have been given for N for professionally exposed groups as considered here [12].

Each professional group has its own dose distribution and own number; this approach allows one to determine the necessary sample volume for staff as a whole. This involves determining the best way of distributing the total sample volume over the professionally exposed groups with the object of reducing the statistical error in measuring the moments. This problem can be solved by analyzing the errors in moment calculation.

The problem is that of defining a conditional turning point. Analytical solutions have been derived for cases where the dose distributions are represented by histograms or analytical relationships. The optimal sample volume has been calculated for each professional group.

The data have been used in calculating the probability of exceeding a specified dose ($\frac{1}{3}$ of the maximum permissible dose) for various professional groups. The value is 0.3 for staff performing x-ray diagnosis and intracavity therapy by traditional methods of source handling; the corresponding value for radioisotope diagnosis by traditional methods is 0.035; the value for teletherapy is $3 \cdot 10^{-5}$; and that for generator operation is 0.3.

It is therefore essential to employ individual monitoring in x-ray diagnosis and in radioisotope diagnosis by means of short-lived isotope generators (in the first stage of use). It is also desirable to perform individual monitoring in automated teletherapy, cavity therapy, and traditional methods of radioisotope diagnosis.

LITERATURE CITED

1. A. M. Petros'yants, From Scientific Research to Nuclear Industry: Current Problems in Nuclear Science and Technology in the USSR [in Russian], 3rd edition, Atomizdat, Moscow (1976).
2. O. G. Pol'skii and V. Ya. Golikov, in: Proceedings of the Third Conference on Radiation Safety [in Russian], Izd. VTsNIIOT, Moscow (1976), p. 7.
3. O. G. Pol'skii, I. P. Korenkov, and V. M. Kaloshin, Izotopy v SSSR, No. 47, 23 (1977).
4. J. Hokr, Yad. Energ., 20, No. 10, 331 (1974).
5. Glenn T. Seaborg, At. Tekh. Rubezhom, No. 4, 38 (1972).
6. Afterloading in Radiotherapy, New York (1971), p. 302.
7. A. S. Pavlov et al., USSR Paper No. 437 at the Fourth Geneva Conference, 1971.
8. A. S. Pavlov, A. M. Pirogov, and A. Kh. Trakhtenberg, Treatment of Lung Cancer [in Russian], Meditsina, Moscow (1978), p. 258.
9. V. I. Ivanov and O. N. Salimov, in: Dosimetry and Radiation Protection [in Russian], Issue 18, Atomizdat, Moscow (1979), p. 65.
10. Sources and Effects of Ionizing Radiation. U. N. Scientific Committee on the Effects of Atomic Radiation. Report to the General Assembly, New York, 1977.
11. O. N. Salimov, V. I. Ivanov, and L. V. Kleimenova, "Distribution in x-ray section staffs in relation to profession," in: Proceedings of the Conference on Working Conditions and Health of Medical Workers [in Russian], Palanga, 19-21 September, 1977.
12. V. Ya. Golikov et al., in: Abstracts for the Second All-Union Conference on Ionizing Radiation Protection for Nuclear-Engineering Systems [in Russian], MIFI, Moscow (1978), p. 93.

NONLINEAR DEPENDENCE OF INTENSITY EFFECTS ON NUMBER OF PARTICLES IN RING CURRENT

S. G. Arutyunyan and G. A. Nagorskii

UDC 621.384.6.01

The design of large-current accelerators and accumulators depends on intensity effects, i.e., on the influence of the intrinsic beam field on the dynamics of its motion. This field is usually found from Maxwell's equations, in the right-hand side of which are substituted averaged values of the beam charge and current.

In addition, it is assumed that the field of the beam charges coincides with the field of charged particles moving uniformly in a straight line [1].

In the present work, the problem of self-action of a ring current is considered (calculations for more complex current configurations are complicated). The accurate Lienar–Vikhert formulas [2] may be written for the field of particles moving over a circle at a constant velocity. Then, using the Plan summation method [3], the Lorentz force acting on one particle from all the others is found. In the formulas obtained, a nonlinear dependence on the number of particles in the ring current is seen. Various particular cases of the formulas obtained will be considered.

It will be shown that in the ultrarelativistic case for the given problem it is impossible to use the approximation of the field of a charge moving in a straight line for any current density.

Instantaneous Picture of the Field

The electrical and magnetic fields produced by particles of energy γ, in units of mc^2, moving over a circle of radius R at an observation point with the coordinates $(\rho+R, \Phi, z)$ in a cylindrical coordinate system at time t are found.

It is expedient to write the vector from the particles at a later time t' directed to the observation point in the form $\frac{R\Delta}{\beta}[\nu_1 e_1(\theta)+\nu_2 e_2(\theta)+\nu_3 e_3]$, where $\mathbf{e}_i$ are the unit vectors of the cylindrical coordinate system; $\theta = -\Delta < 0$, azimuthal angle of the particle at the time t'; βc, particle velocity. The directional cosines ν_1, ν_2, and ν_3 are

Translated from Atomnaya Énergiya, Vol. 48, No. 5, pp. 318-321, May, 1980. Original article submitted January 8, 1979.

0038-531X/80/4805-0323$07.50

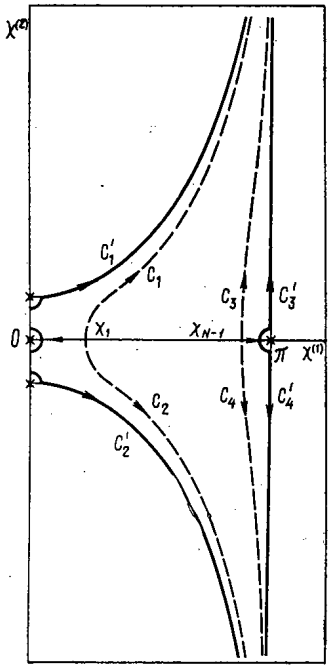

Fig. 1. Complex contour of the applied integration χ of Eq. (9) – – –) c_k (k = 1, 2, 3, 4) contours of integration; ——) c'_k contour of integration in the boundary $N \to \infty$ excluding the segments set of zeros $[0, \chi_1]$, $[\chi_{N-1}, \pi]$ obtained for deformation of c_k from c'_k.

$$\begin{aligned} \nu_1 &= (\beta/\Delta)\,[(1 + \rho/R)\cos(\Phi + \Delta) - 1]; \\ \nu_2 &= (\beta/\Delta)\,[1 + \rho/R]\sin(\Phi + \Delta); \\ \nu_3 &= (\beta/\Delta)\,(z/R). \end{aligned} \tag{1}$$

The following relation is obtained for determining Δ

$$\Delta^2/\beta^2 = 1 + (1 + \rho/R)^2 - 2\,(1 + \rho/R)\cos(\Phi + \Delta) + (z^2/R^2). \tag{2}$$

Using the formulas for the potentials at t', the fields E and H at the point of observation $(\rho + R, \theta, z)$ are written as a function of the parameters $\nu_1, \nu_2, \nu_3, \Delta$:

$$E = \frac{e\beta^2}{(R\gamma\Delta)^2(1-\beta\nu_2)^3}\{[\beta\gamma^2\Delta\,(1-\beta\nu_2) + \nu_1\,(1 - \tag{3}$$

$$-\beta\gamma^2\Delta\nu_1)]\,\mathbf{e}_1(\theta') + (1-\beta\gamma^2\Delta\nu_1)\,[(\nu_2-\beta)\,\mathbf{e}_2(\theta') + \nu_3\mathbf{e}_3]\};$$

$$H = \frac{e\beta^3}{(R\gamma\Delta)^2(1-\beta\nu_2)^3}\{\nu_3\,[(1-\beta\gamma_1\gamma^2\Delta)\,\mathbf{e}_1(\theta') + \gamma^2\Delta\,(1-\beta\nu_2)\,\mathbf{e}_2(\theta') - [\nu_1 + \gamma^2\Delta\nu_2 - \beta\gamma^2\Delta\,(\nu_1^2+\nu_2^2)]\,\mathbf{e}_3\}. \tag{4}$$

Ring Current

The self-action of a ring system of N particles moving at equal intervals over a circle of radius R will be calculated. Using Eqs. (3) and (4) with z = 0 and $\rho = 0$, the radial ($f_\perp$) and tangential ($f_\parallel$) components of the Lorentz force which acts on one particle at an angular distance of Φ from another may be written in the form

$$\frac{4R^2}{e^2} f_\perp = \left[\frac{1+\beta^2}{(1-\beta\cos\chi)\sin\chi} - \frac{\beta^2\sin\chi}{\gamma^2(1-\beta\cos\chi)^3}\right] \equiv g_\perp(\chi); \tag{5}$$

$$\frac{4R^2}{e^2} f_\parallel = \left[\frac{\beta+\cos\chi}{(1-\beta\cos\chi)\sin^2\chi} + \frac{\beta^2(\beta-\cos\chi)}{(1-\beta\cos\chi)^3}\right] \equiv g_\parallel(\chi), \tag{6}$$

where the angle $\chi = (\Phi + \Delta)/2$ satisfies the following expression, which follows from Eq. (2)

$$\chi = \Phi/2 + \beta\sin\chi. \tag{7}$$

The total Lorentz force F acting on each of the N particles is written as a sum

$$F_{\perp,\parallel} = \sum_{j=1}^{N=1} f_{\perp,\parallel}(\chi_j), \tag{8}$$

where χ_j is the solution of Eq. (7) with $\Phi = 2\pi j/N$ (j = 1, ..., N−1).

j in Eq. (8) is replaced by integration over $\chi = \chi(j)$.

As a result, Eq. (8) is replaced by the formula

$$F_{\perp,\parallel} = \frac{1}{2}[f_{\perp,\parallel}(\chi_1) + f_{\perp,\parallel}(\chi_{N-1})] + \frac{N}{\pi}\int_{\chi_1}^{\chi_{N-1}} f_{\perp,\parallel}(\chi)(1-\beta\cos\chi)\,d\chi + \frac{N}{\pi}\sum_{k=1}^{4}\mu_k\int_{c_k}\frac{f_{\perp,\parallel}(\chi)(1-\beta\cos\chi)\,d\chi}{\exp\{2i\varepsilon_k N(\chi-\beta\sin\chi)\}-1}, \tag{9}$$

where $-\mu_1 = -\mu_2 = \mu_3 = \mu_4 = -\varepsilon_1 = \varepsilon_2 = -\varepsilon_3 = \varepsilon_4 = 1$, and the integration contour c_k in the plane $\chi = \chi^{(1)} + i\chi^{(2)}$ is chosen so that the imaginary part of the exponential is constant. The contours c_k, depending on the number of particles N, may expediently be combined with the limiting contours c_k', to which the contours c_k transform as $N \to \infty$. The circumvention of the poles is indicated in Fig. 1. The resulting additional contributions along the real axis are combined with the first integral term in Eq. (9). Reducing the integrals over the contours c_k' to integrals over the real axis leads to the following formula for the radial component of the Lorentz force

$$\frac{4R^2}{e^2}F_\perp = -\frac{2N(1+2\beta^2)}{\pi} - \frac{2\beta^2(1+\beta^2)\gamma^3}{\pi} - \frac{\beta N}{\pi(E-1)}\times$$

$$\times\left[(1+\beta^2)\left(2+\beta\ln\frac{1+\beta}{1-\beta}+1-\beta\right]+\frac{1}{2}[g_\perp(\chi_1) + g_\perp(\chi_{N-1})] + \frac{N(1+\beta^2)}{\pi}\int_0^{\ln\frac{\gamma+1}{\beta\gamma}} dx\ln\frac{\operatorname{ch}x+1}{\operatorname{ch}x-1}\frac{d}{dx^2}\times\right.$$

$$\times\left(\frac{\operatorname{th}x}{\exp\{2N(x-\beta\operatorname{sh}x)\}-1}\right) - \frac{4\beta^2 N}{\pi\gamma^2(1+\beta)^2}\int_0^{\ln\frac{\gamma+1}{\beta\gamma}}\frac{dx}{\gamma(1-\beta)-\operatorname{th}\frac{x}{2}}\frac{d}{dx}\times \tag{10}$$

$$\times\left(\frac{1}{\operatorname{ch}^2\frac{x}{2}\left[\gamma(1-\beta)+\operatorname{th}\frac{x}{2}\right]^2(\exp\{2N(x-\beta\operatorname{sh}x\}-1)}\right) + \frac{N(1+\beta^2)}{\pi}\int_0^\infty dx\ln\frac{\operatorname{ch}x+1}{\operatorname{ch}x-1}\frac{d}{dx^2}\times$$

$$\times\left(\frac{\operatorname{th}x}{\exp\{2N(x+\beta\operatorname{sh}x)\}-1}\right) + \frac{2\beta N}{\pi}\int_0^\pi\frac{dx}{\exp\{2NG\}-1}\left[\frac{(1+\beta^2)(x+A\operatorname{ctg}x)}{x^2+D\operatorname{ctg}^2x}+\right.$$

$$\left.\left.+\frac{A^2(A\operatorname{ctg}x-3x)+D(x-3A\operatorname{ctg}x)}{\gamma^2(A^2+D)^2}\right] + \frac{2N\beta^2}{\pi\gamma^2}\int_0^\infty\frac{dx}{\exp\{2N(x+\beta\operatorname{sh}x)\}-1}\frac{\operatorname{sh}x}{(1+\beta\operatorname{ch}x)^2},\right.$$

while for the tangential component of the Lorentz force

$$\frac{4R^2}{e^2}F_\parallel = \frac{8}{3}\beta^3\gamma^4 + \frac{1}{2}[g_\parallel(\chi_1) + g_\parallel(\chi_{N-1})] + \frac{2\beta N}{\pi}\int_0^\pi\frac{dx}{\exp\{2NG\}-1}\left[\frac{2A}{A^2+D} - \frac{4A^2}{\gamma^2(A^2+D)^2}+\right.$$

$$\left.+\frac{(1+\beta^2)(x+A\operatorname{ctg}x)^2-(A^2+D)\operatorname{ctg}x[2x+(1+\beta^2)\operatorname{ctg}x]}{(x^2+D\operatorname{ctg}^2x)^2}\right] + \frac{2\beta N}{\pi}\int_0^\pi dx\operatorname{ctg}x\frac{d}{dx}\left(\frac{\sin^2x}{(A^2+D)(\exp\{2NG\}-1)}\right), \tag{11}$$

where

$$E = \exp\left\{2N\left(\ln\frac{\gamma+1}{\beta\gamma} - \frac{1}{\gamma}\right)\right\};\quad A = 1 - x\operatorname{ctg}x;$$

$$D = x^2 - \beta^2\sin^2x;\ G = \ln[(x+\sqrt{D})/(\beta+\sin x)] - \sqrt{D}\operatorname{ctg}x.$$

It is evident that the Lorentz force depends on two parameters: N and γ. However, analysis of the exponential behavior shows that the characteristic parameters of the problem are $\overset{*}{N} = N/\gamma^3$ and γ. For existing high-energy particle accelerators and accumulators, $\overset{*}{N} \leqslant 1$ [4]; in this case, almost all the terms in Eqs. (10) and (11), except the last term in Eq. (10), are of the same order, and depend on $\overset{*}{N}$ in a significantly nonlinear manner.

In the ultrarelativistic case, when $\gamma \gg 1$, the functions $F_\perp$ and $F_\parallel$ are expanded in series in inverse powers of γ^2

$$F_{\perp,\parallel} = \gamma^{a_{\perp,\parallel}}\sum_{n=0}^{\infty}F_{\perp,\parallel}^{(n)}(\overset{*}{N})\,\gamma^{-2n}, \tag{12}$$

where $a_\perp = 3$, $a_\parallel = 4$. After replacing the variable of integration x by z/γ, it becomes obvious that only terms to the fourth power appear in the sum. Note that it is possible for $F^{(n)}(\overset{*}{N})$ to depend on $\ln\gamma$. At large γ, only the first nonvanishing term of the expansion in Eq. (12) exists.

The expression obtained for the radial component in the case $\overset{*}{N} \gg \gamma^{-3}$ is of the form

$$F_{\perp}^{(0)}(\overset{*}{N}) = -\frac{3\overset{*}{N}}{\pi} + \frac{2C\overset{*}{N}}{\pi} - \frac{8}{\pi} + \frac{2\overset{*}{N}}{\pi} \ln \frac{8\overset{*}{N}\gamma^4}{\pi} + \frac{4\overset{*}{N}}{\pi(1-M)} + \frac{2(1+u^4)}{u(1+u^2)^3} - \frac{4\overset{*}{N}}{\pi}\int_0^1 dz \ln z \frac{d^2}{dz^2} \times$$

$$\left\{\frac{z}{\exp[k(z)]-1}\right\} - \frac{8\overset{*}{N}}{\pi}\int_0^1 \frac{dz}{(1+z)^3} \frac{\exp[k(z)][1-\overset{*}{N}z(1+z)^2]-1}{\{\exp[k(z)]-1\}^2} + \frac{8\overset{*}{N}}{\pi}\int_0^\infty \frac{dz}{\exp[p(z)]-1}\left[\frac{1}{3+4z} - \frac{3}{(9+4z)^2}\right], \quad (13)$$

where C is an Euler constant; $M = \exp(2\overset{*}{N}/3)$; also

$$u = \left(\sqrt{\frac{9\pi^2}{\overset{*}{N}^2} + 1} + \frac{3\pi}{\overset{*}{N}}\right)^{1/3} - \left(\sqrt{\frac{9\pi^2}{\overset{*}{N}^2} + 1} - \frac{3\pi}{\overset{*}{N}}\right)^{1/3}$$

is the real root of the equation $u^3 + 3u - 6\pi/\overset{*}{N} = 0$; $k(z) = \overset{*}{N}z(1 - z^2/3)$; and $p(z) = (2\overset{*}{N}/3)(1 + 4z/3)\sqrt{(1 + z/3)}$.

In the limiting case $\gamma^{-3} \ll \overset{*}{N} \ll 1$, the first nonvanishing term in Eq. (12) takes the form

$$F_{\perp}^{(0)}(\overset{*}{N} \to 0) = 1/2\pi. \quad (14)$$

In the other limiting case $\overset{*}{N} \gg 1$, the first term of the asymptotic expansion in Eq. (12) takes the form

$$F_{\perp}^{(0)}(\overset{*}{N} \to \infty) = \frac{4\overset{*}{N}}{\pi}\left(\ln \frac{2\overset{*}{N}\gamma^2}{\pi} + C\right). \quad (15)$$

Note that the formula for the radial force obtained in the approximation of the field of a charge moving in a straight line contains an additional factor $\sim\gamma^{-2}$ in comparison with Eq. (15). For $\overset{*}{N} \sim 1$, all the terms in Eq. (13) are comparable in size.

The ratio of the radial component $F_{\perp}$ of the beam self-action to the external force maintaining circular motion of a single particle over a path of radius R may be of the order of unity in certain cases (e.g., in adhesators, where $\gamma \sim 10$, $N \sim 10^{13}$, $R \sim 1$ cm [5]). However, for large electron and proton accumulators and accelerators, the important factor is not this ratio, which is less than unity for such machines, but the frequency shift of the betatron oscillations arising due to beam self-action. The corresponding analysis, while of considerable interest, is beset by great computational difficulties.

For the tangential component in the case $\overset{*}{N} \gg \gamma^{-3}$, the first term of the expansion in Eq. (12) takes the form

$$F_{\parallel}^{(0)}(\overset{*}{N}) = \frac{8}{3} + \frac{2(1+u^2+2u^4)}{u^2(1+u^2)^3} - \frac{\overset{*}{N}^2}{2\pi^2} + \frac{12\overset{*}{N}}{\pi}\int_0^\infty \frac{dz}{\exp\{p(z^2)\}-1}\left[\frac{1}{9+4z^2} - \frac{6}{(9+4z^2)^2} - \right.$$

$$\left. - \frac{3-4z^2}{(3+4z^2)^2}\right] + \frac{18\overset{*}{N}}{\pi}\int_0^\infty \frac{dz}{z}\frac{d}{dz}\left(\frac{1}{(9+4z^2)(\exp\{p(z^2)\}-1)}\right). \quad (16)$$

In the limiting case $\gamma^{-3} \ll \overset{*}{N} \ll 1$, Eq. (16) gives

$$F_{\parallel}^{(0)}(\overset{*}{N} \to 0) = -\left(\frac{1}{3} + \frac{\sqrt{3}}{2\pi}\right). \quad (17)$$

In the opposite limiting case when $\overset{*}{N} \gg 1$, the first term in Eq. (12) is

$$F_{\parallel}^{(0)}(\overset{*}{N} \to \infty) = \frac{112}{3}\frac{\pi^2}{\overset{*}{N}^2}. \quad (18)$$

The results obtained show that in calculating intensity effects it is desirable to take into account accurate formulas for the particle field and the discreteness of the beam current.

In conclusion, thanks are offered to A. Ts. Amatuni for numerous useful discussions of the problem and valuable comments.

LITERATURE CITED

1. G. Bruk, Cyclic Charged-Particle Accelerators [in Russian], Atomizdat, Moscow (1970).
2. L. D. Landau and E. M. Lifschitz, Field Theory [in Russian], Nauka, Moscow (1973).
3. E. T. Whittaker and G. N. Watson, Course of Modern Analysis, Cambridge Univ. Press (1927).
4. A. Ts. Amatuni and S. G. Artyunyan, Preprint EFI-288(13), Erevan (1978).
5. Proceedings of Fifth All-Union Conference on Charged-Particle Accelerators [in Russian], Vol. II, Nauka, Moscow (1977).

ISOTOPE ANALYSIS OF NANOGRAM URANIUM SAMPLES

R. N. Gall', A. M. Korochkin,
V. A. Lednev, B. N. Sokolov,
and V. N. Vyachin

UDC 621.384.83-034.822

Mass-spectometric isotope analysis of solid specimens in nuclear physics, geology, and cosmochemistry frequently involves the use of specimens perhaps as small as 10^{-10} g. Such specimens impose specific requirements on the apparatus and methods, and in particular the sensitivity of the mass spectrometer must be very high. This can be attained by surface ionization in the source, with use of a secondary-electron multiplier in the recording system and point scanning of the mass spectrum, which considerably reduces the sample loss during the analysis, and which also increases the accuracy while reducing the analysis time.

Tight specifications are laid down for the reproducibility of the analytical conditions with small samples, since even minor deviations such as in the working times or in the vacuum can cause appreciable loss of reproducibility. The working times may be standardized by automating the recording system, with subsequent automatic data processing. The provision of identical vacuum conditions makes it desirable not to use ion sources that require the spectrometer to be opened to change the sample. The mass spectrometer should also have low memory for previous samples, which is particularly important if the samples differ greatly in size or isotopic abundance.

These conditions are largely met for high-accuracy measurement of small samples by the MI 1320 mass spectrometer [1, 2]. This instrument has high technical characteristics: sample utilization factor 0.05%, limit of detection $2 \cdot 10^{-13}$ g, isotopic sensitivity $3 \cdot 10^{-6}$, convergence and reproducibility in the measurement of isotope ratios of better than 0.1 and better than 0.05% relative when the isotope ratios vary over the range 1 : 100. These characteristics relate to uranium specimens with near-natural isotope contents, and the accuracy parameters have been derived by the use of relatively large specimens (about 10^{-4} g of uranium).

Here we describe studies on the attainable accuracy with the MI 1320 for nanogram uranium samples. Solutions in nitric acid of concentration 0.3 N in uranyl nitrate were used with the natural isotope abundance (Table 1).

The specimens were deposited with a quartz capillary of diameter 0.2 mm, which was flushed several times with the uranyl nitrate solution before use in order to equilibrate the uranium concentrations in the bulb and within the capillary. Fresh capillaries were used for solutions differing in concentration. The error in determining the mass of the deposited sample was 10-12%. The sample was transferred from the capillary to the evaporator strip in the ion source in small droplets, with the first droplets evaporated at room temperature and the latter ones evaporated by passing a current through the strip. This method prevented the solution from spreading over the evaporator and enabled us to localize the specimen over a section of length 1-1.5 mm in the center.

TABLE 1. Concentrations of Solutions in Terms of Uranium for Various Sample Weights, $^{238}U^{+}$ Ion Current, and Multiplier Voltage

Specimen, g	Conc., g/ml	$^{238}I^{+}$, A	U_{mul}, kV
10^{-6}	10^{-3}	$2{,}5 \cdot 10^{-11}$	2,3
10^{-7}	10^{-4}	$3 \cdot 10^{-13}$	3,4
10^{-8}	10^{-4}	$7 \cdot 10^{-14}$	3,8
10^{-9}	10^{-5}	$2 \cdot 11^{-14}$	4,0

Translated from Atomnaya Énergiya, Vol. 48, No. 5, pp. 321-324, May, 1980. Original article submitted July 4, 1978; revision submitted May 23, 1979.

0038-531X/80/4805-0327$07.50

TABLE 2. Results for R_U with the Electron Multiplier

Analysis No.	Specimen, g			
	10^{-6}	10^{-7}	10^{-8}	10^{-9}
1	136,40±0,22	136,35±0,68	136,34±1,48	137,22±1,66
2	136,52±0,31	136,49±0,49	136,91±0,74	138,06±0,73
3	136,27±0,25	136,51±0,77	137,28±1,02	137,01±1,73
4	136,57±0,41	136,08±0,72	136,99±1,85	137,82±0,90
5	136,29±0,19	136,75±0,49	138,09±0,68	137,34±1,00
6	136,36±0,22	136,46±1,31	137,25±1,11	137,95±1,05
Mean values				
	136,40±0,13	136,44±0,22	137,14±0,57	137,56±0,43
Corrected values				
	137,78	137,82	138,56	138,95
Mean convergence, rel. %				
	0,20	0,54	0,84	0,86
Reproducibility, rel. %				
	0,1	0,16	0,42	0,31

A series of six analyses was performed for each specimen, in each of which 14-16 $^{238}U^+$ and $^{235}U^+$ mass spectra were recorded. These were taken in point readout, and the intensity of each peak was measured with a digital voltmeter of class 0.02, with the results passing to the computer in the mass spectrometer for processing. This processing involved averaging the intensities for each peak, making corrections for the change in ion current with time, correction for the zero drift of the electrometer amplifiers, calculation of the mean isotope ratio, and definition of the convergence in the results. The convergence was judged from the standard deviation of the isotope ratio and was assigned as the error of the analysis.

The series of analyses for each sample was used in calculating the arithmetic mean for the isotope ratio and the reproducibility, which was calculated as the standard deviation and taken as the error of measurement. For each analysis we used a fresh plate bearing evaporators (a tungsten strip $10 \times 0.6 \times 0.02$ mm) and ionizer (a rhenium strip $10 \times 0.8 \times 0.02$ mm).

Before the analysis, this block of ion sources was outgassed for 2-3 h in the chamber for outgassing these units, which involved general heating of the unit under vacuum to 250-300°C and heating the strips by passing currents through the evaporators (2 A) and the ionizer (3 A). The units before outgassing were cleaned mechanically and then washed with pure ethanol. This cleaning in combination with the outgassing ensured a low memory level. The memory effect was tested by using a unit without samples deposited, in which the working source conditions were operated. The multiplier recorded the $^{238}U^+$ ion current. With careful cleaning, the memory level for $^{238}U^+$ was not more than $3 \cdot 10^{-19}$ A, which was at the limit of detection of the instrument.

The outgassed unit bearing the specimens was passed through a gate device to the ion source. The heating current in the ionizer and in the evaporator was raised slowly until 1 A was reached in the evaporators and 3 A in the ionizer, after which only the ionizer current was raised until the working state was reached. This state was checked from the $^{187}Re^+$ ion current, which was 10^{-13} A at the ion-detector collector. This condition provided a reasonably high efficiency in ionization and long-term operation of the ionizer. Then the heating currents in the evaporators were increased until the working $^{238}U^+$ current was set up (Table 1), after which there followed a short delay of 10-12 min before analysis and determination of the isotope ratio $R_U = {}^{238}U/{}^{235}U$. This delay before the analysis is needed to ensure stability in the ion currents. This method of preparing the specimens provided a stable ion current, which varied by less than 10% during the analysis time (10-15 min).

The electron multiplier recorded the $^{238}U^+$ ion current corresponding to a potential difference across the input impedance of the electrometer amplifier of 17 V; this was attained by adjusting the gain in the electron multiplier, which assisted in producing reproducible analysis conditions, since then the error arising from the nonlinearity in the input impedance of the electrometer amplifier was constant.

The measurements were performed with a resolution $R_{10\%} = 400$ in the mass spectrometer and a residual-gas pressure in the analyzer of $p = 5 \cdot 10^{-9}$ mm Hg (1 mm Hg = 133.322 Pa), which provided an isotopic sensitivity for adjacent masses for uranium of about $5 \cdot 10^{-6}$.

Table 2 gives results for R_U for natural uranium for various sample masses made by means of the secondary-electron multiplier, where the results are distorted by discrimination effects in the multiplier [3-5]. Discrimination effects were allowed for by means of a series of analyses of samples of 10^{-6} g in which the

TABLE 3. Results for R_U for Samples of 10^{-6} g Measured with an Ion Collector (reproducibility 0.11 rel. %)

Analysis No.	$^{238}U/^{235}U$	Convergence, rel. %	Analysis No.	$^{238}U/^{238}U$	Convergence, rel. %
1	137,81±0,31	0,22	4	137,78±0,25	0,18
2	138,02±0,38	0,27	5	137,80±0,30	0,21
3	137,66±0,35	0,35	6	137,60±0,31	0,22

multiplier was replaced by a Faraday cylinder (Table 3). A sample of 10^{-6} g made it possible to attain high time-stable $^{238}U^+$ currents of $(2\text{-}3)\cdot10^{-11}$ A, which is quite sufficient for measurement with a reproducibility of about 0.11% relative, i.e., with the same accuracy as for samples of natural uranium 100 times larger (about 10^{-4} g), while the time for the ion source to reach the working state with a mass of 10^{-6} g was reduced by a factor 2-3, with an overall reduction in the analysis time of 50-70%.

Tables 2 and 3 show that the mean values of R_U obtained with the collector and the multiplier differ appreciably, with the multiplier giving the lower values. The values obtained with the collector (Table 3) correspond to published data for natural uranium [6], i.e., the mass spectrometer does not have an appreciable systematic error, and the difference between $R_{U\,mul}$ and $R_{U\,col}$ is to be ascribed to discrimination effects in the multiplier.

The reproducibility of the results for samples of 10^{-6} g was about the same in both cases, i.e., the multiplier makes no appreciable contribution to the random component of the error at this accuracy level. The mean value of R_U increased as the sample mass was reduced (Table 2), and the random error also increased. This rise in R_U is mainly due to two factors: the increased fractionation in the ion source during the run-up to the working state and the differences in voltage dependence of the multiplier gain for ions differing in mass. A third possible factor (uranium isotope fractionation in deposition from the walls of the capillary during sample deposition) has not been examined.

The fractionation in the ion source with small specimens was examined in three successive analyses of the same specimens (10^{-8} g) with a fixed voltage on the multiplier. Each analysis required 10 min. The results were as follows: $R_{U_1} = 138.09$; $RU_2 = 138.59$; $RU_3 = 138.81$, i.e., the $^{238}U/^{235}U$ isotope ratio increased by 0.5% relative in 20 min. The time required by the ion source to reach the working condition when the evaporator heating current was switched on was 20 min for a sample of 10^{-8} g, i.e., enrichment in the ^{238}U of several tenths of a percent could occur.

The differences in gain of the multiplier are due mainly to the electron emission processes at the first dynode on bombardment by the ions; and

$$I_{el} = I_{ion} K_{mul} = I_{ion} \gamma K_{el}, \tag{1}$$

where I_{el} is the output electron current from the multiplier; I_{ion}, input ion current; K_{mul}, gain of the multiplier; γ, secondary ion–electron emission coefficient from the first dynode for the given type of ion; and K_{el}, gain of electron current in the multiplier, and we get for isotopes 1 and 2 for some element that

$$R_{U_{mul}} = \frac{I_{1el}}{I_{2el}} = \frac{I_{1\,ion}}{I_{2\,ion}} \frac{\gamma_1}{\gamma_2} \frac{K_{1el}}{K_{2el}}. \tag{2}$$

If the values of the ion currents I_1 ion and I_2 ion are such that the multiplier is far from saturation, K_{el} is independent of the input ion current and

$$R_{U_{mul}} = R_{U\,col}\,(\gamma_1/\gamma_2) = R_{U_{col}}\,\alpha, \tag{3}$$

where $\alpha = \gamma_1/\gamma_2$ is the multiplier discrimination factor.

There is no mechanism for potential electron ejection in this case (the ionization potential of uranium $U_i = 6.08$ V [7]), and the work function of the copper–beryllium alloy $e\varphi = 4.2$ eV [8], so the energy dependence of γ can be put in the following form [9] for ion velocities $V_i < 3\cdot10^5$ m/sec, which corresponds to energies $E_i <$ 100 keV for uranium:

$$\gamma_i = c_i\,(V_i^2 - V_0^2), \tag{4}$$

where V_0 is the threshold ion velocity corresponding to the onset of kinetic emission and c_i is some constant for a given target–ion pair. If the surfaces are covered with a gas film, $V_0 \approx 0$ [9], and in the presence of an isotope effect for a sample of 10^{-6} g we get

$$1/\alpha = \frac{c_1}{c_2}\left(\frac{V_1}{V_2}\right)^2 = \frac{R_{U\,col}}{R_{U\,mul}} = 1{,}010, \quad (5)$$

whence $c_1/c_2 = C = 0.997$, i.e., the isotope effect due to the mass difference between ^{238}U and ^{235}U is $(0.3 \pm 0.2)\%$ on the basis of the error of measurement. From (3) and (5) we can correct R_U as measured with the multiplier (Table 2). The values from various samples indicate that the main contribution to the rise in R_U on reducing the sample size is the fractionation in the ion source, which begins to become appreciable for samples $< 10^{-7}$ g. The multiplier discrimination factor is due mainly to differences in speed between the isotopes.

The random component of the error increases as the sample is reduced mainly because of the increasing statistical fluctuations in the ^{235}U ion current, since it is impossible with small samples to obtain currents of adequate intensity stable over long periods. For example, $I^{+}_{235_U} \approx 1.5 \cdot 10^{-16}$ A for a sample of 10^{-9} g (Table 1), which results in statistical fluctuations of about 1% during the 10-sec measurement on a single peak. If the analysis time is increased, the error tends to increase on account of an increased effect from fractionation in the ion source. Also, minor variations in the analysis conditions have a marked effect on results for small specimens.

In spite of the above factors, the reproducibility is represented by a spread of not more than 0.45% for samples down to 10^{-9} g. The limit of detection by the MI 1320 is $2 \cdot 10^{-13}$ g, so in principle it is possible to analyze 10^{-10} g of natural uranium, where the content of ^{235}U is $7 \cdot 10^{-13}$ g, which is sufficient to record several mass spectra from the uranium.

LITERATURE CITED

1. V. A. Pavlenko et al., in: Sixth All-Union Symposium on Stable Isotopes in Geochemistry [in Russian], Moscow (1976), p. 227.
2. R. N. Fall' et al., Nauch. Prib., No. 15, 19 (1978).
3. M. Van Gorkom and K. Glick, Int. J. Mass Spectrom. Ion Phys., 4, No. 3, 203 (1970).
4. R. Lao et al., ibid, 10, No. 3, 309 (1973).
5. R. Pottie et al., ibid, 11, No. 1, 41 (1973).
6. H. Kienitz, Massenspektrometrie, Verlag Chemie GmbH, Weinheim (1968).
7. I. N. Bakulina and N. I. Ionov, Zh. Eksp. Teor. Fiz., 36, 1001 (1959).
8. V. S. Fomenko, Emission Parameters of Materials [in Russian], Naukova Dumka, Kiev (1970).
9. L. N. Dobretsov and M. V. Gomoyunova, Emission Electronics [in Russian], Nauka, Moscow (1966).

FIELD ION MICROSCOPY OF RADIATION DEFECTS IN TUNGSTEN IRRADIATED WITH 50-keV W^+ IONS

I. METHOD AND RESULTS

A. F. Bobkov, V. T. Zabolotnyi,
L. I. Ivanov, G. M. Kukavadze,
N. A. Makhlin, and A. L. Suvorov

UDC 539.2:539.12.04

In the interests of the further development of nuclear materials science, we have made a study of the atomic collision cascades in tungsten, like those formed by the action of neutrons during the deuterium–tritium synthesis reaction. This extends extant work [1] to other neutron energy and temperature ranges.

Following our experimental procedure, we irradiated samples (tips) of technically pure tungsten (grade VA-3) that had earlier been prepared and analyzed in the field ion microscope [2] in the Vesuvius-1 ion accelerator with 50-keV tungsten ions at 300°K, corresponding to the second annealing stage. The irradiation doses were 10^{12}, 10^{13}, and $5 \cdot 10^{14}$ ion/cm^2, which according to calculation [3] means the production in the irradiation time of 0.01, 0.1, and 5.5 displacements/atom, or equivalent neutron fluxes of $7 \cdot 10^{18}$, $7 \cdot 10^{19}$, and $3.5 \cdot 10^{21}$ neutrons/cm^2. The rate of generation of defects in tungsten was 10^{-3} displacements/atom, i.e., 10^4 times higher than that expected in thermonuclear reactors. We then analyzed the samples again in the field ion microscope at 78°K. We derived a picture of the spatial distribution of the radiation defects by field evaporation of layers of surface atoms (in the continuous mode). Approximating the sample surface as a hemisphere and the field ion image with a pseudostereographic projection [4], we can use sequential images to construct the defect (vacancy) distribution along the track of the bombarding ions. We corrected for the distortion of the form of the radiation defects by the imaging and evaporating fields by the published method [5, 6] and identified the nature and size of the radiation damage on the basis of our earlier results [6-9].

Field ion microscopic analysis of the irradiated samples revealed the formation of defect regions, which were vacancy clusters (depleted zones) with a halo of interstitials lying at a distance of 25 Å on average (1 Å = 10^{-10} m). We calculated the vacancy concentration in the depleted zones as 30 ± 10 at. %, as isolated vacancies and as vacancy clusters containing up to 30 vacancies. With an irradiation dose of 10^{12} ion/cm^2 we detected vacancy clusters of volume $\sim 1 \cdot 10^3\ \Omega_a$ (here $\Omega_a = 15.85$ Å^3 is the atomic volume of tungsten), containing roughly 300 vacant sites. In some cases close to the large vacancy clusters we observed smaller vacancy clusters consisting of 10-30 vacancies and separated from one another by several tens of angstroms (Fig. 1a, b). Both clusters may well originate as a result of the multiplication of a single cascade into isolated subcascades. On the average, ~1.25 subcascades correspond to each intrinsic ion. The average energy of formation of a subcascade has been estimated as ~30 keV [10]. We calculated the number of displacements in the tungsten lattice produced by one 50-keV tungsten ion from the relation $\nu = k\tilde{E}/2E_d$, where k is the coefficient of the cascade function (0.8); $\tilde{E}$ is the average energy lost by the ion in the production of displacements (37.7 keV); and E_d is the threshold displacement energy of tungsten atoms (50 eV). Hence $\nu \approx 300$.

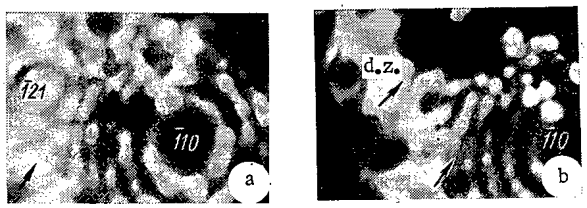

Fig. 1. Field ion images derived by sequential field evaporation of two surfaces of an irradiated tungsten sample with the depleted zone of a single cascade (the arrow indicates the direction of the incident ion beam): a) initial irradiation; b) after removal of eight atomic layers by the field. d.z. – depleted zone.

Translated from Atomnaya Énergiya, Vol. 48, No. 5, pp. 325-326, May, 1980. Original article submitted September 21, 1978; revision submitted January 8, 1980.

0038-531X/80/4805-0331 $07.50

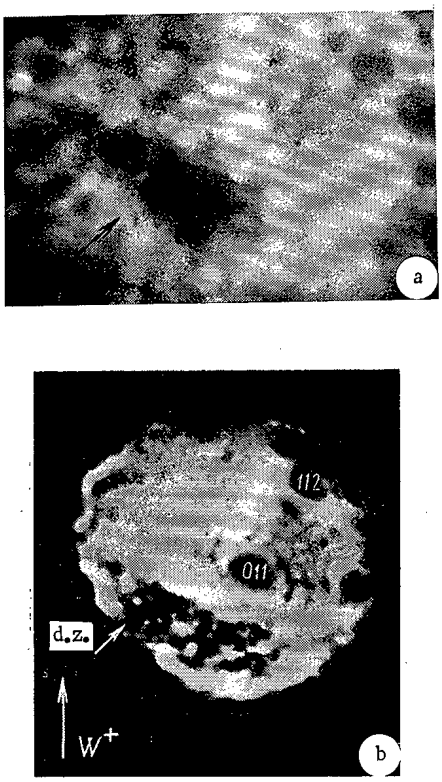

Fig. 2. Field ion images of the surfaces of irradiated tungsten samples demonstrating the formation of vacancy clusters at doses of a) $1 \cdot 10^{13}$ and b) $5 \cdot 10^{14}$ ion/cm^2 (arrows indicate the direction of the incident ion beam). d.z. – depleted zone.

With an irradiation dose of $1 \cdot 10^{13}$ ion/cm^2, in several cases we detected clusters of volume $3 \cdot 10^3\ \Omega_a$, consisting of roughly 10^3 vacancies. One of these clusters, formed by the overlap of three cascades (Fig. 2a), started on the sample surface and extended approximately 90 Å into the bulk along the direction of the incident ion beam. The concentration of these cascades in the samples was 10^{18} cm^{-3} and their average volume was $\approx 2 \cdot 10^3\ \Omega_a$ ($\sim$600 vacancies).

Some of the field ion images revealed the formation of single interstitials at distances of 10 to 50 Å from the edge of the closest vacancy cluster and at depths of at least 45 Å from the surface; the total number of interstitials was $\sim$1% of the number of detected vacancies. We did not observe contrast effects that could be interpreted as interstitial clusters.

After irradiation to a dose of $5 \cdot 10^4$ ion/cm^2 we detected depleted zones with volumes from 1 to $5 \cdot 10^4\ \Omega_a$ (Fig. 2b). The zones started on the surface and extended up to 130 Å into the bulk of the sample along the direction of the incident ion beam. Obviously, this damage was caused by the coalescence of depleted zones belonging to a number of cascades. At all irradiation doses we detected small voids of diameter $\sim$10 Å within the vacancy cluster.

LITERATURE CITED

1. D. Seidman, Surface Sci., 70, 532 (1978).
2. V. A. Kuznetsov, G. M. Kukavadze, and A. L. Suvorov, Prib. Tekh. Eksp., No. 2, 152 (1969).
3. M. Robinson, in: Radiation Damage in Metals, Am. Soc. Met., Metals Park, Ohio (1976), p. 1.
4. D. G. Brandon, J. Sci. Instrum., 41, 373 (1964).
5. A. L. Suvorov, in: Structure and Properties of Single Crystals of Refractory Metals [in Russian], Nauka, Moscow (1973), p. 52.

6. A. L. Suvorov and A. G. Sokolov, Kristallografiya, 17, 1200 (1972).
7. A. L. Suvorov, Usp. Fiz. Nauk, 101, 21 (1970).
8. A. L. Suvorov and A. G. Sokolov, Kristallografiya, 20, 379 (1975).
9. A. F. Bobkov et al., in: Problems in Atomic Physics and Technology. Physics of Radiation Damage and Nuclear Materials Science [in Russian], Vol. 1 (3), Kharkov. Fiz. Tekh. Inst., Kharkov (1976), p. 26.
10. P. Pronko and K. Merkle, in: Proceedings of the Workshop on Correlation of Neutron and Charged Particle Damage, Oak Ridge National Laboratory (1976), p. 177.

FIELD ION MICROSCOPY OF RADIATION DEFECTS IN TUNGSTEN IRRADIATED WITH 50-keV W^+ IONS

II. DISCUSSION OF EXPERIMENTAL RESULTS

V. T. Zabolotnyi, L. I. Ivanov,
N. A. Makhlin, and A. L. Suvorov

UDC 539.2:539.12.04

We decided to compare our experimental results [1] with calculations on radiation damage in tungsten, computer calculations of the development and annealing of cascades, and the results of other experiments [2-5].

We found that the depleted zones of the cascades had maximum linear dimensions (up to 60 Å, 1 Å = 10^{10} m) in the ⟨110⟩ direction. The average number of vacancies generated by one W^+ ion was at least 240, i.e., in the second annealing stage about 80% of the original number of vacancies perist in the cascade. The reason for this low recombination is that in these experiments the overwhelming majority of the interstitials, which have high mobility at the irradiation temperature, emerge onto the surface, acting as the dominant effective sink.

The average separation of the interstitials from the edge of the depleted zone was 25 Å, while their number did not exceed 1% of the calculated number of Frenkel pairs that were formed. The high mobility of the interstitials in tungsten at room temperature is due to the formation of complexes with impurity atoms. The interstitials are usually assumed to be formed by focused replacement sequences [5]. The existence of impurities in the irradiated metal can reduce the sequence length because the sequences are broken at impurity atoms [6]. However, in the present case the impurity concentration was less than 0.2 at. % and could not substantially alter the average sequence length. Consequently, we can conclude that the formation of interstitial–impurity atom is not due to this sequence breaking but takes place as a result of the capture of interstitials by impurity traps during thermal migration.

Since we detected interstitials only in the region 10-50 Å from the edge of the depleted zones, we can conclude that thermal migration has only a small effect on their original distribution. Otherwise a uniform interstitial distribution should be generated in the volume in question, i.e., the average separation of the interstitials from the edges of the depleted zones corresponds to the average length of the focused replacement sequences in tungsten at room temperature. The average sequence length is 65 Å in the irradiation of tungsten at 18°K with 20-keV W^+ ions [5]. Thus, increase in the irradiation temperature from 18 to 300°K reduces the sequence length to approximately one-third; this is due to the increase in the energy losses as a result of thermal vibrations when the replacement sequence propagates.

In these as in earlier experiments [5] we did not detect complexes of interstitials, although their existence has been predicted by computer calculations of the development and annealing of cascades [2, 3, 7]. The origin of this discrepancy could be that in these calculations the replacing collisions were not examined, while the recombination volume of the interstitials was chosen arbitrarily.

In addition to the depleted zones containing several hundreds of vacancies, we also detected smaller clusters containing about ten vacancies. The distance between the small and the large vacancy clusters was several tens of angstroms. These clusters seem to be the depleted zones of subcascades of energy ~1 keV. The over-

Translated from Atomnaya Énergiya, Vol. 48, No. 5, pp. 326-327, May, 1980. Original article submitted December 15, 1978; revision submitted January 8, 1980.

0038-531X/80/4805-0333 $07.50

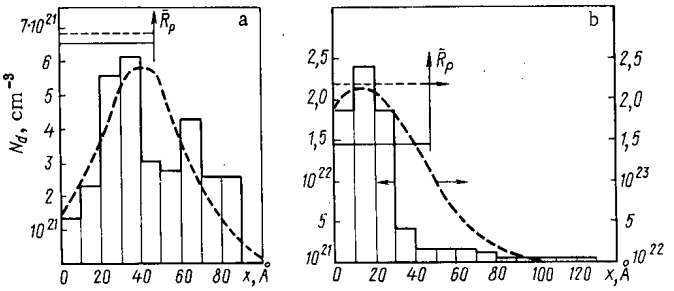

Fig. 1. Depth distribution of defects derived from the collection of field ion images of the surface layers with irradiation doses of a) $1 \cdot 10^{13}$ and b) $5 \cdot 10^{14}$ ions/cm^2.

lap of cascades with simultaneous annealing of the damage within them has so far received comparatively little attention. The sole method with which this process can be examined on the atomic level seems to be field ion microscopy.

The depth distribution of defects is among the most important parameters needed for comparison of, e.g., swelling due to neutron irradiation and simulation experiments. Such information is extremely difficult to derive experimentally, particularly when the bombarding ions have comparatively low energy. Figure 1 shows the depth distribution of the vacancies with various irradiation doses; here the direction of the x axis coincides with that of the incident ion beam. We plotted theoretical curves (broken line) in addition to the experimental histograms. The average vacancy density (continuous line) and the average displacement density (broken line), derived from the histogram and the theoretical curve, respectively, differ by 4.4%. The displacement of the maximum of the histogram toward the surface on increase in the irradiation dose is due to sample sputtering. The change in the defect distribution gives the sputtering coefficient as 60-70 atoms/ion. The calculations indicate that the average displacement concentration for a given dose should be $2.2 \cdot 10^{23}$ cm^{-3}. However, the observed value is $1.45 \cdot 10^{22}$ cm^{-3}. The reason for this discrepancy resides in the detailed development of the cascade in a crystal having a high vacancy concentration. The displaced atoms formed in the cascade can encounter existing vacancies, thus reducing the total number of defects that are created.

As we have said, the radiation damage with an irradiation dose of $1 \cdot 10^{12}$ ions/cm^2 is principally the depleted zones of single cascades. Because of the overlap of the cascades, at a dose of $1 \cdot 10^{13}$ ions/cm^2 defect regions are additionally generated from the coalescence of several depleted zones. When the irradiation dose is increased to $5 \cdot 10^{14}$ ions/cm^2 the overlap of numerous cascades takes place and is accompanied by the appearance of extensive defect regions. The overlap of cascades reduces the efficiency of the formation of radiation defects. Thus, while at an irradiation dose of $1 \cdot 10^{12}$ and $1 \cdot 10^{13}$ ions/cm^2 each ion forms on average 300 vacancies, only 22 vacancies are formed when the dose is $5 \cdot 10^{14}$ ions/cm^2. The average vacancy concentration in the damaged layer at a dose of $1 \cdot 10^{12}$ ions/cm^2 is $(3.5\text{-}7.0) \cdot 10^{-3}$ atomic fraction, but 10 times lower at a dose of $1 \cdot 10^{13}$ ions/cm^2, while it does not exceed 0.09-0.17 atomic fraction at a dose of $5 \cdot 10^{14}$ ions/cm^2. The volume of a vacancy in tungsten is $0.42\,\Omega_a$ [8]. Thus, the average vacancy swelling of the damaged layer at the maximum irradiation dose can be 7%. We did not detect the formation of voids with dimensions greater than 10 Å at high irradiation doses, but the existing small voids under the corresponding thermal conditions could act as the nucleation centers for the larger voids.

LITERATURE CITED

1. A. F. Bobkov et al., At. Energ., 48, 325 (1980).
2. D. Doran, Radiat. Effects, 2, 249 (1970).
3. J. Beeler and M. Beeler, in: Proceedings of the International Conference on Fundamental Aspects of Radiation Damage in Metals, Gatlinburg, 6-10 October 1975, US ERDA CONF-751006-P1, Vol. 1, p. 28.
4. V. V. Kirsanov, in: Nuclear Materials Science [in Russian], Vol. 1, Izd. TsNIIatominform, Moscow (1978), p. 340.
5. L. A. Beavan, R. M. Scanlan, and D. N. Seidman, Acta Met., 19, 1339 (1971).
6. V. V. Kirsanov, Fiz. Tverd. Tela, 19, 1184 (1977).
7. J. R. Beeler, Jr. and H. H. Yoshikawa, Materials Research and Standards, 11 (2), 29 (1971).
8. M. W. Thompson, Defects and Radiation Damage in Metals, Cambridge Univ. Press (1969).

EFFECTS OF GAS DISSOLVED IN WATER ON CRITICAL HEAT LOADINGS

V. V. Fisenko, Yu. D. Katkov,
A. P. Lastochkin, and V. I. Maksimov

UDC 621.039

Reliability specifications for nuclear power station components are steadily tightening, particularly for the cores of power reactors, and therefore various papers have appeared in the USSR and elsewhere on the heat-transfer crisis in the forced flow of water in pipes. In 1976 tabular data were published [1] for use in calculating the heat-transfer crisis for water boiling in uniformly heated circular tubes. The tables gave carefully tested and consistent experimental data on critical heat loads and limiting steam contents obtained for water boiling in technically smooth tubes of diameter 8 mm with a relative length of $l/d \geq 20$, pressures between 3 and 20 MPa, mass speeds from 0.5 to 5.0 Mg/m^2·sec, deviations from the boiling point from 0 to 75°K, and a step in the relative enthalpy change of 0.05.

Surveys have also been published [2, 3] of data obtained in experiments with outgassed water and with water in which the gas concentration either was not measured at all or else was measured after outgassing with an inadequate accuracy. It is therefore desirable to estimate the size of the difference between the critical heat loadings calculated from the recommendations of [1] and the values found by experiment with nearly zero dissolved gas.

For this purpose we built a system with a gas and steam volume compensation system for the coolant, as well as a system for simulating and monitoring the dissolved gas. The error in determining the dissolved gas concentration was not more than ± 5%. The purification system allowed us to produce a residual dissolved gas concentration not more than 30 neutrons·cm^3 of N_2/kg H_2O.

The system was a cylindrical channel made of 0Kh18N10T steel of length 1.0 m and internal diameter $8 \cdot 10^{-3}$ m with uniform electrical heating along the length. The coolant moved upwards with a mass flow rate ρW = 2000 kg/m^2·sec (constant in all experiments), and the input was supplied with outgassed water having

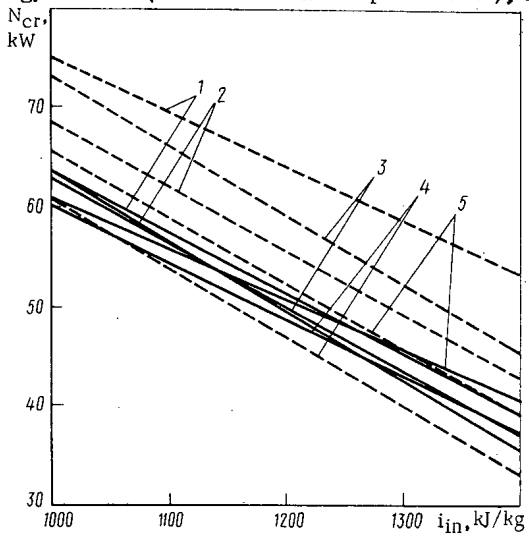

Fig. 1

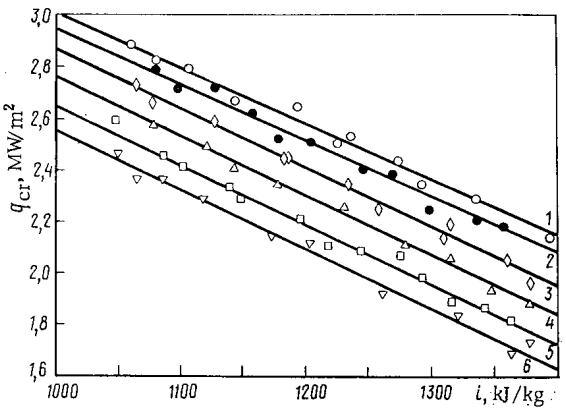

Fig. 2

Fig. 1. Comparison of experiment (broken line) and calculation (solid line) [1] for pressures of 18.0 (1); 16.0 (2); 14.0 (3); 12.0 (4), and 10.0 (5) MPa.

Fig. 2. The $q_{cr} = f(i_{in})$ relation for P = 18 MPa given by experiment for $\bar{C}$ = 0 (○); 500 (●); 1200 (◇); 220 (△); 3200 (□); 3500 (▽) in cm^3 N_2/kg H_2O.

2200?

Translated from Atomnaya Énergiya, Vol. 48, No. 5, pp. 327-328, May, 1980. Original article submitted December 4, 1978; revision submitted December 11, 1979.

0038-531X/80/4805-0335 $07.50

various temperature deviations from the saturation point. The critical heat flux was detected from the sharp rise in the channel wall temperature. The following ranges in the initial parameters were used: P = 10-18 MPa, Δt_i = 10-100 °K.

Figure 1 shows a calculation in accordance with the recommendation of [1] and experimental values. The discrepancy between the theoretical and observed values is minimal at a pressure of 10-12 MPa. The discrepancy is over 25% for P = 18 MPa and water near its boiling point. Figure 2 gives our experimental results on the effects of gas concentration on the critical heat load.

It has therefore become necessary to examine the effects of dissolved gas on the critical heat load over a wide range in the initial parameters. The effect may be substantial in any system where there is a gas volume-compensation system for the coolant.

LITERATURE CITED

1. "Tabular data for calculating the heat-transfer crisis in the boiling of water in uniformly heated circular tubes," Teploenergetika, No. 9, 90 (1976).
2. V. I. Subbotin et al., in: Studies on the Heat Transfer to Steam and Water Boiling in Tubes at High Pressures [in Russian], Atomizdat, Moscow (1958).
3. G. V. Alekseev, B. A. Zenkevich, and V. I. Subbotin, Trudy TsKTI, Kotloturbostroenie, Issue 58, 123 (1965).

EFFECT OF FLUORESCENCE ON γ-RAY BUILDUP FACTORS IN LEAD

I. N. Butueva and I. N. Trofimov

UDC 539.121.72:539.122

Shields against γ radiation with energies of 200 keV and less are generally calculated by using the attenuation rates given in the handbook [1], which are based on amply large values of the buildup factors. In a number of practical problems, however, it is required to reduce the mass of a lead shield to a minimum, and this requires more accurate calculations of the buildup factors.

For low-energy photons in lead coherent scattering and fluorescence are important. The γ-ray buildup factors which take account of these processes are calculated by the Monte Carlo method. The authors previously developed a modification of this method [2] which permits the calculation of buildup factors in a shield up to 20 mfp thick. The essence of the modification involves specifying first collision sources uniformly over the whole thickness of the shield plus splitting. The modification was tested by comparing calculated buildup factors in water, iron, and lead with results obtained by the moments method [3].

Using this modification dose buildup factors were calculated with and without taking account of coherent scattering and fluorescence for energies of 200, 150, 120, and 100 keV. The coherent scattering cross section

TABLE 1. Dose Buildup Factors in Pb for a Point Isotropic Source, Taking Account of Coherent Scattering

Energy, MeV	μx						
	1	2	4	7	10	15	20
0,2	1,12	1,23	1,4	1,7	1,9	2,4	2,9
0,15	1,1	1,15	1,25	1,45	1,65	1,9	2,3
0,12	1,1	1,12	1,2	1,3	1,45	2	4,3
0,10	1,06	1,1	1,24	2	5,3	73	2300

TABLE 2. Dose Buildup Factors in Pb for a Point Isotropic Source, Taking Account of Coherent Scattering and Fluorescence

Energy, MeV	μx						
	1	2	4	7	10	15	20
0,2	1,2	1,3	1,55	1,9	2,5	3,8	5,4
0,15	1,4	1,6	1,8	2,1	2,4	3,1	3,9
0,12	1,7	2,3	3,7	6,7	12,7	40	130
0,10	2,2	3,2	6,4	22	80	810	10000

Translated from Atomnaya Énergiya, Vol. 48, No. 5, pp. 328-329, May, 1980. Original article submitted March 26, 1979.

0038-531X/80/4805-0336$07.50

μ_{coh} was obtained from data in the handbook [4] by taking the difference between the total cross sections with and without taking account of coherent scattering. The angular distribution of γ photons in coherent scattering was found by the conventional method [5]. It was assumed that the fluorescence yield in the photoelectric absorption process was 0.96, the energy of the fluorescent photons was 75 keV, and the angular distribution was isotropic.

The calculations were performed for a plane isotropic source, and the results were then converted for a point isotropic source by the well-known relation (cf. [2]). The results of the calculations are listed in Tables 1 and 2. The lower limit of the energy spectrum was chosen equal to 10 keV. The standard statistical error of the results varied linearly from 5% for $\mu x = 1$ to 30% for $\mu x = 20$.

The effect of coherent scattering on the buildup factors turned out to be small. The present calculations completely confirmed the assumption of Goldstein [3] that buildup factors can be calculated without taking account of coherent scattering if the coherent scattering cross section is subtracted from the total cross section. If the coherent scattering cross section is taken into account in the total cross section, the increase in the buildup factors is given by the factor $\exp(\mu_{coh}x)$. It is clear that in this case the straight-ahead approximation is valid.

Fluorescence has a more important effect on the buildup factors. It is characteristic of fluorescence that there is a huge jump in the cross section for the photoelectric effect at the K-level, and the energy of the fluorescent γ photons is lower than that at the jump, and therefore the mean free path of fluorescent γ photons is frequently longer than that of the source photons. The tables show that taking account of fluorescence increases the values of the buildup factors by a factor of 10 and more in a number of cases.

For the L-levels the jumps in the photoelectric absorption cross section are small, and it is expected that the effect of fluorescence at the L-levels on the buildup factors will be negligible.

LITERATURE CITED

1. L. R. Kimel' and V. P. Mashkovich, Shielding Against Ionizing Radiations [in Russian], Atomizdat, Moscow (1972).
2. I. N. Butueva et al., At. Energ., 45, No. 2, 125 (1978).
3. H. Goldstein and J. Wilkins, The Shielding of Nuclear Powered Vehicles [Russian translation], IL, Moscow (1961).
4. E. Storm and H. Israel, "Photon cross sections from 1 keV to 100 MeV for elements Z = 1 to Z = 100," Nucl. Data, 7A, 565 (1970).
5. Radiation Field of a Point Monodirectional γ-Ray Source [in Russian], Atomizdat, Moscow (1974).

SPATIAL AND ENERGY DISTRIBUTIONS OF THE THERMAL NEUTRONS IN A CELL OF A REACTOR AT BILIBINSK NUCLEAR POWER STATION

G. G. Panfilov, A. A. Vaimugin,
A. V. Gusev, A. P. Korneeva,
A. G. Kostromin, V. I. Kulikov,
S. S. Lomakin, V. F. Lyubchenko,
and V. N. Sharapov

UDC 621.039.512.45:539.125.52

An activation method has been used with a zero-power uranium–graphite assembly to determine the neutron spectral characteristics T_n (neutron temperature) and r (proportion of epithermal neutrons) for the combination $r\sqrt{T_n/T_0}$ [1].

The channels in the core were of design and fuel composition analogous to those in a reactor in the nuclear power station [2]. The central insert consisted of 25 channels. This number is sufficient to obtain a characteristic equilibrium neutron spectrum at the center of the assembly [3].

The characteristics of the neutron spectrum in the assembly were measured by activating foil detectors made from alloys of aluminum with lutecium, manganese, and indium, and also pure copper foils. The neutron-screening coefficients G_{th} and G_{epi} for the detectors were close to one, apart from the copper detector ($G_{epi} = 0.858$) and the indium ones ($G_{th} = 0.996$, $G_{epi} = 0.850$). The Westcott parameter S_0 was taken from [1].

The foil activities were measured with γ-ray detectors and single-channel differential analyzers and also with a Protoka β-counting system. The foils were calibrated in the thermal column of an F-1 reactor [1].

The neutron temperature was determined at points 1-6 in the central cell of the assembly at the height of the center of the core in channels containing water and at points 1-6, 1', 3', and 3" in channels without water (Fig. 1). The detectors at point 2 reproduced the cross section of the fuel rod. These were placed in a cross section and were screened on two sides from fission fragments by aluminum foils. The cadmium ratio was measured with screens of thickness 0.5 mm. Tables 1 and 2 give the results obtained in the central cell (R_{Cd} is the cadmium ratio and I is the spectral index [1]).

Figure 2 gives not only the observed neutron temperatures but also values derived from theoretical neutron spectra for a cell in the Bilibinsk reactor. The spectra were calculated in the P_3 approximation by the spherical-harmonic method for cylindrical geometry [4], where the cell was split up into five homogeneous concentric zones: water, steel, graphite, fuel rods, and graphite again (from the center to the edge).

TABLE 1. Spectral Characteristics of Cell for Channels Containing Water

Point No.	Distance, mm, from center	R_{Cd}^{Cu}	$r\sqrt{T_n/T_0}$	I_{Cu}^{Lu}	T_n, K
1	0	10,6±0,5	0,088±0,003	1,00±0,02	318±13
2	27	5,5±0,3	0,177±0,005	1,21±0,02	439±17
3	47	8,0±0,4	0,119±0,003	1,13±0,02	375±15
4	74	8,5±0,4	0,102±0,003	1,13±0,02	372±15
5	100	8,7±0,4	0,108±0,003	1,11±0,02	363±14
6	141	9,1±0,5	0,103±0,003	1,12±0,02	369±14

Translated from Atomnaya Énergiya, Vol. 48, No. 5, pp. 329-331, May, 1980. Original article submitted June 15, 1979.

0038-531X/80/4805-0338 $07.50

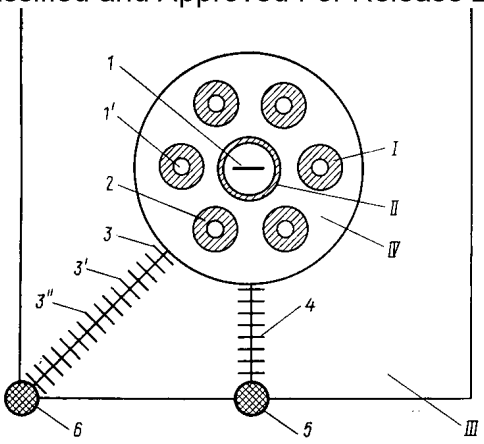

Fig. 1

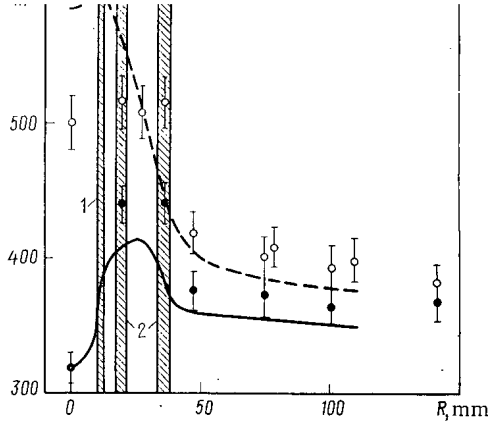

Fig. 2

Fig. 1. Disposition of the detectors in the central cell with channels: I) fuel rod; II) central tube; III) cell graphite; IV) channel graphite.

Fig. 2. Distribution of T_n over cell: broken line and open circles) calculation and measurement for channels without water; solid line and filled circles) same for channels with water; 1) wall of central tube; 2) fuel pin.

TABLE 2. Spectral Characteristics of Cell for Channels without Water

Point No.	Distance, mm, from center of of cell	I_{Cu}^{Lu}	I_{Mn}^{Lu}	I_{Mn}^{In}	R_{Cd}^{Cu}	$r\sqrt{T_n/T_0}$		T_n, K	
						R_{Cd}	I_{Mn}^{In}	I_{Cu}^{La}	I_{Mn}^{Lu}
1	0	1,24±0,02	1,40±0,03	4,08±0,08	4,8±0,3	0,209±0,006	0,224±0,007	472±19	534±21
1′	27	—	1,40±0,03	3,70±0,07	—	—	0,193±0,006	—	508±20
2	27	1,30±0,02	1,42±0,03	3,88±0,08	4,6±0,3	0,220±0,007	0,207±0,006	512±21	422±21
3	47	1,18±0,02	1,32±0,03	3,05±0,06	6,2±0,3	0,156±0,005	0,141±0,004	410±16	426±17
3′	78	—	1,28±0,03	2,92±0,06	—	—	0,131±0,004	—	407±16
3″	109	—	1,27±0,03	2,81±0,06	—	—	0,123±0,004	—	398±16
4	74	1,17±0,02	—	—	6,8±0,4	0,141±0,004	—	401±16	—
5	100	1,16±0,02	—	—	7,2±0,4	0,131±0,004	—	392±16	—
6	141	1,14±0,02	1,22±0,02	2,84±0,06	7,7±0,4	0,122±0,004	0,125±0,004	381±15	382±15

In accordance with the experimental method of [1], the neutron temperature was determined in the calculation from the condition for equality of the ratios of the ^{63}Cu and ^{176}Lu cross sections averaged over the thermal region of the neutron energies the first time for a Maxwellian spectrum M(E) and the second time from the spectrum Φ(E) derived from thermalization calculations. Integration was replaced by summation over the individual groups of neutrons for the energy range from 0 to 0.11 eV, which is the limit of the Maxwellian neutron spectrum.

The calculated and observed T_n for channels with and without water in the main describe identically the spatial variation in the temperature over the cell (Fig. 2). The calculated neutron temperature for the fuel rods was below the measured value, evidently because all the material in the fuel-rod zone was taken as homogeneously distributed in the calculation. On the other hand, the observed neutron temperature in the central tube was about 100° below the calculated value for the channels without water. The core height in the physical assembly was small, so the discrepancy is due to additional activation of the detectors arising from neutrons in the low-energy spectrum derived from the end reflectors.

We are indebted to O. V. Komissarov for assistance in performing the calculations.

LITERATURE CITED

1. S. S. Lomakin et al., Tr. Soyuz. Nauchn.-Issled. Inst. Priborostr., Issue 12, Atomizdat, Moscow (1970), p. 230.
2. V. M. Abramov et al., At. Energ., 35, No. 5, 299 (1973).
3. Yu. Yu. Glazkov et al., ibid., 10, No. 4, 381 (1961).
4. G. I. Marchuk et al., ibid., 13, No. 6, 534 (1962).

VIABILITY OF RESISTANCE THERMOMETERS UNDER REACTOR CONDITIONS

M. N. Korotenko, V. A. Salamakha, S. O. Slesarevskii, and V. P. Maksimenko

UDC 621.039.5

Resistance thermometers are of interest for temperature measurement on account of their high stability and high accuracy under ordinary conditions. Reactor conditions give rise to additional errors caused by radiation effects. These additional errors are dependent in a complicated way on the combined effects of radiation intensity, neutron fluence, temperature, device design, heat-transfer conditions, mechanical stress level, degree of order in the material, and certain others. The data on this subject are relatively scanty [1-3].

We have examined the viability of six commerical resistance thermometers under reactor conditions; the sensitive element was Pl-2 platinum wire of diameter 50 μm. The resistances R_0 of the thermometers at 0°C were 46.00 ± 0.02 Ω, while the ratios were $R_{100}/R_0 = 1.391 \pm 0.0007$. The design and manufacturing technology have been described [4]. The thermometers were irradiated in a VVR-M reactor, where the neutron-flux densities were respectively φ_T (E = 0.025 eV) ~ $9 \cdot 10^{13}$ neutrons/(cm^2·sec); φ_f (E = 1.15 MeV) ~ $3.5 \cdot 10^{13}$ neutrons/(cm^2·sec), and the rate of internal heat production in the steel q_g was 2.3 W/g. The thermometers were calibrated before and after irradiation outside the reactor by the reference-point method at temperatures of 100, 231.8, and 327.2°C.

The additional errors due to radiation can be divided into components due to change in physical parameters of the material, effects of radiation heating, and deterioration in the dielectric parameters of the insulation.

The change in physical parameters of the resistance were examined up to a fast-neutron fluence of $2 \cdot 10^{20}$ neutrons/cm^2. The thermometers were irradiated at various temperatures, but the conditions were otherwise identical. Figure 1 shows the results. Evidently, the more rapid annealing of radiation damage during irradiation at about 500°C is responsible for the much smaller changes in R_0 and R_{100}/R_0 by comparison with those at $t_{ir} \approx 80$°C.

When a given neutron fluence had been reached, the thermometers were recalibrated; Fig. 2 shows the resistance change, and it is clear that annealing during calibration at a temperature exceeding the irradiation

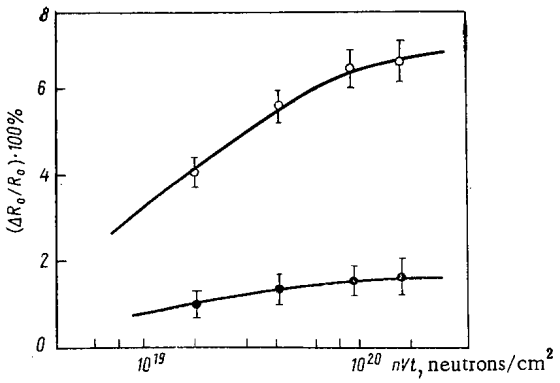

Fig. 1

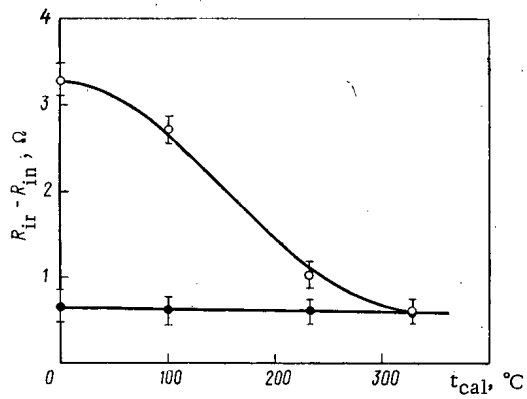

Fig. 2

Fig. 1. Effects of neutron fluence on the resistance change in resistance thermometers (irradiation temperatures ~80 (○) and ~500°C (●), calibration temperature 0°C).

Fig. 2. Resistance change in irradiated resistance thermometer in relation to calibration temperature (irradiation temperatures ~80 (○) and ~500°C (●), neutron fluence about $2 \cdot 10^{20}$ neutrons/cm^2).

Translated from Atomnaya Énergiya, Vol. 48, No. 5, pp. 331-332, May, 1980. Original article submitted June 26, 1979.

0038-531X/80/4805-0340$07.50

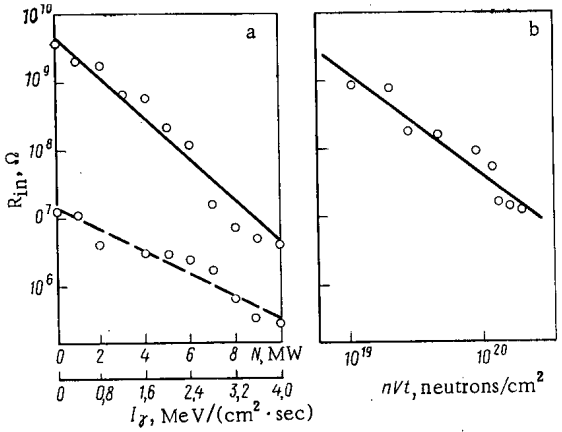

Fig. 3. Transient (a) and residual (b) changes in thermometer insulation resistance.

temperature largely restores the initial value of the resistance. The effective annealing at relatively low temperatures (≳250°C) is explained [5] by the low activation energy and low stability of radiation damage by comparison with the changes produced by plastic strain. The recovery in the resistance on annealing indicates that the change in resistance at this neutron fluence is caused not by radiation-induced recrystallization of the platinum but by the formation of lattice defects. Fast neutrons have the predominant effect on the resistance change. It is therefore best to use a resistance thermometer under conditions where the fast-neutron fluence is $<(2\text{-}4)\cdot 10^{19}$ neutrons/cm^2, while the temperature of the medium is over 250°C. The additional error arising from the resistance change is no more than 3°K.

The errors due to radiation heating are observed only under irradiation and are dependent on the rate of internal heat production in the materials of the thermometer and on the total thermal impedance between the sensitive element and the medium. These errors can be estimated analytically by means of standard heat-transfer equations [6]. The error from this source with this design of device was 2-4°K for a rate of internal heat production in steel q_g = 0.5 W/g but rose to 14-18°K for q_g = 2.3 W/g (heat-transfer coefficient α about $3\cdot 10^4$ W/m$^2\cdot$K).

The dielectric parameters of the insulating materials deteriorate under irradiation in the main due to deviation from equilibrium concentration in the charge carriers and the production of radiation damage, and also because the insulator contains new atoms of impurity elements. The resulting errors can be estimated for a given measurement scheme with particular values of the parameters by the method of [7].

Figure 3a shows the resistance change in the insulation in the initial period of irradiation in relation to the γ-ray intensity; the broken line shows the resistance change in the insulation after exposure to a neutron fluence of $2\cdot 10^{20}$ neutrons/cm^2. Figure 3b shows the effects of the neutron fluence on the residual changes in insulation resistance. The measurements were made at U = 100 V. Annealing at about 600°C (for about 1 h) reduced the residual change in the insulation resistance by 50-80%.

The considerable change in the insulation resistance indicates the need to increase the low insulation resistance allowed by the All-Union State Standard for resistance thermometers for reactor use. These measures should be accompanied by improved design and proper choice of materials to improve the viability of resistance thermometers under reactor conditions.

LITERATURE CITED

1. W. Browning and C. Miller, in: Temperature Measurements in Novel Technology [Russian translation], Mir, Moscow (1963), p. 53.
2. P. Madsen, UKAEA Report, AERE-M/R-649 (1951).
3. R. R. Svoup, Vopr. Rak. Tekh., 4, 38 (1971).
4. V. A. Salamakha et al., in: New Researches in Thermometry [in Russian], Vishcha Shkola, Lvov (1974), p. 41.
5. S. T. Konobeevskii, V. I. Kutaitsev, and N. F. Pravdyuk, Effects of Irradiation on the Structure and Properties of Constructional Materials [in Russian], Atomizdat, Moscow (1955).
6. V. P. Isachenko, V. A. Osipova, and A. S. Sukhomel, Heat Transfer [in Russian], Énergiya, Moscow (1975).
7. B. I. Gil' et al., [4], p. 5.

RECOVERY OF THE FAST-NEUTRON SPECTRUM IN A MODEL FOR A LIQUID-SALT BLANKET IN A FUSION REACTOR

V. M. Novikov, A. A. Shkurpelov,
V. A. Zagryadskii, D. Yu. Chuvilin,
and Yu. V. Shmonin

UDC 539.125.5.164.4

It is of interest to measure the energy spectra of the fast neutrons in systems that simulate the blanket zones in a fusion reactor not only in order to refine calculation methods and nuclear constants but also to assist the practical development of reactors. One of the simplest and yet reasonably precise methods of neutron spectrometry is activation, in which only minor perturbations in the neutron spectrum at the point of measurement are combined with the scope for measurement in the presence of strong γ-ray fluxes. The activation method allows one to measure neutron spectra in the range 0.5-14 MeV if the substances are chosen properly, i.e., in the range of energies characteristic of the blanket zones of fusion reactors.

Methods have been developed for recovering the neutron energy spectrum from activation data, in particular expansion in terms of orthonormalized functions, iterative methods, and maximum likelihood [1]. Although these methods are widely used, they have major disadvantages. The recovery results are sensitive to the number of detectors and to the distribution of the energy thresholds.

Recently, greater significance has been attached to recovery by means of a priori information [2, 3], by which is meant the results from all past experiments or calculations that provide data on the physical features of the spectrum. This method is stable under variation in the number and combination of the threshold detectors. It has been found to work reliably for fast-neutron spectra in various fissile media. It is desirable to use this method in researching neutron spectra in systems that simulate fusion blankets.

The recovery is performed in finite-dimension form via a system of effective constants. The a priori information is supplied as a set of integral spectra, which characterize the unknown integral spectrum with a certain degree of confidence. The set may include spectra calculated via the BLANK program for the model [4]. Neutron spectra above 0.1 MeV are calculated in this program by a Monte Carlo technique.

Numerical experiments were used to check the accuracy of the method; some given input neutron spectra were used to calculate the activation integrals, which were then input to the recovery program. The input data included those for monoenergetic neutrons of energy 14 MeV, a set of single lines with various neutron energies, and the characteristic spectrum for fusion neutrons. The recovered spectra agreed with the input ones to within 2%.

This method was then applied to the neutron spectrum in a model for a liquid-salt blanket. The model was a sphere uniformly filled with a eutectic mixture of LiF and BeF_2 in the 50 : 50 mol.% relation. The outside diameter of the model was 400 mm. Within the model was a spherical cavity of radius 60 mm. The design of the model has been described [5].

The neutrons of energy 14 MeV were provided by an NGI-200 neutron generator; the titanium tritium target lay at the center of the model. The neutron yield was up to 10^{10} neutrons/sec. Activation methods were used to measure the absolute rates of the following reactions: $^{115}In(n', n)^{115m}In$; $^{58}Ni(n, p)^{58}Co$; $^{56}Fe(n, p)^{56}Mn$; $^{27}Al(n, \alpha)^{24}Na$; $^{65}Cu(n, 2n)^{64}Cu$; $^{19}F(n, 2n)^{18}F$; $^{63}Cu(n, 2n)^{62}Cu$; $^{58}Ni(n, 2n)^{57}Ni$.

The diameters of the activation detectors were 10 mm; the thicknesses were 0.1-1.0 mm. The detectors were distributed radially in the model, and the spaces between them were filled with salt of the same composition. The induced activity was measured with a scintillation spectrometer (NaI, size 63 × 63 mm) from the γ-ray photopeaks. The method of determining the photopeak area and the efficiency of the γ-ray spectrometer has been described [6] along with the electronic equipment used in the experiments.

Translated from Atomnaya Énergiya, Vol. 48, No. 5, pp. 332-334, May, 1980. Original article submitted July 2, 1979.

0038-531X/80/4805-0342 $07.50

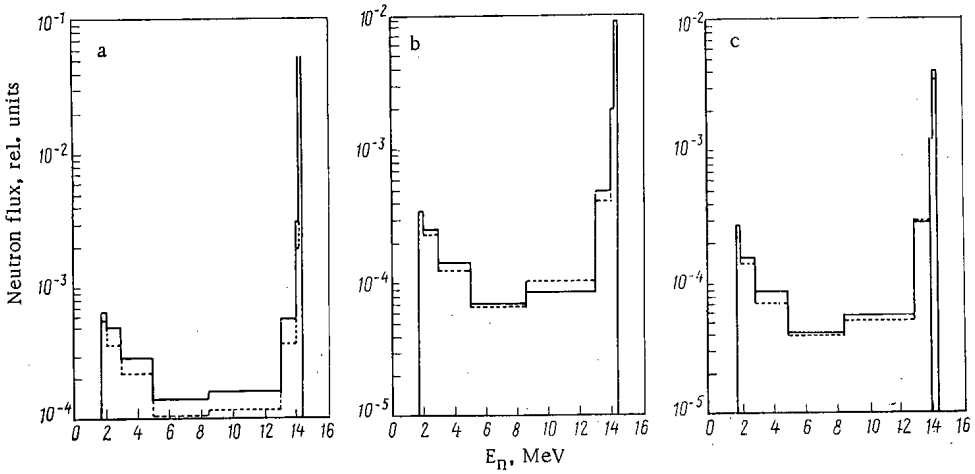

Fig. 1. Group neutron fluxes in relation to energy at points at the following distances from the neutron source: 76 mm (a), 124 (b), and 155 (c): solid line from theory, broken line from experiment.

There were fluctuations in the neutron intensity due to instability in the ion beam and to target burnup, which were corrected for at the same time as the normalization of the activities to the mean neutron flux, which was performed in accordance with [7]. The overall error in measuring the absolute activities of the detectors was 7-9%. The errors in the cross sections of the activation detectors were utilized in calculating the spectra, which are given [8] as 20-30%. The resulting maximum error in the recovered spectrum was 38%. Therefore, the error is determined in the main in this method by the uncertainty over the cross sections of the activation detectors.

Figure 1 shows group neutron fluxes (in the range 1.8-14.1 MeV) as measured and as calculated from the BLANK program. The calculations were performed in spherical geometry with a point 14.1-MeV source. The resulting statistical error in the calculation was not more than 5%.

The following normalization was used in comparing the theoretical and experimental results; the group fluxes from both sources were referred to the same flux in the source group (energy 14.1-14.2 MeV) at a point lying on the internal interface between the salt and air. The value of the neutron flux at this point is determined essentially by the distance to the source, which is 60 mm. This normalization allowed us to refer the theoretical and observed spectra to a single neutron source intensity. Figure 1 shows that the calculation reproduces the energy spectrum satisfactorily in the activation measurements. There are discrepancies in the group fluxes, which amount to about 40% for the point closest to the source (r = 76 mm), but this is within the overall error of the spectrum recovery and calculation. The present study thus demonstrates that a neutron energy spectrum can be recovered for the range 1-14 MeV from activation measurements.

LITERATURE CITED

1. E. A. Kramer-Ageev, V. S. Troshin, and E. G. Tikhonov, Activation Methods in Neutron Spectrometry [in Russian], Atomizdat, Moscow (1976).
2. A. A. Shkurpelov, V. F. Zinchenko, and B. A. Levin, At. Energ., 44, No. 4, 352 (1978).
3. K. I. Zolotarev et al., ibid, 46, No. 2, 96 (1979).
4. S. V. Marin, D. V. Markovskii, and G. E. Shatalov, Preprint IAE-2832, Moscow (1977).
5. V. M. Novikov et al., At. Energ., 47, No. 2, 127 (1979).
6. V. M. Novikov et al., Preprint IAE-3165, Moscow (1979).
7. Fam Zui Hien, At. Energ., 42, No. 5, 414 (1977).
8. W. McElrow and L. Kellogg, Nucl. Technol., 25, No. 2, 180 (1975).

OPTIMUM NEUTRON SPECTRUM FOR ACTIVATING FUEL PINS IN DELAYED-NEUTRON MONITORING

B. P. Maksyutenko

UDC 621.039.54

The relative yields of delayed-neutron groups (relative yields from pure precursors) vary from one fissile substance to another, so it is possible to determine the concentrations of such substances in a mixture. The yield of any one group is proportional to the number of nuclei of a given substance and to the fission cross section, and from the usual mixing rule one can find the ratio of the yield Y_m of group m to the yield of the first group for a mixture of k substances in accordance with

$$Y_m = \frac{\sum_{i=1}^{k-1} Y_{mi} L_i M_i \eta_i + \left(1 - \sum_{i=1}^{k-1} \eta_i\right) Y_{mk} L_k M_k}{\sum_{i=1}^{k-1} M_i L_i \eta_i + \left(1 - \sum_{i=1}^{k-1} \eta_i\right) L_k M_k}, \quad (1)$$

where Y_{mi} is the ratio of the yield of group m to the yield of the first group for substance i; L_i, ratio of the yield of the first group for substance i to the yield of the first group for the substance taken as the first; M_i, ratio of the fission cross section for substance i to the same for the first substance; and n_i, concentration of substance i. The value of L_i is almost independent of the neutron energy E over the range 0-4 MeV, while M_i is a function of energy.

We consider a binary mixture to determine how the error in concentration determination is dependent on the neutron energy. Equation (1) takes the following form for a two-component mixture:

$$Y_m = \frac{Y_{m1}\eta_1 + Y_{m2} X (1 - \eta_1)}{\eta_2 + X (1 - \eta_1)}, \quad (2)$$

where $X = L_2 M_2$.

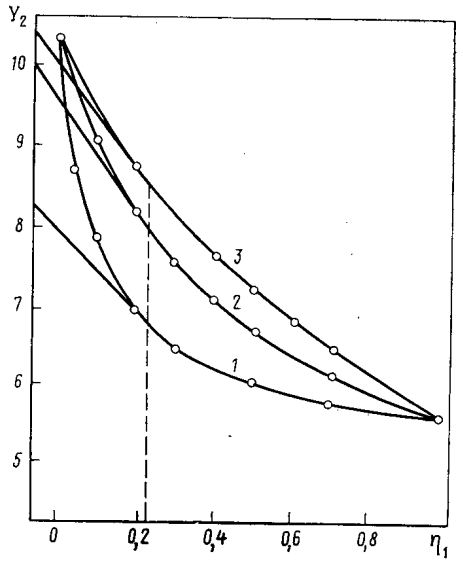

Fig. 1. Ratio of the yield of the second group of delayed neutrons to that of the first for a $^{235}U-^{238}U$ mixture as a function of the ^{235}U concentration for E (MeV) of 1.35 (1), 1.70 (2), 2.0 (3); symbols from experiment, broken line randomly chosen concentration $\eta = 0.23$.

Translated from Atomnaya Énergiya, Vol. 48, No. 5, pp. 334-335, May, 1980. Original article submitted July 2, 1979; revision submitted October 29, 1979.

0038-531X/80/4805-0344 $07.50

As $Y_m(\eta_1)$ is a hyperbola, (2) may be more conveniently represented in a system of asymptotic axes:

$$Y'_m\eta' = \frac{(Y_{m2}-Y_{m1})X}{(1-X)^2}, \tag{3}$$

where $Y'_m = Y - Y_{as}$ as $\eta' = \eta - \eta_{as}$.

The resolution is the name given to the minimum difference $\Delta\eta$ in the percent contents of a given substance in two mixtures that can be distinguished from the relative group yields. The relative yields for two given concentrations are considered as distinct if

$$|Y'^{(2)}_m - Y'^{(1)}_m| \geqslant \Delta Y^{(1)}_m + \Delta Y^{(2)}_m.$$

Here $Y'^{(2)}_m$ and $Y'^{(1)}_m$ are relative yields of group m for concentrations of the first fissile substance $\eta'^{(1)}_1$ and $\eta'^{(2)}_1$, while $\Delta Y^{(1)}_m$ and $\Delta Y^{(2)}_m$ are the corresponding standard deviations. We take these errors as equal to get the resolution as

$$\Delta\eta = \frac{2\Delta Y_m}{\partial Y'/\partial\eta'} \tag{4}$$

or

$$\Delta\eta = -\frac{2\Delta Y_m}{Y_{m2}-Y_{m1}} \frac{[(\eta-1)X-\eta]^2}{X}. \tag{5}$$

The minimum value of the second factor in (5), i.e., the best resolution, is attained with

$$X = \eta/(1-\eta), \tag{6}$$

and therefore the step along the η axis is as follows for the best resolution:

$$\Delta\eta' = \frac{8\Delta Y_m}{Y_{m2}-Y_{m1}} \eta(1-\eta). \tag{7}$$

Therefore, the best resolution for a given concentration is attained at a particular value of X, which is proportional to the ratio of the fission cross section and therefore is a function of the neutron energy. There are no strictly monoenergetic sources, so one can estimate the permissible spectrum width by differentiating (6):

$$\Delta X = \Delta\eta/(1-\eta)^2. \tag{8}$$

It is virtually never the case that the material is not a reactor fuel whose composition is not approximately known, so the ratio of the fission cross sections can be determined in advance, and so one can state what sources can be used for which mixture.

The three curves in Fig. 1 show the ratio of the yield of the second group to that of the first in relation to the ^{235}U concentration for a $^{235}U-^{238}U$ mixture for three values of the neutron energy. For a randomly selected concentration $\eta = 0.23$ the slopes of the tangents give $\partial Y'/\partial\eta'$, which means from (4) that the best resolution should occur for curve 2. Figure 1 also shows that the variation in the relative yield is particularly large for low ^{235}U concentrations (over 70% over the range 0-20%). The resolution is therefore best in this part. Threshold substances give this scope for selection. For certain combinations of two substances (e.g., $^{235}U-^{239}Pu$) the ratio of the fission cross section is virtually constant over a wide range, so there is no such special point, but then the spectrum width in the source can be very great.

The neutron energy range 0.2-4.0 MeV is the best for activating fuel rods; lower energies can give information only about the concentration in the outer layers on account of the high fission cross sections, while higher energy is inapplicable because the reactions of (n, nf) type cause a rapid variation in the relative yields of the groups over a narrow energy range, which may cause complications in the calculations.

In the same way one can define the conditions for the optimum energy for a multicomponent mixture.

EFFECTS OF γ RAYS ON THE INHERENT RESOLUTION OF A THALLIUM-ACTIVATED SODIUM IODIDE CRYSTAL

É. L. Vinograd, N. Yu. Gurevich, and Yu. A. Tsirlin

UDC 539.1.074.3:548.55:546.33.15.683

NaI(Tl) scintillation spectrometers are widely used under conditions of varying temperature and radiation flux. These conditions cause the spectrometric characteristics to alter. For example, x and γ rays reduce the light yield from NaI(Tl) crystals [1-3]. This is due to deterioration in the transmission of the luminescence [4-6]. Here we consider the effects of γ irradiation on the inherent resolution r of NaI(Tl) crystals after irradiation at 20-100°C, particularly to determine the factors responsible for change in r.

The measurements were made on detectors in routine production of sizes 40 × 40 and 40 × 80 mm; the specimens were irradiated with ^{137}Cs at dose rate of 1 Gr/h. The temperature was kept constant during the irradiation by means of an NBE ultrathermostat. The inherent resolution was measured in accordance with [7].

Figure 1 shows the change in the inherent resolution of the NaI(Tl) crystals in relation to γ-ray dose at normal temperature; the deterioration in r is monotone and tends to a limit at a dose of about 1 Gr. There are also substantial differences in the relative change in resolution between specimens of crystals grown by the same technique and having identical sizes.

Figure 2 shows the effects of temperature on the relative change in r after a dose of 1 Gr; the $\Delta r(D)$ and $\Delta r/r_0(T)$ relations (Figs. 1 and 2) follow the form of the coloring curves $\Delta\tau/\tau_0(D)$ and $\Delta\tau/\tau_0(T)$ [5] for NaI(Tl) crystals. This indicates that the radiation damage responsible for the deterioration in resolution is also related to the reduction in transmission for the luminescence.

Parallel measurements were made of the change in r and in transmission at $\lambda \approx 410$ nm by the method of [8] for detectors manufactured by the same technology and given the same dose of 1 Gr of γ rays. These measurements showed that all the crystals gave virtually identical changes in transmission in spite of a major spread in $\Delta r/r_0$. The anomalously large loss of resolution in certain detectors ($\Delta r/r_0 \approx 130\%$) was due to an inhomogeneous distribution of the scintillation efficiency C produced by the γ irradiation.

Measurements were made with a collimated source of the distribution of the scintillation efficiency for a detector with a large value of $\Delta r/r_0$; the detector was found to contain parts A and B differing slightly in per-

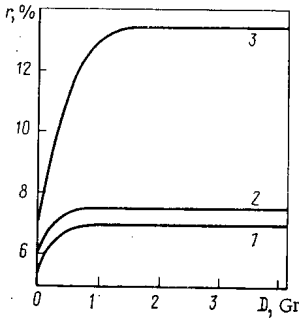

Fig. 1

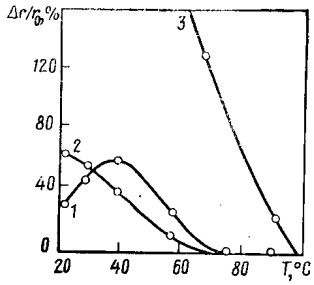

Fig. 2

Fig. 1. Resolution of 40 × 40 mm detectors made of NaI(Tl) in relation to γ-ray dose at dose rate of 1 Gr/h and a temperature of 20°C: 1-3) specimens made by the same technique.

Fig. 2. Effects of temperature on the radiation-induced change in resolution for NaI(Tl) crystals 40 × 40 mm receiving doses of 1 Gr: 1-3) specimens made by the same technique; circles observed points.

Translated from Atomnaya Énergiya, Vol. 48, No. 5, pp. 335-336, May, 1980. Original article submitted July 3, 1979.

0038-531X/80/4805-0346 $07.50

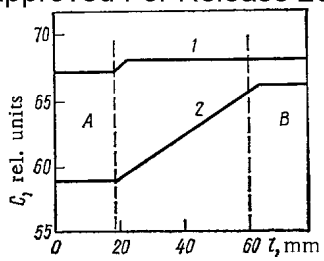

Fig. 3

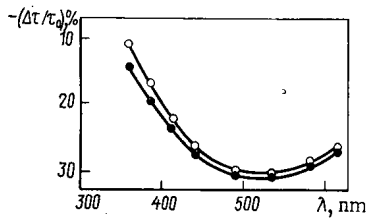

Fig. 4

Fig. 3. Distribution of scintillation efficiency along the length of an NaI(Tl) detector of dimensions 40 × 80 mm: 1) before irradiation; 2) after (irradiation at room temperature, dose 1 Gr).

Fig. 4. Relative reduction in the light-collection coefficient for various wavelengths for detectors irradiated at room temperature to a dose of 100 rad showing different radiation-induced changes in r: ○) $\Delta r/r_0 \approx 10\%$; ●) $\Delta r/r_0 \approx 100\%$.

formance before irradiation but having substantially different C afterwards (Fig. 3). These parts also differed in luminescence spectrum; part A had more green light ($\lambda > 410$ nm) than did part B. It is found [9] that the increase in contribution to the green emission is due to elevated amounts of activator, whereupon the main emission centers ($\lambda_{max} = 410$ nm) are accompanied by compound thallium centers (λ_{max} of 450 and 470 nm). Chemical analysis also showed an elevated amount of thallium in part A ($\rho_A = 2.1 \cdot 10^{-1}$ mass% Tl, $\rho_B = 7 \cdot 10^{-2}$ mass% Tl).

Measurements were also made of the light-collection factors for the NaI(Tl) detectors at 350-650 nm before and after irradiation; the color centers produced by the γ rays reduce the transmission in the green region (450-470 nm) much more than that in the blue region (400-420 nm) (Fig. 4).

Therefore, it is possible for NaI(Tl) crystals to have good resolution and a uniform distribution of the scintillation efficiency before irradiation but to consist of parts differing in composition between the emission centers, whereupon the specimen after irradiation shows differences arising from selective reduction in the green transmission. The part of the crystal having the strong green emission due to the elevated actuator content will then give the weaker signal, which substantially distorts the amplitude spectrum and adversely affects the resolution. The contribution of compound thallium centers becomes appreciable [9] at a concentration of $8 \cdot 10^{-2}$ mass %, and the value increases with the activator concentration.

Therefore, it is not essential to have a strictly uniform bulk distribution of the activator in a NaI(Tl) crystal, which is difficult to attain in practice, but the crystal can work well under irradiation if the thallium concentration varies only within narrow limits and nowhere exceeds $8 \cdot 10^{-2}$ mass %. It is also clear that crystals with low average concentrations show less fall in light yield on exposure to γ rays.

We conclude that a working temperature for NaI(Tl) 40-50° above normal temperature reduces the resolution by a factor 2-3 when the detector is exposed to γ rays.

LITERATURE CITED

1. Ya. M. Zakharko and V. V. Chepelev, Izv. Akad. Nauk SSSR, Ser. Fiz., 29, No. 1, 78 (1965).
2. Z. B. Baturicheva, N. Yu. Gurevich, and Yu. A. Tsirlin, Opt. Spektrosk., No. 18, 129 (1965).
3. N. Yu. Gurevich et al., in: Single Crystals and Technology [in Russian], Issue 1, Izd. VNIImonokristallov, Kharkov (1970), p. 53.
4. N. Yu. Gurevich, in: Abstracts for the Fifth All-Union Conference on Scintillator Synthesis, Production, and Use [in Russian], Izd. VNIImonokristallov, Kharkov (1968), p. 57.
5. Yu. A. Tsirlin et al., At. Energ., 45, No. 1, 69 (1978).
6. R. Ford et al., IEEE Trans. Nucl. Sci., NS-24, No. 1, 264 (1977).
7. GOST 17038-71: Scintillation-Type Ionizing-Radiation Detectors: Methods of Measuring Scintillation Characteristics [in Russian], Standartov, Moscow (1971).
8. N. Yu. Gurevich, Yu. A. Tsirlin, and A. Ya. Berlovskii, Byull. Izobret., No. 30, 193 (1969).
9. R. Kh. Mustafina and A. N. Panova, [3], p. 81.

CALCULATION OF PHOTON-RADIATION MASS ATTENUATION COEFFICIENT

V. I. Gudima and G. V. Pekina

UDC 539.122

The values of the mass attenuation coefficient for photon radiation of different energies are given in tabular form [1, 2]. For certain calculations and the modeling of processes, it is expedient to have formulas relating the mass attentuation coefficient μ/ρ with the photon-radiation energy E.

For the energy range 0.3-3 MeV, which covers most sources of ionizing radiation used, e.g., in measuring technology, this dependence is satisfactorily approximated by the expression $\mu/\rho = a_0 + a_1/E + a_2/E^2 + a_3/E^3$.

The coefficients a_i (i = 0, 1, 2, 3) have been calculated by the least-squares method for 94 elements using the data of [1]. Table 1 shows the values of a_i for 50 elements often encountered in calculations. The maximum error of the approximation δ in the given energy range does not exceed 5%. The exceptions are rhenium (5.1%), gold (5.2%), and thorium (5.3%).

TABLE 1. Coefficients a_i for Calculating Mass Attenuation Coefficient (cm^2/g) from Photon-Radiation Energy (MeV) and Error of Approximation δ (%)

Element	a_0	a_1	a_2	a_3	δ	Element	a_0	a_1	a_2	a_3	δ
Hydrogen	0,03049	0,1314	—0,408	0,005312	1,4	Iron	0,01996	0,05164	—0,01356	0,001858	1
Helium	0,01711	0,06145	—0,0174	0,002094	2,3	Cobalt	0,02223	0,04436	—0,04436	0,001091	0,8
Lithium	0,01432	0,05482	—0,01625	0,002042	1,5	Nickel	0,01943	0,05603	—0,01582	0,002294	2,4
Beryllium	0,01502	0,05538	—0,01593	0,001939	1,5	Copper	0,02129	0,04673	—0,01064	0,001409	0,5
Boron	0,01647	0,05615	—0,01594	0,001948	2	Zinc	0,02023	0,05054	—0,01318	0,001941	1,7
Carbon	0,01695	0,0629	—0,01878	0,002412	1,1	Germanium	0,02147	0,04346	—0,009204	0,001294	0,2
Nitrogen	0,0183	0,0593	—0,01638	0,001976	1,7	Arsenic	0,02047	0,04645	—0,01134	0,001751	1,6
Oxygen	0,01796	0,06048	—0,01708	0,002091	1,1	Selenium	0,02131	0,04199	—0,008757	0,001354	0,7
Fluorine	0,01731	0,05658	—0,01568	0,001876	0,8	Bromine	0,021	0,04491	—0,0104	0,001698	1,5
Neon	0,01873	0,05792	—0,01563	0,001836	1,5	Molybdenum	0,02416	0,03864	—0,005819	0,001229	1,2
Sodium	0,01749	0,05787	—0,01648	0,002048	0,9	Silver	0,0225	0,04373	—0,009175	0,002397	3,4
Magnesium	0,01808	0,05976	—0,01698	0,002097	0,9	Cadmium	0,02362	0,03866	—0,006148	0,001915	2,5
Aluminum	0,01806	0,0575	—0,01616	0,001997	0,6	Tin	0,02504	0,03418	—0,003334	0,001646	1,5
Silicon	0,01918	0,05824	—0,0159	0,001933	0,6	Antimony	0,02433	0,03565	—0,004311	0,001009	2,2
Phosphorus	0,01845	0,05727	—0,01593	0,001967	0,8	Iodine	0,02513	0,03347	—0,002268	0,001712	2,2
Sulfur	0,01797	0,062	—0,01843	0,002415	1	Barium	0,0245	0,03446	—0,00352	0,002367	2,8
Chlorine	0,01917	0,0549	—0,01464	0,001772	0,5	Tungsten	0,03053	0,02334	0,00825	0,003233	2,5
Argon	0,018	0,05175	—0,01393	0,001724	0,4	Platinum	0,03011	0,02555	0,00819	0,004091	3,5
Potassium	0,02109	0,05183	—0,01262	0,001467	0,8	Gold	0,02843	0,03057	0,005736	0,004758	5,2
Calcium	0,01957	0,05869	—0,01634	0,002097	0,8	Mercury	0,02991	0,02658	0,008452	0,004546	3,7
Scandium	0,01884	0,05386	—0,0147	0,001894	0,8	Lead	0,03233	0,01968	0,01415	0,003848	2,4
Titanium	0,0188	0,05258	—0,01434	0,001876	0,9	Radon	0,03143	0,02359	0,0147	0,005061	4,2
Vanadium	0,01954	0,049	—0,01231	0,001539	0,4	Thorium	0,02982	0,0278	0,01362	0,005697	5,3
Chromium	0,02028	0,04948	—0,01222	0,00153	0,4	Uranium	0,03359	0,01764	0,02201	0,004697	3,9
Manganese	0,02019	0,04854	—0,0119	0,001518	0,6	Plutonium	0,03294	0,02234	0,01982	0,005848	4

LITERATURE CITED

1. E. Strom and H. Israel, Nucl. Data Tables, A7, No. 6, 565 (1970).
2. O. F. Nemets and Yu. V. Gofman, Nuclear Physics Handbook [in Russian], Naukova Dumka, Kiev (1975).

Translated from Atomnaya Énergiya, Vol. 48, No. 5, p. 337, May, 1980. Original article submitted July 23, 1979.

0038-531X/80/4805-0348 $07.50

A MONTE CARLO ALGORITHM FOR LOCAL EVALUATION OF PERTURBATIONS IN γ-RAY TRANSPORT PROBLEMS

V. G. Zolotukhin, A. I. Ksenofontov, and A. P. Gnutikov

UDC 519.283

Monte Carlo methods, e.g., with correlated paths, may be ineffective in calculating perturbations in radiation-field functionals arising from the introduction of additional inhomogeneity; in fact, only a small proportion of the paths intersecting the inhomogeneity can give useful information if the size of the perturbing body is small.

The perturbations can be defined by constructing paths from the perturbing region [1] using a bilinear relation between flux and value. The following equation exists [2] for the perturbation in functional J:

$$\delta J = J' - J = -\int \delta\Sigma_t \Phi\Phi^{+'}\, d\mathbf{r}\, d\Omega\, dE + \int \Phi\, d\mathbf{r}\, d\Omega\, dE \int \delta\Sigma_s \Phi^{+'}\, d\Omega''\, dE'', \tag{1}$$

where Φ is the flux in the unperturbed medium; $\Phi^{+'}$, value in the perturbed medium; and $\delta\Sigma_t$ and $\delta\Sigma_S$, perturbations in the total cross sections and the scattering cross sections, respectively.

We consider the case where the perturbation is due to the introduction of an absolute absorber, for which the transfer equation reduces to

$$\Sigma_t' \Phi^{+'}(\mathbf{r}, \Omega, E) = \Omega\nabla\Phi^{+'}(\mathbf{r}, \Omega, E), \tag{2}$$

where $\Sigma_S' = \Sigma_S$ and $\Sigma_t \to \infty$.

We divide the volume of the perturbing body into sufficiently small parts, within which Φ alters only slightly, and we apply Gauss's formula to refer the volume integral to an integral over the surface of the absorber, on the basis that $\Phi^{+'} = 0$ for $\mathbf{n}\Omega < 0$ ($\mathbf{n}$ is the exterior normal to the surface). Then the final expression for the perturbation in a functional is

$$\delta J = -\int |\mathbf{n}\Omega|\, \Phi(\mathbf{r}_s, \Omega, E)\, \Phi^{+'}(\mathbf{r}_s, \Omega, E)\, dS\, d\Omega\, dE, \tag{3}$$

where S is the surface of the perturbing body. The equations for Φ' and Φ^+ are derived analogously.

The solution of (3) by Monte Carlo methods amounts to choosing a point ($\mathbf{r}_S$, Ω, E) on the surface from which one constructs a conjugate path in order to estimate the unperturbed flux Φ with weight $|\mathbf{n}\Omega|$ for a point source S. In the strictly opposite direction ($\mathbf{r}_S$, $-\Omega$, E) we perform a direct simulation of the path of a quantum and estimate $\Phi^{+'}$ for the point of observation D.

The main difficulties in the computational algorithm lie in defining a local estimator for the flux in the conjugate random walk for a monoenergetic source S, and also in simulating the transport of particles (pseudoquanta) in accordance with the conjugate kinetic equation. In that case, Compton scattering of the pseudoquanta involves increasing the energy. To avoid the difficulties arising from energy sampling from an unnormalized distribution [3-5] we propose to use a biased distribution $\hat{f}$ with a normalization of the form

$$\hat{f}(E)\, dE = \frac{d\sigma}{d\Omega}(E \to E')\, \frac{dE}{\sigma_s(E)} \Big/ \int_{E'}^{E_0'} \frac{d\sigma}{d\Omega}(E \to E')\, \frac{dE}{\sigma_s(E)}, \tag{4}$$

where

$$\frac{d\sigma}{d\Omega}(E \to E') \text{ and } \sigma_s(E) = \int_0^E \frac{d\sigma}{dE}(E \to E')\, dE'$$

are the microscopic differential and total cross sections for Compton scattering, $E_0' = \min(E_0, E'/1-2E')$ for

Translated from Atomnaya Énergiya, Vol. 48, No. 5, pp. 337-339, May, 1980. Original article submitted July 23, 1979; revision submitted January 2, 1980.

0038-531X/80/4805-0349 $07.50

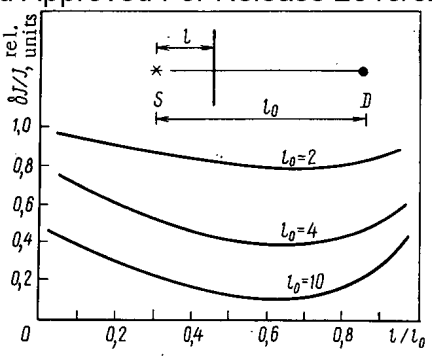

Fig. 1

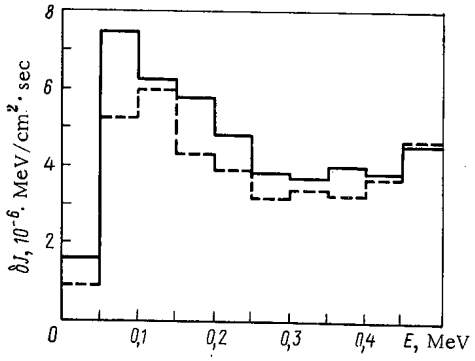

Fig. 2

Fig. 1. Perturbations of the intensity due to scattering in water for a point isotropic source with $E_0 = 0.5$ MeV in relation to distance l between the source S and the surface of an absorbing disk of radius 5.5 cm (J is the intensity of the scattered radiation without the absorbing disk).

Fig. 2. Energy distribution for the scattered radiation intensity: solid line ordinary calculation by Monte Carlo method ($l_0 = 2$); broken line calculation by perturbation theory ($l_0 = 2$ and $l = 0.1$).

$E' < 0.5$, and $E'_0 = E_0$ for $E' \geq 0.5$. The deviation of the function from the true distribution is compensated by the weight equal to the denominator in (4).

For the purpose of conjugate local estimation we take the source as monoenergetic, and therefore the flux is computed from point n in the scattering via the intermediate point n' lying on the vector Ω_n for the motion of a pseudoquantum of energy E_n, which is defined by the condition

$$E_0 = E_n \Big/ 1 - \frac{E_n}{m_0 c^2}(1 - \Omega_n \cdot \Omega^*), \tag{5}$$

where Ω^* is the direction from point n' to the source S.

The estimator for the flux for the point source is found from

$$\Phi_n = k \frac{d\sigma}{d\Omega}(E_0 \to E_n) \frac{1}{\sigma_s(E_0)} \prod_{i=0}^{n} W_{1_i} W_{2_i} \left(\frac{d\varphi}{dE_n}\right) \frac{1}{4\pi R \sin\theta} \exp\left(-\frac{R}{\sin(\theta+\varphi)} \times \right.$$
$$\left. \times [\Sigma_t(E_0)\sin\theta + \Sigma_t(E_n)\sin\varphi]\right), \tag{6}$$

in which R is the distance between the scattering point n and S, with W_{1i} the survival weight of the pseudoquantum ($W_0 = \Sigma_s(E_0)/\Sigma_t(E_0)$), W_{2i} is the weight of the biased function $\hat{f}$, $(d\varphi/dE_n) = (m_0c^2/E_n^2)[1/\sin(\theta+\varphi)]$ is the Jacobian related to the transfer from spatial variables to energy ones in accordance with (5), $\varphi = \arccos(\Omega_n \cdot \Omega^*)$, and θ is the angle between Ω_n and the direction from point n to S. The results obtained by conjugate local estimation agree well with the data of [6] for a point isotropic monoenergetic source of γ rays.

Results are given for the geometry of Fig. 1 from calculation by this method for a thin disk lying on the source–detector line in such a way that any quantum striking the surface is absorbed. The perturbations in the scattered intensity are minimal if the disk is about halfway between the source and the detector and increase as the disk approaches either the source or the detector, where the screening effect is greater in the region near the source and decreases as l_0 increases.

An important feature of this algorithm is that it is possible to estimate the linear radiation-field functional by means of the bilinear relation (3). If we employ complete screening for $J' = 0$ in the perturbed case, then the perturbation is $\delta J = -J$; this corresponds approximately to the disk being placed near the source (Fig. 2), where we show perturbations in the spectrum along with the unperturbed functional J(E) for $l = 0.1$ mean free path. We thus have a novel method of solving some radiation-transport problems by forced perturbation of the initial geometry.

LITERATURE CITED

1. V. G. Zolotukhin, Preprint FM-91, FÉI, Obninsk (1967).
2. G. I. Marchuk and V. V. Orlov, in: Neutron Physics [in Russian], G. A. Krupchitskii (editor), Atomizdat, Moscow (1961), p. 35.

3. M. Kalos, Nucl. Sci. Eng., 33, 284 (1968).
4. D. Irving, Nucl. Eng. Design, 15, 273 (1971).
5. A. De Matteis and R. Simonini, Nucl. Sci. Eng., 67, 309 (1978).
6. V. G. Zolotukhin et al., in: Monte Carlo Simulation in Mathematical Physics [in Russian], G. I. Marchuk (editor), Izd. VTs Sib. Otd. Akad. Nauk SSSR, Novosibirsk (1976), p. 48.

CHANGING YOUR ADDRESS?

In order to receive your journal without interruption, please complete this change of address notice and forward to the Publisher, 60 days in advance, if possible.

(Please Print)

Old Address:

name

address

city

state (or country) zip code

New Address

name

address

city

state (or country) zip code

date new address effective

name of journal

THE LANGUAGE OF SCIENCE
Plenum
PUBLISHING CORPORATION

227 West 17 Street, New York, New York 10011

Declassified and Approved For Release 2013/02/01 : CIA-RDP10-02196R000800030004-0

A Plenum Sampler

Mass Spectrometry of Priority Pollutants

by **Brian S. Middleditch, Stephen R. Missler,** and **Harry B. Hines**
University of Houston

Designed to expedite access to mass spectral information, this volume offers both the experienced mass spectroscopist and novice a convenient source of comprehensive information on 129 priority pollutants. Included are molecular formulas, molecular weight, CAS name and registry number, *Merck Index* reference, and line diagrams. approx. 275 pp., illus., 1980, $29.50

Skeletal Growth of Aquatic Organisms

Biological Records of Environmental Change

edited by **Donald C. Rhoads** and **Richard A. Lutz**
Yale University

Skeletal Growth in Aquatic Organisms applies ontogenetic and demographic analytical methods to a wide range of paleoecological and ecological problems. Internationally renowned researchers examine topics such as the application of skeletal data to problems in paleoclimatology, paleobathymetry, paleooceanography, biogeography, pollution biology, and fisheries management. *Topics in Geobiology, Volume 1*. approx. 750 pp., illus., 1980, $47.50

Electronic Interpretation of Organic Chemistry

A Problems-Oriented Text

by **Fredric M. Menger** and **Leon Mandell**
Emory University

The purpose of this book is to familiarize the student with the principles governing organic reactivity and to provide a "feel" for organic chemistry that cannot be developed by memory alone. 214 pp. + index, 1980, $27.50, **text edition:** $12.50

Principles of Genetic Toxicology

by **David Brusick**
Litton Bionetics, Inc., Kensington, Maryland

This book provides nongeneticists with an introduction to the fundamentals of genetic toxicology. Suitable for use as a textbook, *Principles of Genetic Toxicology* also serves as a reference for toxicologists, chemists, and administrative personnel seeking information on biological and chemical safety evaluation. approx. 300 pp., illus., 1980, $25.00

Current Developments in Anthropological Genetics

Volume 1
Theory and Methods

edited by **James H. Mielke** and **Michael H. Crawford**
The University of Kansas

Topics covered in this important new work include historical demography, perspectives on the evolutionary theory of sociality, a review of the structure of subdivided populations, genetic epidemiology and cultural transmission, and segregation analysis. approx. 500 pp., illus., 1980, $45.00

Lipids in Evolution

by **William R. Nes** and **W. David Nes**
Drexel University

Lipids in Evolution examines the similarities and differences of lipids in various biological contexts, and offers a critical correlation of this information within evolutionary parameters. Topics covered include the origin of oxygen, the role of temperature and pH, and phylogenetics. A volume in *Monographs in Lipid Research.* approx. 225 pp., illus., 1980, $29.50

Nutrition and Food Science

Present Knowledge and Utilization

edited by **Walter J. Santos, J. J. Barbosa, Dagoberto Marques de Miranda Chaves,** and **Nabuco Lopes**
Brazilian Nutrition Society
and **José Carlos Valente**
National Food and Nutrition Institute and Associação Brasileira de Nutrologia

in three volumes

This timely work gives an exhaustive account of the most up-to-date research in nutrition and food science. Representing internationally renowned researchers from more than ninety countries, these volumes will be of great value to those interested in one of the most challenging problems facing contemporary and future societies.

Volume 1
Food Nutrition Programs and Policies
approx. 825 pp., 1980, $75.00*

Volume 2
Nutrition Education, Food Science, and Technology
approx. 900 pp., 1980, $79.50*

Volume 3
Nutritional Biochemistry and Pathology
approx. 775 pp., 1980, $69.50*

*three volume set price: $195.00

THE LANGUAGE OF SCIENCE
Plenum
PUBLISHING CORPORATION
227 West 17 Street, New York, New York 10011

Declassified and Approved For Release 2013/02/01 : CIA-RDP10-02196R000800030004-0

NEW RUSSIAN JOURNALS

IN ENGLISH TRANSLATION

BIOLOGY BULLETIN

Izvestiya Akademii Nauk SSSR, Seriya Biologicheskaya

The biological proceedings of the Academy of Sciences of the USSR, this prestigious new bimonthly presents the work of the leading academicians on every aspect of the life sciences—from micro- and molecular biology to zoology, physiology, and space medicine.

Volume 7, 1980 (6 issues) $195.00

SOVIET JOURNAL OF MARINE BIOLOGY

Biologiya Morya

Devoted solely to research on marine organisms and their activity, practical considerations for their preservation, and reproduction of the biological resources of the seas and oceans.

Volume 6, 1980 (6 issues) $115.00

WATER RESOURCES

Vodnye Resursy

Evaluates the water resources of specific geographical areas throughout the world and reviews regularities of water resources formation as well as scientific principles of their optimal use.

Volume 7, 1980 (6 issues) $215.00

HUMAN PHYSIOLOGY

Fiziologiya Cheloveka

A new, innovative journal concerned *exclusively* with theoretical and applied aspects of the expanding field of human physiology.

Volume 6, 1980 (6 issues) $195.00

SOVIET JOURNAL OF BIOORGANIC CHEMISTRY

Bioorganicheskaya Khimiya

Features articles on isolation and purification of naturally occurring, biologically active compounds; the establishment of their structure, methods of synthesis, and determination of the relation between structure and biological function.

Volume 6, 1980 (12 issues) $245.00

SOVIET JOURNAL OF COORDINATION CHEMISTRY

Koordinatsionnaya Khimiya

Describes the achievements of modern theoretical and applied coordination chemistry. Topics include the synthesis and properties of new coordination compounds; reactions involving intraspheral substitution and transformation of ligands; complexes with polyfunctional and macromolecular ligands; complexing in solutions; and kinetics and mechanisms of reactions involving the participation of coordination compounds.

Volume 6, 1980 (12 issues) $255.00

THE SOVIET JOURNAL OF GLASS PHYSICS AND CHEMISTRY

Fizika i Khimiya Stekla

Devoted to current theoretical and applied research on three interlinked problems in glass technology; the nature of the chemical bonds in a vitrifying melt and in glass; the structure-statistical principle; and the macroscopic properties of glass.

Volume 6, 1980 (6 issues) $145.00

LITHUANIAN MATHEMATICAL JOURNAL

Litovskii Matematicheskii Sbornik

An international medium for the rapid publication of the latest developments in mathematics, this quarterly keeps western scientists abreast of both practical and theoretical configurations. Among the many areas reported on in depth are the generalized Green's function, the Monte Carlo method, the "innovation theorem," and the Martingale problem.

Volume 20, 1980 (4 issues) $175.00

PROGRAMMING AND COMPUTER SOFTWARE

Programmirovanie

Reports on current progress in programming and the use of computers. Topics covered include logical problems of programming; applied theory of algorithms; control of computational processes; program organization; programming methods connected with the idiosyncracies of input languages, hardware, and problem classes; parallel programming; operating systems; programming systems; programmer aids; software systems; data-control systems; IO systems; and subroutine libraries.

Volume 6, 1980 (6 issues) $115.00

SOVIET MICROELECTRONICS

Mikroelektronika

Reports on the latest advances in solutions of fundamental problems of microelectronics. Discusses new physical principles, materials, and methods for creating components, especially in large systems.

Volume 9, 1980 (6 issues) $160.00

Send for Your Free Examination Copy

PLENUM PUBLISHING CORPORATION, 227 West 17th Street, New York, N.Y. 10011
In United Kingdom: 88/90 Middlesex Street, London E1 7EZ England
Prices slightly higher outside the U.S. Prices subject to change without notice.